

1-1-2008

Overload Detection/Health Monitoring Landing Gear Sensor System Proposal

Bradley, W. Baird
Ryerson University

Follow this and additional works at: <http://digitalcommons.ryerson.ca/dissertations>

 Part of the [Aerospace Engineering Commons](#)

Recommended Citation

Baird, Bradley, W., "Overload Detection/Health Monitoring Landing Gear Sensor System Proposal" (2008). *Theses and dissertations*. Paper 1157.

OVERLOAD DETECTION/HEALTH MONITORING
LANDING GEAR SENSOR SYSTEM PROPOSAL

by

Bradley William Baird
B. Eng, Ryerson University, 2001

A thesis

Presented to Ryerson University

in partial fulfillment of the
requirements for the degree of
Masters of Applied Science
in the Program of
Aerospace Engineering

Toronto, Ontario, Canada, 2008

© Brad Baird, Goodrich Aerospace Canada Ltd.

I hereby declare that I am the sole author of this thesis.

Under the terms of the agreement between Goodrich Corporation and RIADI, distribution of this thesis is limited to Dr. Zouheir Fawaz and the referees who will review this thesis. Due to the proprietary nature of this document, Goodrich Corporation does not authorize Ryerson University to distribute this thesis in the public domain.

BRITE PROJECT OVERLOAD DETECTION/HEALTH MONITORING LANDING GEAR SENSOR SYSTEM PROPOSAL

Bradley William Baird

Ryerson University, Masters of Applied Science, Aerospace Engineering. 2008

In recent years, both the major aircraft manufacturers and airline customers have asked landing gear suppliers to begin the development of a viable overload detection/health monitoring system (ODHMS) for in-service and future aircraft landing gear projects. At present, there is no reliable/quantifiable means of determining whether a landing gear has been overloaded during both landing and ground maneuvering conditions. Instead, airlines and aircraft manufacturers rely on a combination of the pilot's judgment and flight recorder data. This thesis outlines current overload detection methods and their shortcomings. It also proposes two possible ODHMS system configurations and provides the basic algorithms required to predict the applied loads acting on the landing gear. Both ODHMS systems require the use of strain gauges and potential gauge types are reviewed. Finally, a technology development test plan is outlined to produce a mature ODHMS to be placed on the next generation single aisle aircraft platform.

ACKNOWLEDGEMENTS

I would like to take this opportunity to thank Dr. Zouheir Fawaz for his support over the past five years while I have been trying to complete this thesis. I would also like to thank Dr. Kamran Behdinin, Dr. Cheug Poon, and Dr. Jeffrey Yokota for their support over the years as well. Finally, I would like to thank Paul Vanderpol and V-Bond Lee who have been very supportive over the years in allowing me to complete this thesis at Goodrich Landing Gear.

TABLE OF CONTENTS

| <u>Section</u> | <u>Description</u> | <u>Page No.</u> |
|----------------|---|-----------------|
| | DECLARATION | ii |
| | ABSTRACT | iii |
| | ACKNOWLEDGEMENTS | iv |
| | TABLE OF CONTENTS | v |
| | LIST OF FIGURES | vii |
| | LIST OF TABLES | viii |
| | DEFINITION OF TERMS | ix |
| 1.0 | INTRODUCTION | 1 |
| 1.1 | Descriptions of Landing Gear Types | 3 |
| 1.1.1 | Nose Landing Gears (NLG) | 3 |
| 1.1.2 | Main/Wing Landing Gears (MLG/WLG) | 5 |
| 1.1.3 | Body Landing Gears (BLG) | 7 |
| 1.2 | Overload Types | 8 |
| 1.2.1 | Hard Landing | 8 |
| 1.2.2 | Ground Maneuvering | 8 |
| 2.0 | HISTORICAL BACKGROUND | 9 |
| 2.1 | Overload Detection | 9 |
| 2.1.1 | Inspection Procedures | 9 |
| 2.1.2 | Qualitative Tables | 12 |
| 2.2 | Boeing Overload Detection Method | 15 |
| 2.3 | Health Monitoring | 18 |
| 2.3.1 | Civil Engineering Industry | 18 |
| 2.3.2 | Aerospace Industry | 19 |
| 3.0 | SENSING SYSTEM OPTIONS | 21 |
| 3.1 | Strain Gauges | 21 |
| 3.1.1 | Resistance Strain Gauge | 21 |
| 3.1.2 | Fibre Bragg Grating Fibre Optic Strain Gauges | 22 |
| 3.1.3 | Fabyr-Perot Fibre Optic Strain Gauge | 23 |
| 3.1.4 | Goodrich Silicon MEMS Technology | 23 |
| 3.2 | Accelerometers | 24 |
| 3.3 | Thesis Proposed System | 25 |
| 3.3.1 | Cantilever/Aft Articulated – Wheel Loads | 26 |
| 3.3.2 | Cantilever – Post Loads | 27 |
| 3.3.3 | Aft Articulated – Post Loads | 28 |
| 3.4 | Strain Gauge Attachment to Structure | 29 |
| 4.0 | LANDING GEAR ANALYSIS THEORY | 30 |
| 4.1 | Landing Gear Structural Modelling | 30 |
| 4.2 | Superposition Principle | 31 |
| 4.3 | Discrete Section Analysis | 32 |
| 4.4 | Finite Element Analysis | 38 |
| 5.0 | STATIC ANALYSIS – OVERLOAD DETECTION | 39 |
| 5.1 | Yielding Criteria | 39 |
| 6.0 | FATIGUE ANALYSIS | 40 |
| 6.1 | Stress-Life Theory (S-N) | 40 |
| 6.2 | Strain-Life Theory (E-N) | 42 |
| 6.2.1 | Monotonic Stress-Strain Relationship | 42 |
| 6.2.2 | Cyclic Stress-Strain Relationship | 42 |
| 6.2.3 | Strain-Life Equation Derivation | 44 |
| 6.2.4 | Strain-Life Equation – Mean Stress Correction | 46 |
| 6.3 | Notch Correction | 47 |
| 6.4 | Random Loading History | 48 |
| 6.5 | Miner's Rule | 49 |
| 7.0 | LOAD PREDICTION ALGORITHM DEVELOPMENT | 50 |

| | | |
|-------|--|---|
| 7.1 | Axle Equations | 1 |
| 7.1.1 | Governing Equations:..... | 1 |
| 7.2 | FEA Study for Strain Gauge Calibration | 1 |
| 7.2.1 | Drag/Vertical Ground Load Calibration | 1 |
| 7.2.2 | MX / MZ Ground Load Calibration | 1 |
| 7.2.3 | Side Load Results | 1 |
| 7.2.4 | Calculating Ground Loads Based on Calibration Equations | 1 |
| 7.2.5 | Newton's Method for Solving Nonlinear Systems of Equations | 1 |
| 7.3 | Post Equations..... | 1 |
| 7.3.1 | Torque Link Strain Measurement | 1 |
| 7.3.2 | Governing Equations..... | 1 |
| 7.4 | G650 NLG Study..... | 1 |
| 7.4.1 | Finite Element Model of G650 Piston and Torque Links | 1 |
| 7.4.2 | Unit Load Results..... | 1 |
| 7.4.3 | Post Load Equation Development for G650 | 1 |
| 7.5 | Strain Gauge Data Acquisition..... | 1 |
| 7.6 | Sensitivity to Temperature | 1 |
| 7.7 | Strain Gauge Time-Lag..... | 1 |
| 7.7.1 | Sample Dynamic Landing Event..... | 1 |
| 7.7.2 | Sensitivity to Time-Lag Results..... | 1 |
| 7.8 | Sensitivity of Load Predictions to Strain Gauge Placement | 1 |
| 7.8.1 | Sensitivity Analysis Results – Vertical and Drag..... | 1 |
| 7.8.2 | Sensitivity Analysis Results – Vertical and Side..... | 1 |
| 7.9 | Data Reduction for Static and Fatigue Analysis..... | 1 |
| 7.9.1 | Intermediate Data Point Elimination..... | 1 |
| 7.9.2 | Small-Strain Vibration Elimination..... | 1 |
| 8.0 | SOFTWARE DEVELOPMENT | 1 |
| 8.1 | Modules..... | 1 |
| 8.2 | ODHMS Section Definition 1.0..... | 1 |
| 8.2.1 | Traditional Section Cut Analysis | 1 |
| 8.2.2 | FEM Nodal Stress Analysis..... | 1 |
| 8.2.3 | Load Equation Definitions | 1 |
| 8.3 | ODHMS Strain Interpreter 1.0..... | 1 |
| 8.3.1 | Elimination of Superfluous Strain Data | 1 |
| 8.3.2 | Calculation of Wheel/Post Loads..... | 1 |
| 8.4 | ODHMS Overload Prediction 1.0 | 1 |
| 8.5 | ODHMS Life Prediction 1.0..... | 1 |
| 9.0 | TEST PLAN | 1 |
| 9.1 | Cantilever Beam Demonstration Test..... | 1 |
| 9.1.1 | Calibration Loads | 1 |
| 9.1.2 | Strain Gauge Placement..... | 1 |
| 9.1.3 | Finite Element Calibration | 1 |
| 9.1.4 | Load Equation Development..... | 1 |
| 9.1.5 | Test Cases..... | 1 |
| 9.2 | G650 NLG Drop Test..... | 1 |
| 9.3 | G650 NLG Static Test..... | 1 |
| 9.4 | G650 NLG Fatigue Test..... | 1 |
| 9.5 | G650 Flight Test | 1 |
| 10.0 | DISCUSSION..... | 1 |
| 11.0 | CONCLUSION | 1 |
| | REFERENCES..... | 1 |

LIST OF FIGURES

| | |
|---|----|
| Figure 1-1: Example of an Aft-Articulated NLG | 3 |
| Figure 1-2: Example of Cantilever – Trunnion Type NLG | 4 |
| Figure 1-3: Example of Cantilever – Truss Type NLG | 4 |
| Figure 1-4: Example of an Aft-Articulated MLG..... | 5 |
| Figure 1-5: Example of a Cantilever MLG | 6 |
| Figure 1-6: Example of a Cantilever WLG..... | 6 |
| Figure 1-7: Example of BLG | 7 |
| Figure 2-1: Example of In-Stop Design | 10 |
| Figure 2-2: Overload Qualitative Table Example..... | 14 |
| Figure 2-3: Proposed Strain Measurement Locations - Boeing | 15 |
| Figure 2-4: Typical Load Transfer from Landing Gear to Airframe | 16 |
| Figure 2-5: Example Load Case and Resulting Reactions..... | 17 |
| Figure 3-1: Wheel Load Monitoring Configuration..... | 26 |
| Figure 3-2: Post Load Monitoring Configuration – Cantilever Type..... | 27 |
| Figure 3-3: Post Load Monitoring Configuration – aft articulated Type | 28 |
| Figure 4-1: An Example of a Structural Beam model..... | 30 |
| Figure 4-2: Examples of Landing Gear Finite Element Analysis | 38 |
| Figure 6-1: Sample S-N Curve | 41 |
| Figure 6-2: Hysteresis Loop for Cyclic loading..... | 43 |
| Figure 6-3: Strain-Life Curve | 45 |
| Figure 6-4: Effect of Mean Stress on Strain-Life Curve..... | 46 |
| Figure 6-5: Sample Rainflow Counting Example and Resulting Hysteresis Loop..... | 48 |
| Figure 7-1: Applied Loads at Wheel Centreline..... | 51 |
| Figure 7-2: Finite Element Model of Axle Region..... | 55 |
| Figure 7-3: Finite Element Contact Model of Axle Interface | 55 |
| Figure 7-4: Axle Interface Supports..... | 56 |
| Figure 7-5: Ground Load Application to Axle..... | 56 |
| Figure 7-6: Gauge 1 DV Results | 58 |
| Figure 7-7: Gauge 2 DV Results | 58 |
| Figure 7-8: Gauge 3 DV Results | 59 |
| Figure 7-9: Gauge 4 DV Results | 59 |
| Figure 7-10: Gauge 5 DV Results | 60 |
| Figure 7-11: Gauge 6 DV Results | 60 |
| Figure 7-12: Gauge 7 DV Results | 61 |
| Figure 7-13: Gauge 8 DV Results | 61 |
| Figure 7-14: Gauge 1 RM Results..... | 64 |
| Figure 7-15: Gauge 2 RM Results..... | 64 |
| Figure 7-16: Gauge 3 RM Results..... | 65 |
| Figure 7-17: Gauge 4 RM Results..... | 65 |
| Figure 7-18: Gauge 5 RM Results..... | 66 |
| Figure 7-19: Gauge 6 RM Results..... | 66 |
| Figure 7-20: Gauge 7 RM Results..... | 67 |
| Figure 7-21: Gauge 8 RM Results..... | 67 |
| Figure 7-22: Definition of Post Loads | 73 |
| Figure 7-23: Strain Gauge Measurement Locations at Piston | 74 |
| Figure 7-24: Potential Strain Gauge Arrangement at Piston | 75 |
| Figure 7-25: Relating Torque Link Apex Loads to MV Moment | 76 |
| Figure 7-26: Calibrating Strain Gauge Results to Apex Force | 77 |
| Figure 7-27: Definition of Wheel Centreline | 78 |
| Figure 7-28: Free Body Diagram for Loads at Section A-A | 79 |
| Figure 7-29: G650 NLG FE Model for Strain Gauge Calibration | 82 |
| Figure 7-30: Applied Loads and Boundary Conditions | 83 |
| Figure 7-31: Proposed Strain Gauge Locations | 83 |
| Figure 7-32: Von Mises Stress Plots for Unit Cases | 84 |
| Figure 7-33: Skinning of Piston and Torque Link | 85 |

| | |
|---|---|
| Figure 7-34: Sample Locations for Piston Barrel..... | 1 |
| Figure 7-35: Strain Gauge Location on Torque Link Assy..... | 1 |
| Figure 7-36: Sample Locations for Piston Barrel..... | 1 |
| Figure 7-37: Sample Locations for Piston Barrel..... | 1 |
| Figure 7-38: Sample Locations for Piston Barrel..... | 1 |
| Figure 7-39: Summary of Side Load Error (Vertical + Drag) | 1 |
| Figure 7-40: Summary of Side Load Error (Vertical + side) | 1 |
| Figure 7-41: Example of Intermediate Data Elimination | 1 |
| Figure 7-42: Comparison of Applied Loads to Absolute strain | 1 |
| Figure 7-43: Small-Strain Vibration Events Elimination | 1 |
| Figure 7-44: Example of Small-Strain Vibration Event Removal | 1 |
| Figure 8-1: Landing Gear Health Monitoring 1.0 | 1 |
| Figure 8-2: Sample Use of FEA Results | 1 |
| Figure 8-3: Sample Load Equations Development..... | 1 |
| Figure 8-4: Sample Load Equations Development from Beam Model | 1 |
| Figure 8-5: Unit Post Loads Applied to Beam Model..... | 1 |
| Figure 9-1: Cantilever Beam Demonstration Test Article | 1 |
| Figure 9-2: Calibration Loads for Cantilever Beam Test | 1 |
| Figure 9-3: Strain Gauge Placement on Cantilever Beam | 1 |
| Figure 9-4: Cantilever Beam Finite Element Model..... | 1 |
| Figure 9-5: Sample Von Mises Stress Plots | 1 |

LIST OF TABLES

| | |
|--|---|
| Table 3-1: Pros and Cons of Strain Gauge Attachment Methods | 2 |
| Table 7-1: Internal Load Types Generated at Piston..... | 7 |
| Table 7-2: Raw FEM Stress Results | 8 |
| Table 7-3: Unit Stress/Strain Data..... | 8 |
| Table 7-4: Sample Dynamic Landing Event | 9 |
| Table 7-5: Sensitivity to Strain Gauge Time-Lag..... | 9 |
| Table 7-6: Calculated Strain Levels for The 90 deg Configuration..... | 9 |
| Table 7-7: Side Load Error for the 90 deg Configuration..... | 9 |
| Table 7-8: Unit Stress/Strain Data (30 deg Config) | 9 |
| Table 7-9: Calculated Strain Levels for The 30 deg Configuration..... | 9 |
| Table 7-10: Side Load Error for the 30 deg Configuration..... | 9 |
| Table 7-11: Unit Stress/Strain Data (45 deg Config) | 9 |
| Table 7-12: Calculated Strain Levels for The 45 deg Configuration..... | 9 |
| Table 7-13: Side Load Error for the 45 deg Configuration..... | 9 |
| Table 7-14: Unit Stress/Strain Data (60 deg Config) | 9 |
| Table 7-15: Calculated Strain Levels for The 60 deg Configuration..... | 1 |
| Table 7-16: Side Load Error for the 60 deg Configuration..... | 1 |
| Table 7-17: Summary of Side Load Error (Vertical + drag Case)..... | 1 |
| Table 7-18: Landing Simulation Ground Loads and Strains..... | 1 |
| Table 9-1: Summary of Predicted Coefficients for Cantilever Beam..... | 1 |
| Table 9-2: Gulfstream G650 Business Jet | 1 |

DEFINITION OF TERMS

| | |
|------------------|---|
| Approach Speed | The horizontal velocity of the aircraft at the instant of landing gear initial contact with the ground during landing. |
| AOG | Aircraft on Ground |
| Assy | Assembly |
| BLG | Body Landing Gear |
| CS | Coordinate System |
| E | Young's Modulus / Modulus of Elasticity |
| GLG | Goodrich Landing Gear |
| Hard Landing | Conditions during landing that produce high impact loads on the landing gear that may cause overloading of landing gear/airframe components |
| MLG | Main Landing Gear |
| MLW | Maximum Landing Weight |
| NDT | Non-Destructive Testing |
| NLG | Nose Landing Gear |
| ODHMS | Overload Detection and Health Monitoring System |
| Sink Rate | The downwards velocity of the aircraft at the instant of landing gear initial contact with the ground during landing. |
| Stbd | Starboard |
| Sustained Stress | Components that are constantly under stress (i.e. pressure fit grease fittings on lugs/sockets, axle roots under 1g static loads) |
| WLG | Wing Landing Gear |
| Zxx, Zyy, Zzz | Bending Moduli of Rupture |

Chapter 1: Introduction

The purpose of this thesis is to outline a potential platform for developing a landing gear overload detection / health monitoring system for both in-service and future aircraft programs. The proposed system will enable airlines, aircraft manufacturers, and landing gear suppliers to measure and predict the following:

- Aircraft Weights and Balance
- Overload Detection during Landing/Ground Maneuvering
- Long-Term fatigue life prediction of landing gear components (Health Monitoring)

In recent years, both the major aircraft manufacturers and airline customers have asked landing gear suppliers to begin the development of a viable overload detection system for in-service and future aircraft landing gear projects. At present, there is no reliable/quantifiable means of determining whether a landing gear has been overloaded during both landing and ground maneuvering conditions. Instead, airlines and aircraft manufacturers rely on a combination of the pilot's judgment and flight recorder data (such as sink rate, approach speed, and aircraft acceleration).

The current means of assessing whether an overload condition has occurred has many shortcomings, a few of which are listed below:

1. Individual pilots will have varying opinions on what constitutes a hard landing (i.e. the assessment is qualitative in nature). Furthermore, if the pilot has a tight schedule of flights, he/she may be under pressure to continue flying without reporting potential hard landing conditions.
2. It is very difficult, even with sink rate, approach speed, and acceleration data to predict the impact loads on the landing gear. This data requires a large amount of engineering analysis from both a dynamics and structural point of view with no guarantees on the validity of the predicted loads.

If the pilot does report a hard landing, then the aircraft is grounded (AOG). Once the aircraft is grounded, various levels of inspection are required up to, and including, removal of the landing gear from the aircraft. This scenario can create large expenses to airlines and also cause loss of revenue.

Due to recent technology developments, the ability for landing gear manufacturers to provide an overload detection system for both current and future products has become achievable. This thesis will outline a proposed means of detecting hard landings utilizing the latest strain gauge technologies. Due to the measuring techniques utilized for hard landing detection, this system also provides the following additional data:

1. aircraft weights and balance to the pilot before take-off
2. long-term fatigue life monitoring and prediction

The main goals of this thesis are the following:

- To propose a framework for a landing gear overload detection/health monitoring system (ODHMS)
- To develop a system that uses a minimum amount of strain gauges to monitor ground loads applied to the landing gear for in-service aircraft
- To develop mathematical algorithms to convert sensor readings into ground loads

1.1 Descriptions of Landing Gear Types

This section outlines typical landing gear designs used in commercial aircraft.

1.1.1 **Nose Landing Gears (NLG)**

Nose landing gears are typically located below and forward of the cockpit. In general, nose landing gears react 10-15% of the aircraft weight. There are three types of nose landing gears typically used in the commercial market:

1. Aft Articulated
2. Cantilever – Trunnion Type
3. Cantilever- Truss Type

Aft Articulated

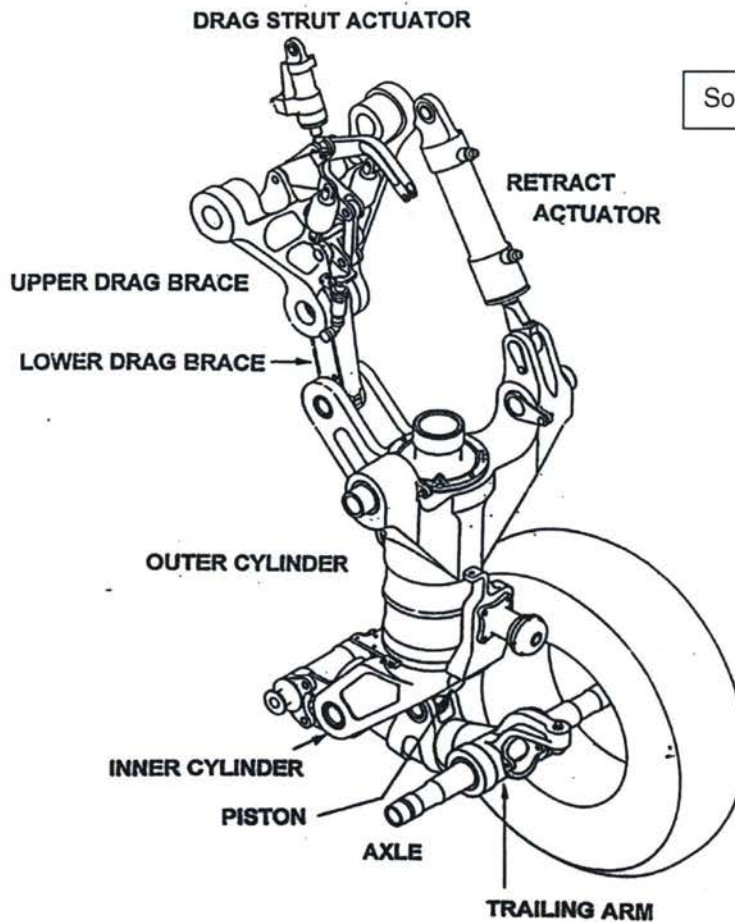


FIGURE 1-1: EXAMPLE OF AN AFT-ARTICULATED NLG

Cantilever – Trunnion Type

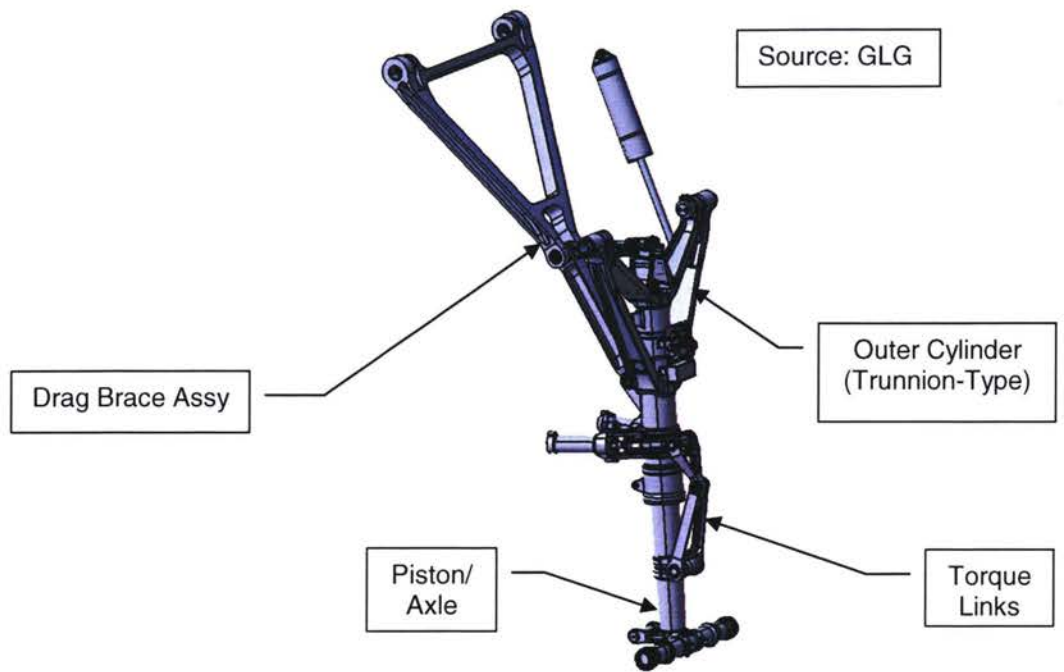


FIGURE 1-2: EXAMPLE OF CANTILEVER – TRUNNION TYPE NLG

Cantilever – Truss Type

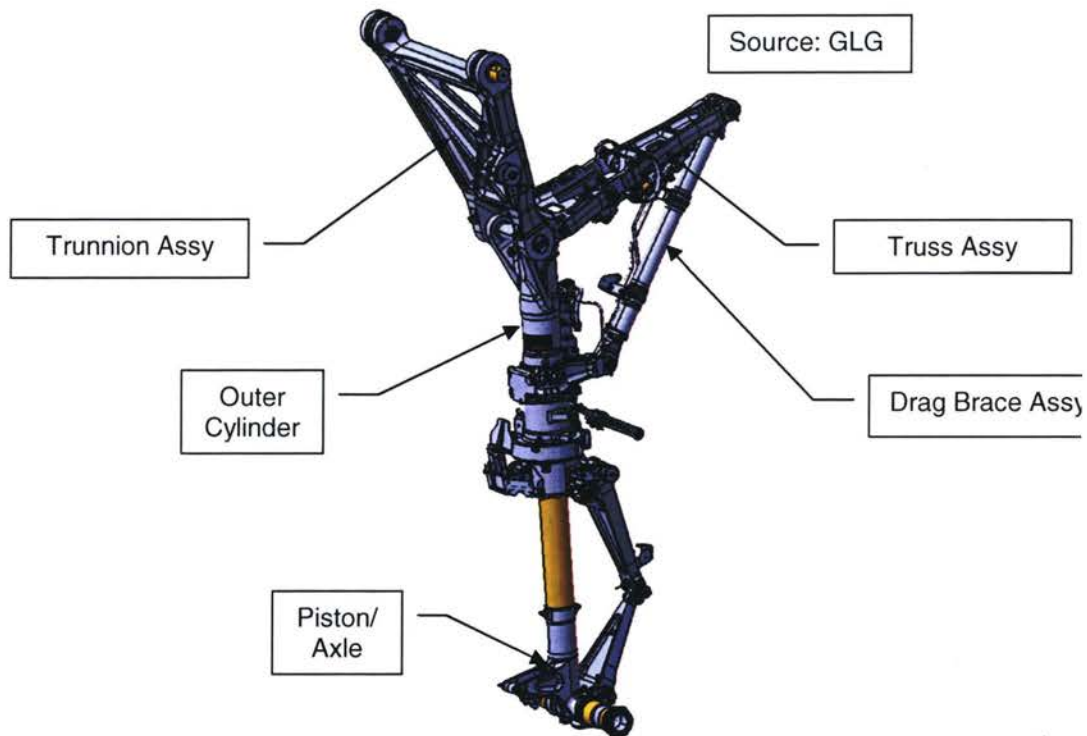


FIGURE 1-3: EXAMPLE OF CANTILEVER – TRUSS TYPE NLG

1.1.2

Main/Wing Landing Gears (MLG/WLG)

Main/Wing landing gears are generally attached at the root of the wing. Main/Wing landing gear designs for commercial aircraft can include 1-6 wheels. There are two types of main landing gears typically used in the commercial market:

- 1. Aft Articulated
- 2. Cantilever

Aft Articulated MLG

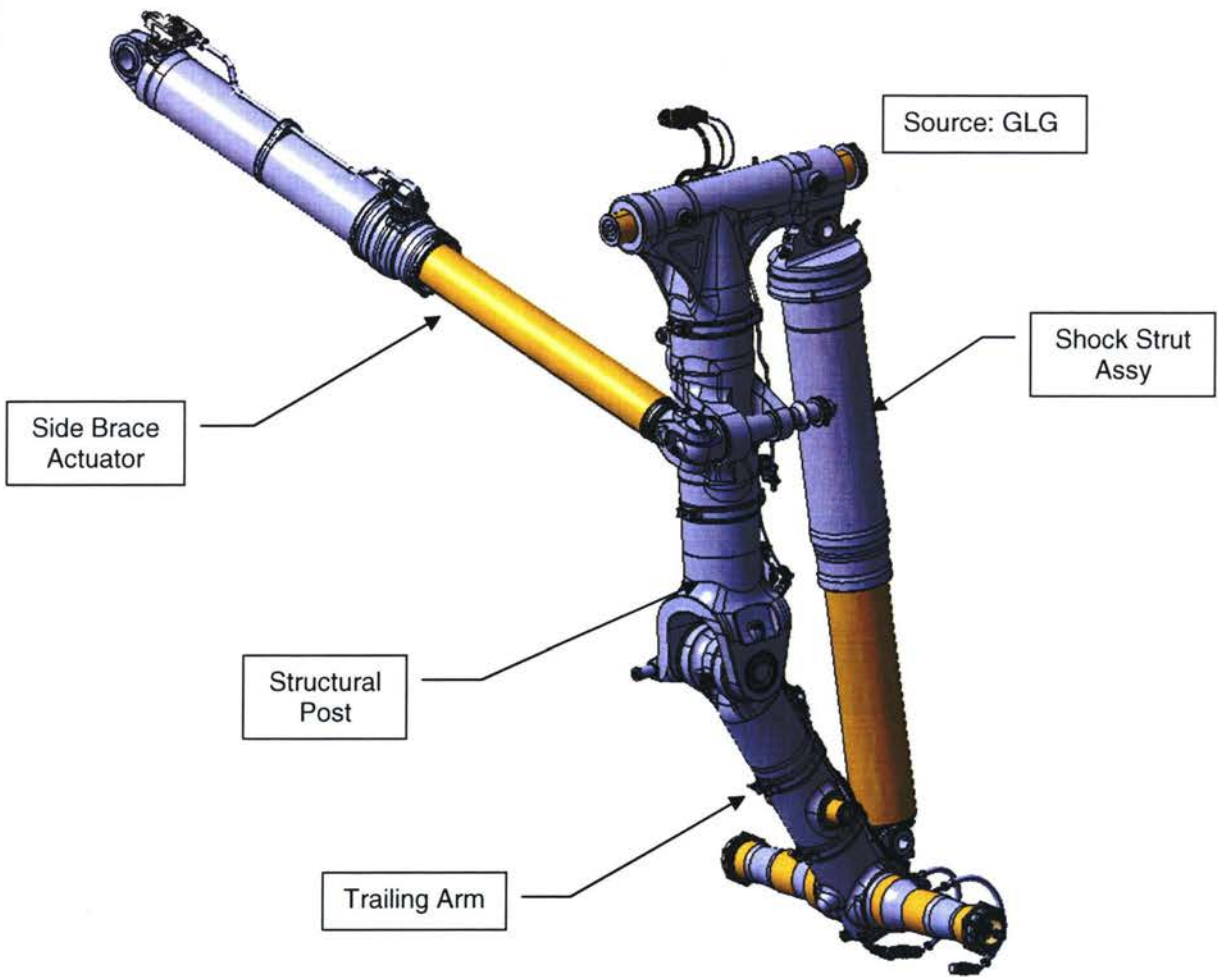


FIGURE 1-4: EXAMPLE OF AN AFT-ARTICULATED MLG

Cantilever MLG

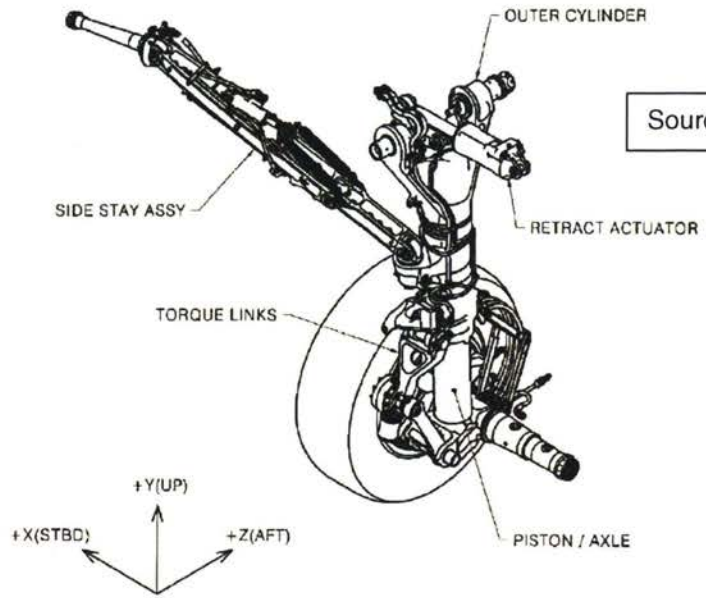


FIGURE 1-5: EXAMPLE OF A CANTILEVER MLG

Cantilever WLG

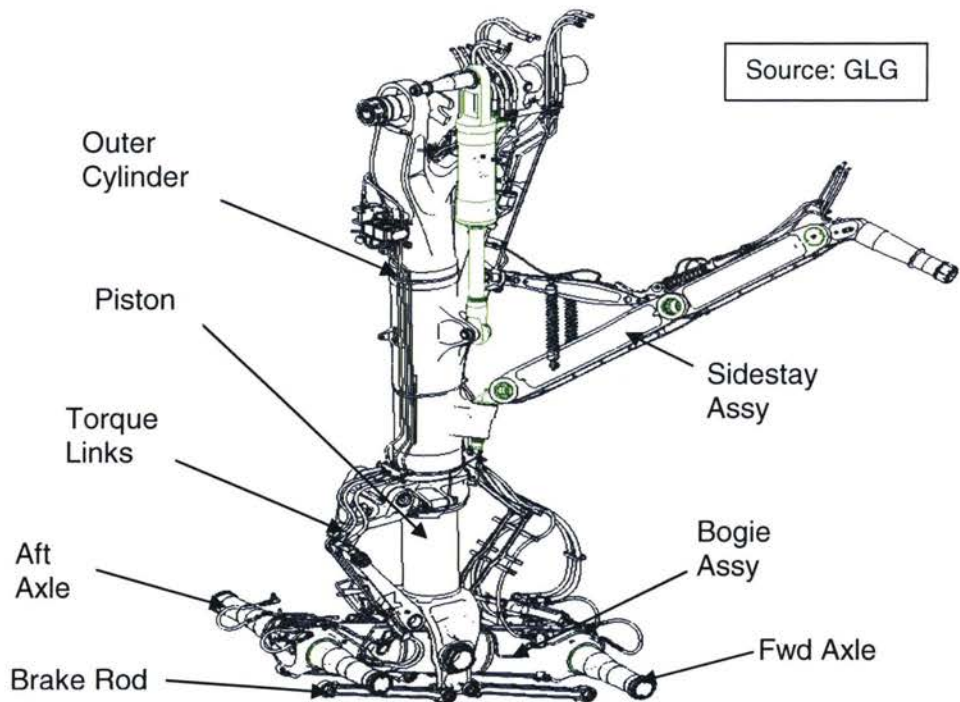


FIGURE 1-6: EXAMPLE OF A CANTILEVER WLG

1.1.3

Body Landing Gears (BLG)

Body (or Centreline) landing gears are limited to large commercial aircraft such as the A340, A380, and 747. All three of these aircraft utilize cantilever style designs.

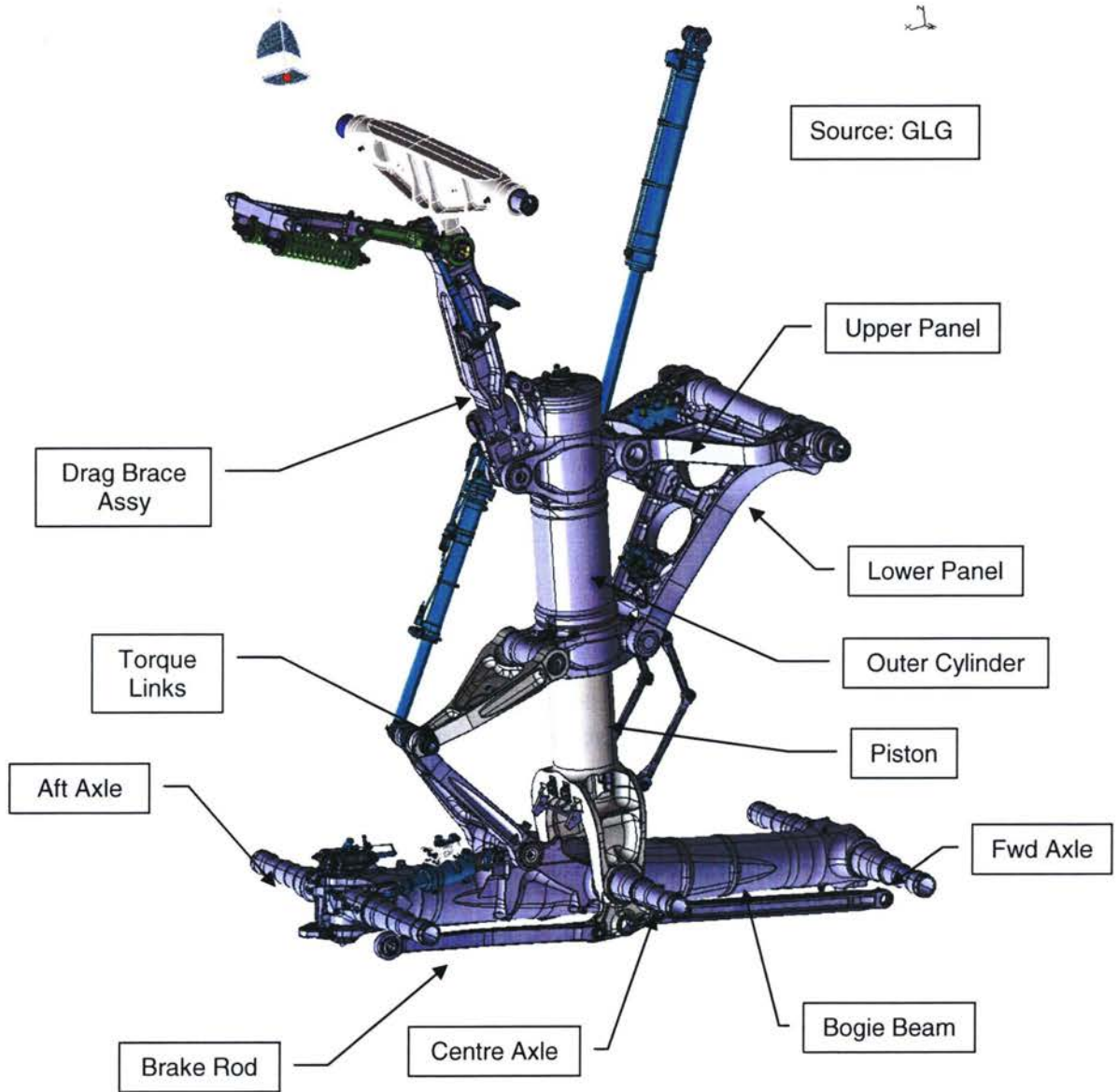


FIGURE 1-7: EXAMPLE OF BLG

1.2 Overload Types

Overload conditions for landing gear can be classified into two categories:

1. Hard Landing
2. Ground Maneuvering

1.2.1 Hard Landing

Typically, hard landings are caused by one or more of the following:

1. The aircraft landing weight exceeds the maximum allowable landing weight (MLW)
2. High sink rate (i.e. ≥ 10 ft/s which is considered the limit load scenario)
3. Nose landing gear touchdown prior to main landing gear
4. Aircraft roll angle at touchdown is such that one main landing gear absorbs initial impact
5. Aircraft overshoots/undershoots the runway
6. Drift landings that cause high drag/side loads on the landing gear

1.2.2 Ground Maneuvering

Overload conditions can also be caused while the aircraft is on the ground and maneuvering. Some conditions that may cause overloading of the landing gear are as follows:

1. High speed turn that produces high lateral g-levels
2. High deceleration due to braking
3. Excessive pivoting
4. Towing incidents (overload or overrun)
5. Wheel/tire failure
6. Tire burst and tread throw
7. Maximum nose wheel steering angle exceeded

Chapter 2: Historic Background

2.1 Overload Detection

References 8, 13

Overloading can be defined as any combination of ground loads acting on the landing gear which causes one or more individual components to yield. Overloading scenarios can occur during both landing and ground maneuvers. Historically, overload detection has been limited to pilot opinion.

Currently, there is no viable quantitative means of assessing whether a hard landing has occurred on a landing gear. As a result, if the pilot reports that a hard landing has occurred, complex inspections may result.

2.1.1 Inspection Procedures

Historically, when a hard landing has been reported by the pilot, a series of inspections are required before the landing gear can be cleared for further flights. Initially, the inspection requirements will be limited to visual inspections conducted while the landing gear is still attached to the aircraft.

These initial inspections are typically named Phase I inspections and will include inspection of the following:

1. Tires and Wheels
2. Shock strut fluid leakage
3. Airframe attachment pin distortion (i.e. ovalization of pins)
4. Bushing migration
5. In-stops for shock strut bottoming indication (see below)¹

¹ To prevent the piston from impacting the top of the outer cylinder, mechanical stops are typically included in the design of the shock strut.



FIGURE 2-1: EXAMPLE OF IN-STOP DESIGN

If, after these initial inspections, there are indications that an overload has occurred, a Phase II inspection is required. Phase II inspections are much more involved and require the aircraft to be put on jacks so that the landing gear no longer supports the aircraft weight. Once the aircraft is on the jacks, the following procedures are typically completed:

1. Retract/extend the nose and main landing gears with the normal system to ensure that joints or components have detrimentally deformed. If the landing gears do not retract normally, this would be a strong indication that an overload scenario has occurred.
2. Retract/extend the main and nose landing gears using the manual system for similar reasons as 1.
3. Examine principal structural elements of the landing gear for damage/deformation (such as axles, outer cylinder, torque links, piston, drag brace, side brace, shock strut, etc.)
4. Complete a check on the shock strut fluid level

If any of these visual inspections indicate that an overload may have occurred, the landing gear is removed from the aircraft and sent to a qualified facility for detailed Non-Destructive Testing (NDT). Depending on the component material, the following NDT tests may be performed in order to detect cracking:

- Magnetic Particle Inspection
- Die Penetrant Inspection

If, after completion of the NDT tests, there are no indications of cracking, one of the following two steps will be taken:

1. The landing gear will be cleared for flight and re-installed on the aircraft

2. If the component material is prone to stress corrosion cracking, the component may be placed on a shelf for 2-6 months. If, after this period, no cracks have formed, the component will be cleared for flight and re-installed on the aircraft.

Due to the space limitations in aircraft structure and the significant loads that landing gears are subjected to, high strength steels and aluminums are utilized. Both of these materials can be prone to stress corrosion cracking when exposed to relatively high sustained stresses. These components can also fail due to stress corrosion once they have undergone plastic deformation. If a component undergoes relatively high tensile plastic deformation without rupturing, the component will fail due to long-term exposure to the atmosphere. For further details on stress corrosion cracking, refer to reference 1.

2.1.2 Qualitative Tables

In the past five years, GLG has worked in conjunction with an aircraft manufacturer to develop a more efficient method of qualitatively assessing whether a hard landing has occurred. This qualitative assessment requires the airframe manufacturer to identify the type of overload scenario (i.e. high sink rate, drift landing, nose wheel over-steering, etc.). Once the overloading scenario has been identified, engineers and aircraft maintenance personnel utilize a series of tables and figures to identify which components on the landing gear require inspection.

Based on this methodology, the airframe manufacturer must still rely on flight recorder data for g levels, sink rates, approach speeds, etc. However, during ground maneuvering and towing scenarios, the flight recorder data may not contain any valuable data for overload prediction. In either scenario, the pilot will still be relied up to report and evaluate the severity of the overload event.

For this method to be successful, the landing gear supplier must identify key components on the landing gear that could be detrimentally deformed during an overload event. As an example, torque links transfer torque acting on the landing gear from the piston/axle to the outer cylinder. Under a hard landing event which produces high vertical loads on the landing gear, the torque link would not be significantly loaded. As a result, the landing gear supplier would not recommend the inspection of the torque links for this type of event.

An example of a qualitative table is provided on the following page. In this chart, a specific type landing scenario has been assumed:

- Various Drag and Vertical Load Combinations
- A set shock strut stroke of 435 mm
- A side load based on 0.35 x the vertical force
- All loads are evenly distributed amongst the wheels

For ease of understanding, assume that the airframe manufacturer has determined from the flight data recorder that a drift landing has occurred with the following post loads:

Vertical = 2000 kN

Drag = 1500 kN

Side = 700 kN

Based on the data above, a point can be drawn on Figure 2-2. Based on this point on the curve the airline maintenance personnel would be directed to inspect, as a minimum, the drag brace f

pin and outboard main pintle pin. If, after these initial inspections, there are indications that these pins have yielded, a more thorough inspection of other components would be required.

DVS Domain Results: Stroke = 435mm Pitch = 0 deg, S = 0.35, 50/50 Distribution

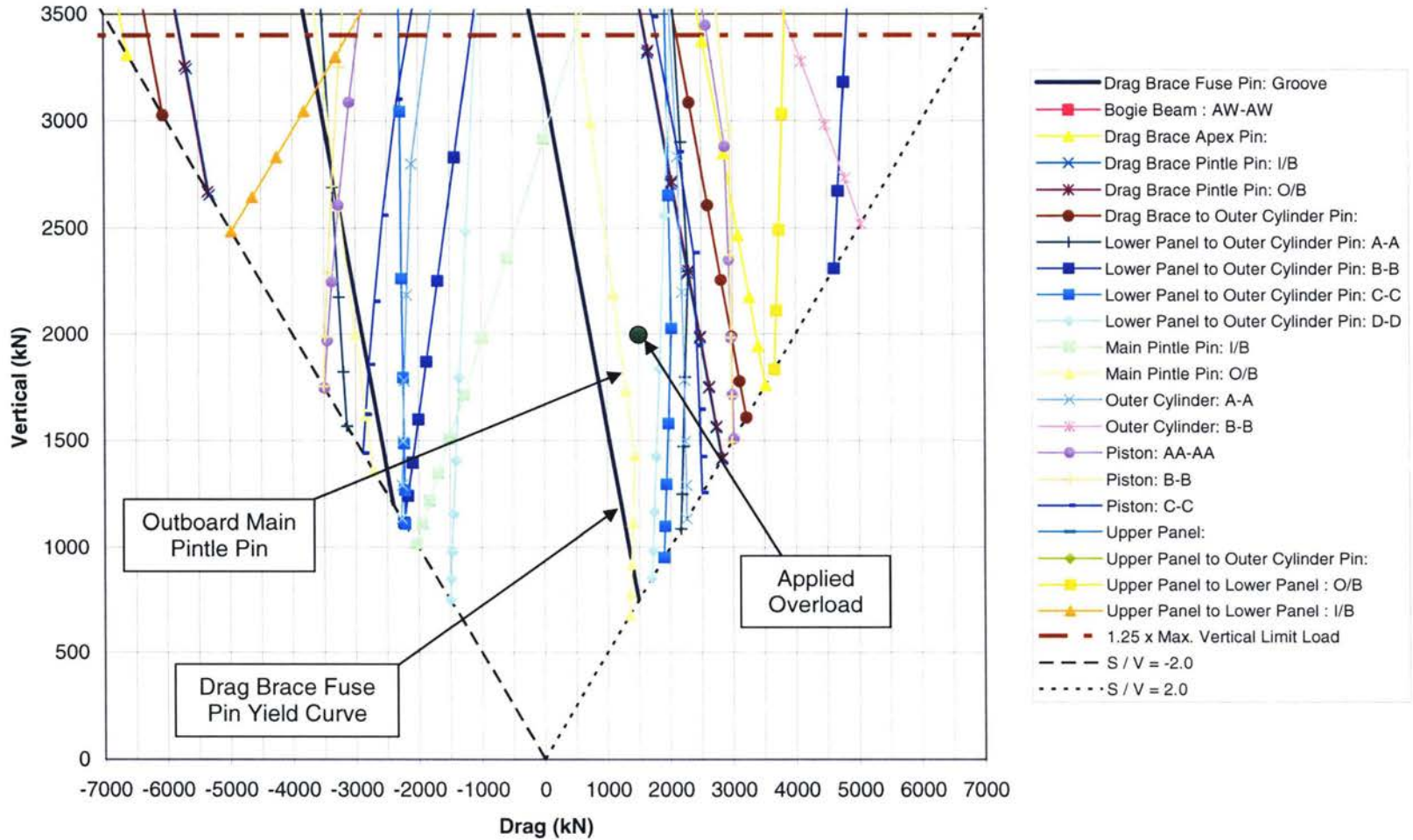


FIGURE 2-2: OVERLOAD QUALITATIVE TABLE EXAMPLE

Boeing Overload Detection Method

On the Boeing 777 program, an overload detection system was developed and patented by Boeing (see reference 10). This system utilizes resistance strain gauges placed at key locations on the main landing gear system and surrounding aircraft structure. The intent of the system is to quantitatively measure the forces that can cause structural damage to an airplane that has experienced a hard landing event. The goal of the system is to make the decision that the aircraft requires a hard landing inspection before it is allowed to fly again.

As with the system proposed by in this thesis, the key measurement to determine the applied ground loads is strain. The system is able to utilize any strain measuring device that outputs an electronic signal. In the patent, Boeing offers suggested locations for strain gauge measurement but does not specifically specify where the ideal measurement points should be located. Some of the suggested locations are shown in the figure below:

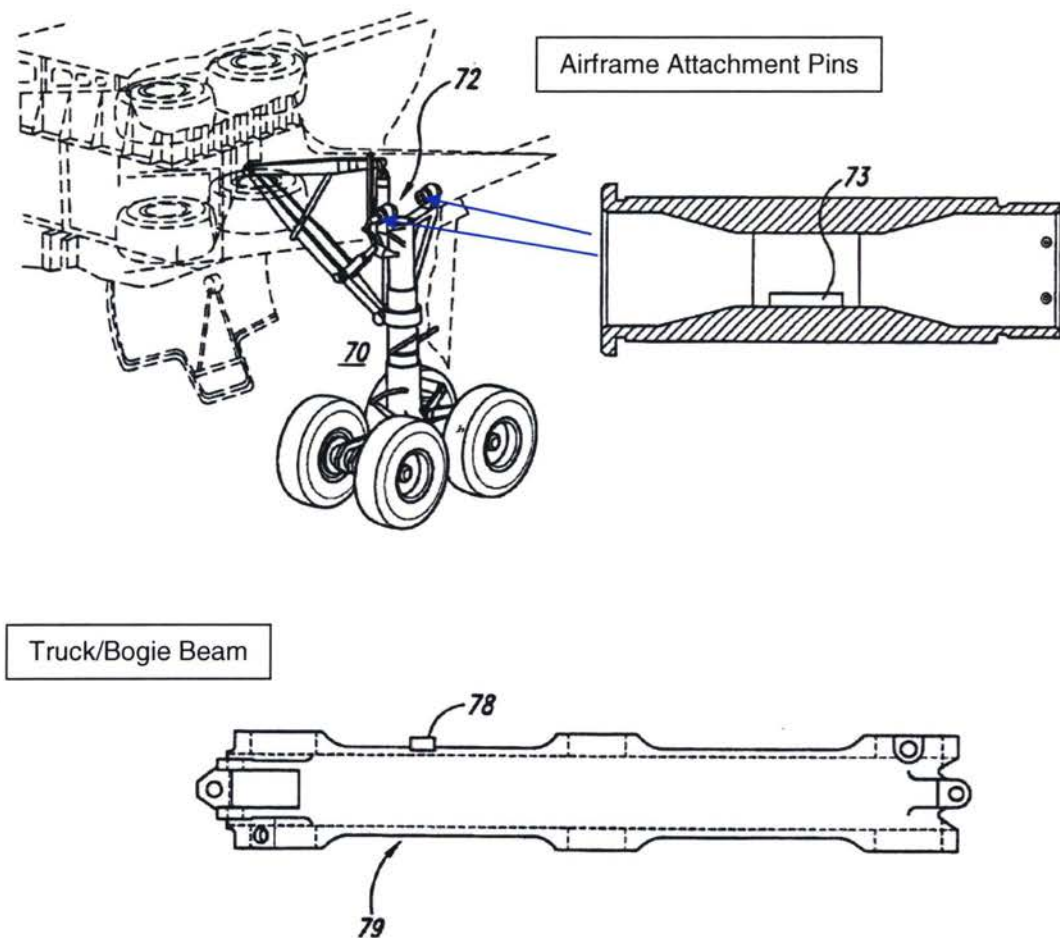


FIGURE 2-3: PROPOSED STRAIN MEASUREMENT LOCATIONS Source: Boeing

For landing gear systems with more than two wheels, a bogie/truck beam is required in the design to attach the 2+ axles to the shock strut. For this configuration, measuring strain levels at the bogie beam would be advantageous. If this configuration was utilized, a minimum of six strain gauges would be needed at both the fore and aft sides of the bogie beam (with reference to the shock strut axis). Measuring strains at the bogie beam would provide the fore/aft split of the overall post loads being applied to the landing gear.

Boeing also proposes measuring strain levels at the airframe attachment pin locations. Generally speaking, measuring strain levels at the aircraft attachment pins will provide some indication of the applied forces to the landing gear. Due to the means by which aircraft attachment pins are connected to the aircraft, only shear forces will be able to be measured by the pins (see figure below):

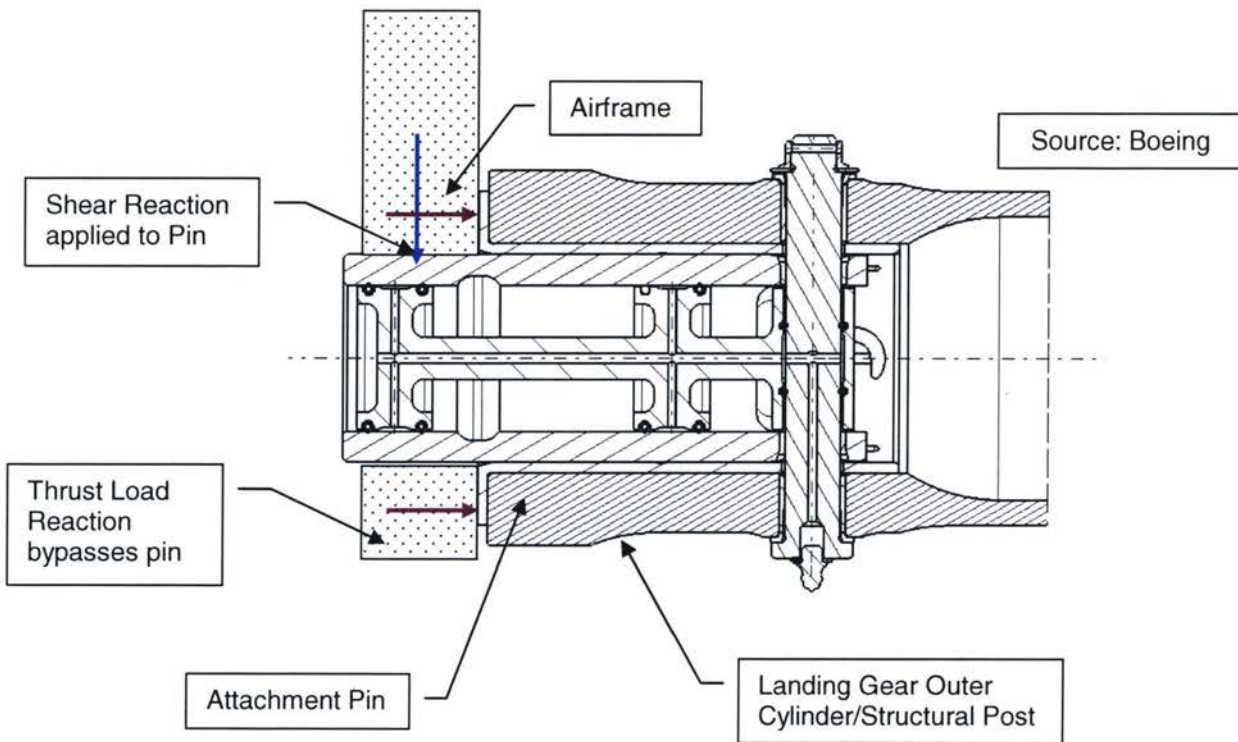


FIGURE 2-4: TYPICAL LOAD TRANSFER FROM LANDING GEAR TO AIRFRAME

Depending on the landing gear configuration, the thrust load reactions at the airframe will either be a direct result of the applied drag or side loads to the landing gear. These two applied loads will also produce a shear couple reaction at the airframe attachments but this will be difficult to separate from the shear reaction due to the vertical force and applied moments at the post. An example case with drag, braking torque, and vertical loads is provided on the following page.

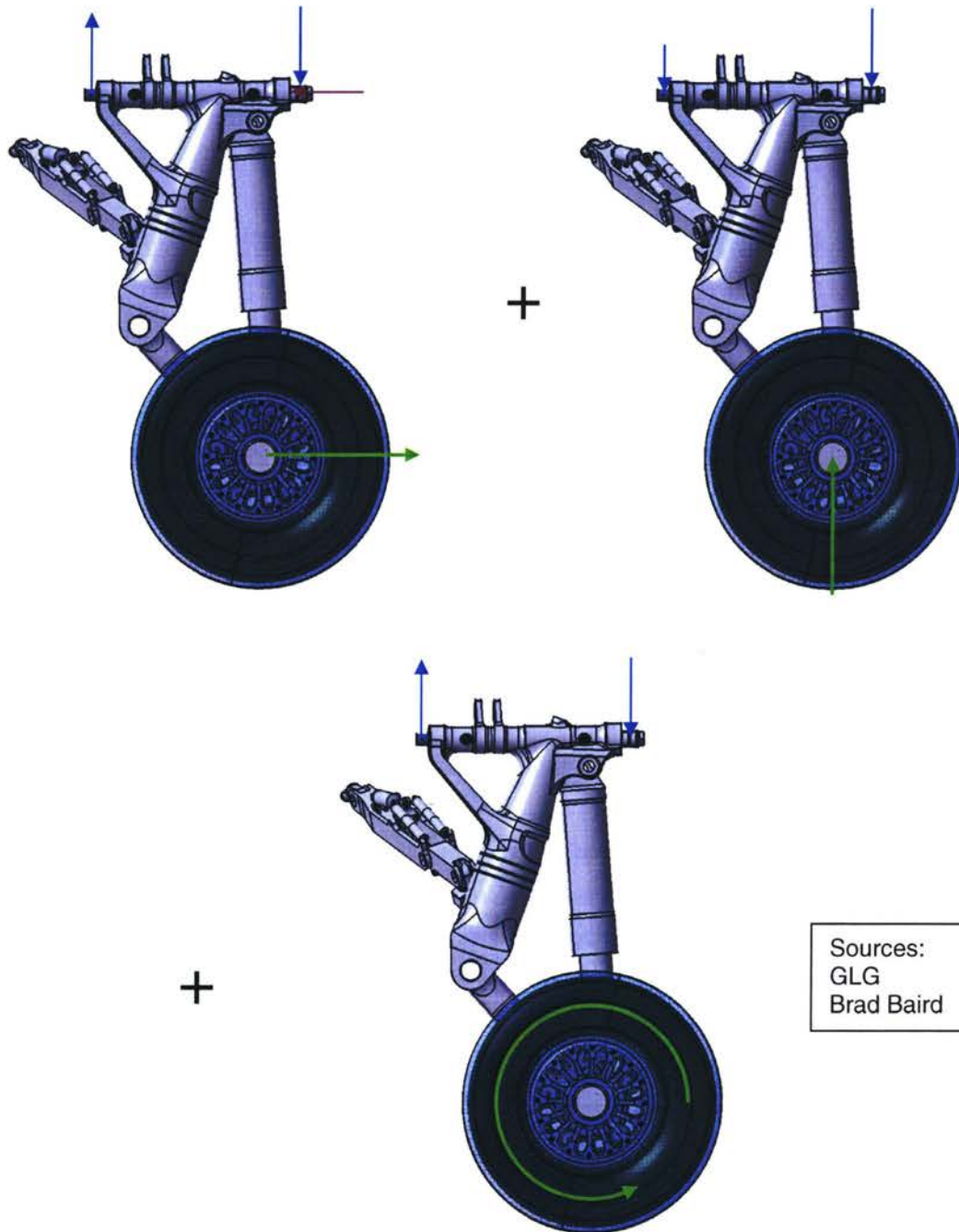


FIGURE 2-5: EXAMPLE LOAD CASE AND RESULTING REACTIONS

From the figure above, the three post loads applied produce two shear reactions at the aircraft attachment points and one thrust reaction component. Since the pin solution does not have the capability to measure the thrust reaction, the shear measurements in the pin will not provide adequate data to solve for the three unknowns. As a result, this system can only be used during landing when it is known that the brakes are not powered.

2.3

Health Monitoring

In recent years, many engineering disciplines have been developing systems to monitor the loads acting on structures for extended periods of time. Typically, the loads are monitored indirectly by measuring strain levels at key regions within the structure. The strains are then converted into loads via calibration from testing, finite element analysis, or traditional hand calculations.

By continuously monitoring the ground loads acting on a landing gear while in service, the fatigue life of individual components can be predicted. Therefore, components that have seen higher fatigue loads than predicted can be removed from the landing gear before failure occurs in service. Conversely, landing gear components that have theoretical life limitations may see fatigue loads significantly lower than predicted. As a result, components with life limitations may have service lives extended due to health monitoring.

A structural health monitoring (SHM) system includes the following elements:

- Structure
- Sensors
- Data acquisition systems
- Data transfer and storage mechanism
- Data management
- Data interpretation and diagnosis

An example of this technology is embedding sensors in structures like bridges and aircraft. These sensors provide real time monitoring of various structural changes like stress and strain. In the case of civil engineering structures, the data provided by the sensors is usually transmitted to a remote data acquisition centre.

This section outlines the uses of health monitoring in both the civil engineering and aerospace fields.

2.3.1 Civil Engineering Industry

Although many engineering disciplines have begun to develop health monitoring systems, the civil engineering industry has become the leaders in this technology development. As the designs and construction of civil structures continues to evolve, it has become crucial that these structures be monitored for their health. If these structures are monitored over long periods of time, premature catastrophic failures can be prevented or their lives may be extended.

In Canada, it is estimated that infrastructure systems have a total asset value of \$2 trillion dollars. Many of these structures are deteriorating over time due to the following:

- inadequate maintenance
- excessive loading
- adverse environment conditions

Generally speaking, infrastructure systems are not monitored for their health. As a result, it is difficult for engineers to predict the state of health of these structures.

Over the past decade, SHM's have been developed to conduct long-term health monitoring. The first civil structure worldwide to incorporate a full SHM system into its initial design is the Taylor Bridge in Headingly, Manitoba. The health of this bridge will be monitored remotely for its lifetime.

Typically, structural health monitoring in the civil engineering industry involves the use of Fibre-Bragg fibre optic strain gauges. These strain gauges are bonded to key regions of structure such as bridges and these strain levels are monitored over long periods of time.

2.3.2 Aerospace Industry

See reference 8 for details.

Structural health monitoring could play a significant role in maintaining the safety of both new and aged aerospace structures that are subject to cyclic loading. For such structures, the development of an integrated sensory system able to monitor, collect, and predict the structural health is essential. The commercial aerospace applications of an SHM are in their infancy but both airframe manufacturers and airline customers are interested in developing SHM systems.

Aging aircraft are of major concern to the engineering community because of the following issues encountered in-service with these aircraft:

- Multi-site fatigue damage
- Hidden cracks in hard to reach locations
- Corrosion

Creating a health monitoring system for new and aging fleets is the subject of major research in universities, government labs, and industry. Prevention of fatigue failures on in-service aircraft could be greatly improved by implementing a reliable SHM system. In fact, such a system would be capable of assessing the aircraft's structural integrity and would be able to detect initial damage before catastrophic failure occurs.

Another added benefit of introducing an SHM system is the ability to reduce maintenance costs throughout an aircraft's life. Today, inspections and structural health monitoring are completed manually. Manual inspections are costly to airlines for two key reasons – the cost of labour and the loss of revenue while the aircraft is grounded.

Chapter 3: Sensing System Options

3.1 Strain Gauges

The strain gauge setup described in section 7.0 does not limit the choice of strain gauge to be used for ground load measurement. The following strain gauges could potentially be placed on a landing gear load monitoring system:

- Resistance
- Fibre Bragg Grating fibre optic
- Fabry-Perot fibre optic
- Goodrich Silicon MEMS technology

As will be discussed in detail in section 7.0, the algorithms developed to predict the ground loads applied to the landing gear require strain outputs. The type of sensing system developed for the ODHMS system does not require that strain be measured directly. In other words, if a more efficient sensing system can be developed that measures displacement instead of strain, it would not affect the algorithms developed in this thesis. The only requirement for the system is to convert the direct measurement of displacement into strain levels.

3.1.1 Resistance Strain Gauge

The resistance strain gauge has been used in test flight programs for many aircraft with success. Resistance strain gauge technology is mature and well understood and, for these reasons, could be a potential candidate for use in an load monitoring system. However, using a system based on resistance strain gauge technology may be difficult for the following reasons:

- Frequent need to zero gauges due to strain drift (i.e. maintenance required)
- Could cause electromagnetic interference (EMI) with critical aircraft/landing gear systems

3.1.2 Fibre Bragg Grating Fibre Optic Strain Gauges

Fibre Bragg Grating (FBG) fibre optic strain gauges are a more recent development in strain gauge technology. Currently, it is being used heavily in civil engineering as a measurement tool for long term health monitoring of bridges. In the aerospace industry, FBG gauges have been imbedded in composite structures in order to monitor loads and to detect the onset of debonding. FBG technology has many benefits:

- Robust
- Does not need to be zeroed (i.e. less maintenance)
- Electrically passive (i.e. does not produce EMI)
- Only one cable required for all strain gauges
- Less time to install than electrical resistance gauges
- Insensitive to transverse strain
- Highly resistant to temperature and moisture

On the other hand, FBG technology has some disadvantages as well:

- If bulb burns out, no data can be acquired for any gauge
- The bulb is relatively expensive to replace
- If cable is damaged, no data can be acquired for any gauge
- Each gauge requires second gauge for temperature correction
- During retraction and extension of the landing gear, the fibre optic cable would bend significantly. If the bending radius required is too severe, the fibre could fail statically or due to fatigue

3.1.3

Fabyr-Perot Fibre Optic Strain Gauge

The Fabyr-Perot (FP) type fibre optic strain gauge has many of the same advantages as the FBG type fibre optic gauge. Some distinctive advantages are as follows:

- No need for second gauge to correct for temperature
- Separate cable for each gauge
- Separate light source for each gauge
- Light source is extremely cheap to replace relative to FBG gauge

The disadvantages to using an FP fibre optic gauge are as follows:

- More maintenance required (i.e. bulb replacement/cable repair)
- More installation required than FBG due to multiple cables
- During retraction and extension of the landing gear, the fibre optic cable would bend significantly. If the bending radius required is too severe, the fibre could fail statically or due to fatigue

3.1.4

Goodrich Silicon MEMS Technology

Goodrich Sensor Systems designs, develops and produces micro electro-mechanical systems (MEMS) for high-performance sensors and actuators. In recent years, Goodrich Sensors has developed a silicon MEMS strain gauge that could be used in landing gear load monitoring applications. Using a MEMS style strain gauge would have the following advantages:

- Sensor package is smaller and lighter
- Higher reliability and less expensive than other sensor systems
- High Precision

Although this strain gauge type has some advantages to other systems, this sensor type does not have a large amount of in-service history and, as such, the product is not mature.

3.2

Accelerometers

Another load monitoring system that has been proposed is to place accelerometers at key locations on the landing gear. These key locations would be the following:

- Axle tip
- Shock Strut

The axle tip would be an ideal location to place an accelerometer because it has a relatively high amount of deflection that will occur when load is applied at the wheels. The shock strut is also ideal since it will displace significantly during the initial touchdown phase and during taxiing. This system would be relatively simple to implement in today's airline market since accelerometers are used extensively on in-service aircraft.

There are three fundamental problems with the accelerometer sensing approach:

1. An accurate stiffness/mass distribution of the landing gear and support structure is required.
2. The shock strut dynamic airspring curve must be accurately known. During in-service use the airspring curve may deviate from the design curve due to leakage of shock strut oil and nitrogen.
3. Accelerometers will aid in the prediction of highly dynamic loading events (such as landing only). For ground maneuvering cases that are quasi-static in nature, accelerations at the shock strut and axle tips are relatively low. Therefore, these readings will not aid in calculating the applied ground loads.

Thesis Proposed System

Generally speaking, airline customers are hesitant to implement new types of sensing systems unless it is required by the airframe manufacturer and/or the aviation authorities. Introducing additional sensing systems to the aircraft can create additional costs to the airliner due to increased maintenance due to increased risks of system failures. In other words, as system complexity increases, the probability of systems related maintenance increases.

For both airframe manufacturers and airlines to accept an ODHMS type system, the landing gear designer must provide a system that fulfills the following requirements:

- Minimum complexity
- Reliable ground load predictions
- Ability to achieve either the overhaul life (typical half of the aircraft life) or full life
- Minimum power and weight impact to aircraft

All of these requirements point to the need to design an ODHMS architecture that is as simple as possible. To achieve the need for simplicity, it is imperative to keep the amount of sensors to a minimum while still maintain accurate ground load measurements. In order to keep the amount of sensors required to predict the ground loads applied to the landing gear to a minimum, it is imperative to place the sensors as close to the load application points as possible (i.e. the wheels). As a result, I propose to investigate two different configurations of strain gauge monitoring systems:

- Wheel load measurement at axle root
- Post load measurement

These two configurations are illustrated conceptually for the following types of landing gear designs:

- Cantilever
- Aft Articulated

Refer to the following pages for the strain gauge system proposals outlined above.

3.3.1 Cantilever/Aft Articulated – Wheel Loads

For both cantilever and aft articulated landing gear designs, a series of strain gauges can be placed at the axle root to measure the applied wheel loads. For further details on this strain gauge configuration, refer to section 7.1.

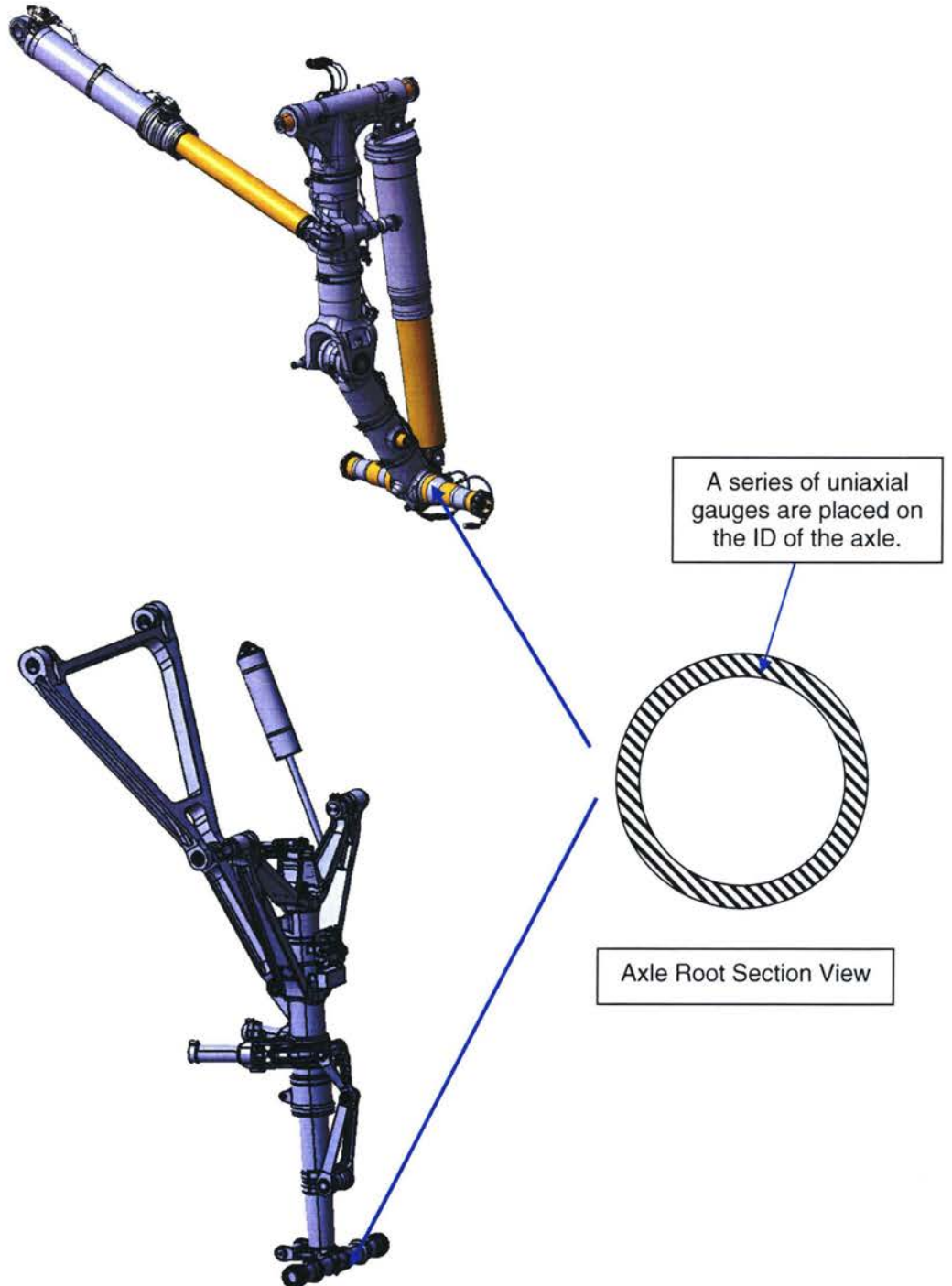


FIGURE 3-1: WHEEL LOAD MONITORING CONFIGURATION

3.3.2

Cantilever – Post Loads

For cantilever landing gear designs, a series of strain gauges can be placed at the base of the piston and on the torque links to measure the applied post loads. For further details on this strain gauge configuration, refer to section 7.3.

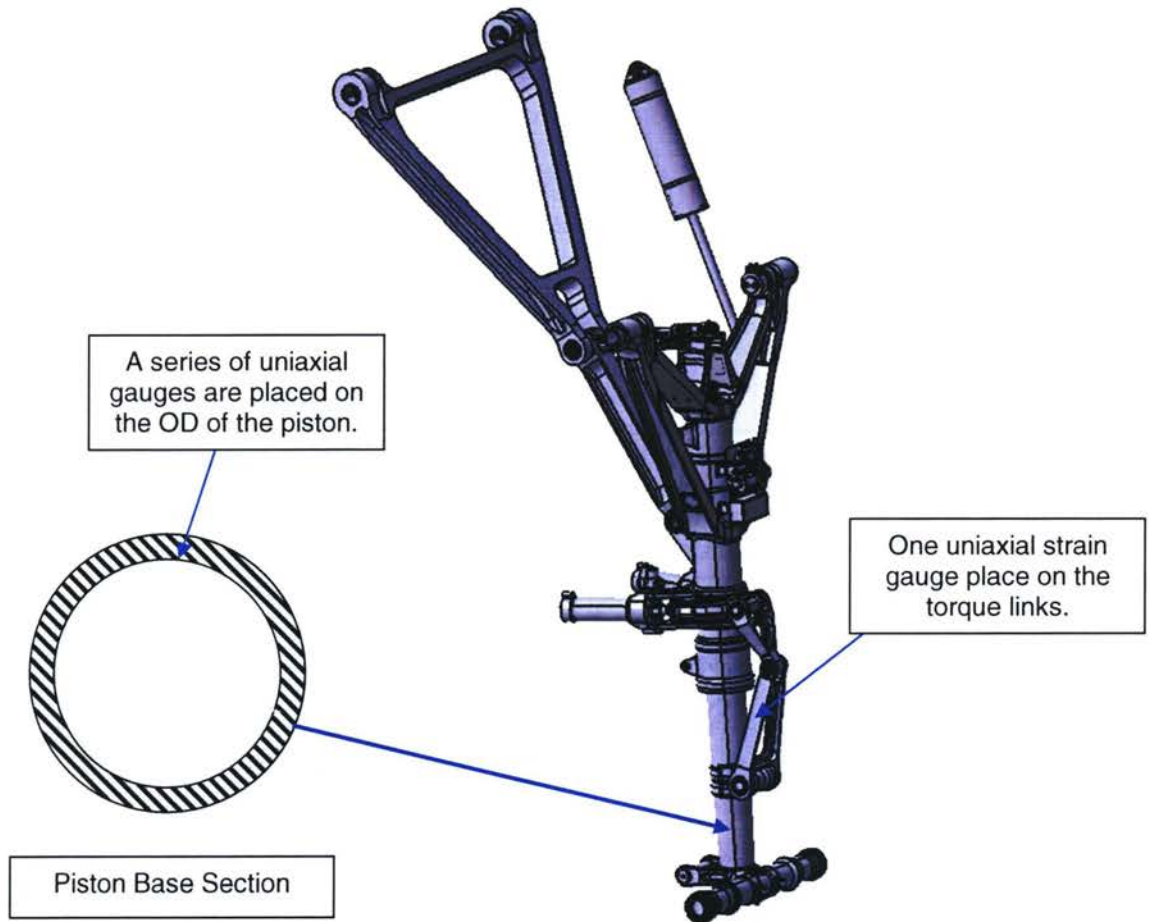


FIGURE 3-2: POST LOAD MONITORING CONFIGURATION – CANTILEVER TYPE

3.3.3 Aft Articulated – Post Loads

For aft articulated landing gear designs, a series of strain gauges can be placed at the base of the structural post and on the shock strut to measure the applied post loads. At this time, GLG does not intend to develop a specific strain gauge configuration for this type of landing gear. As such, do not cover any type of algorithm or calibration development.

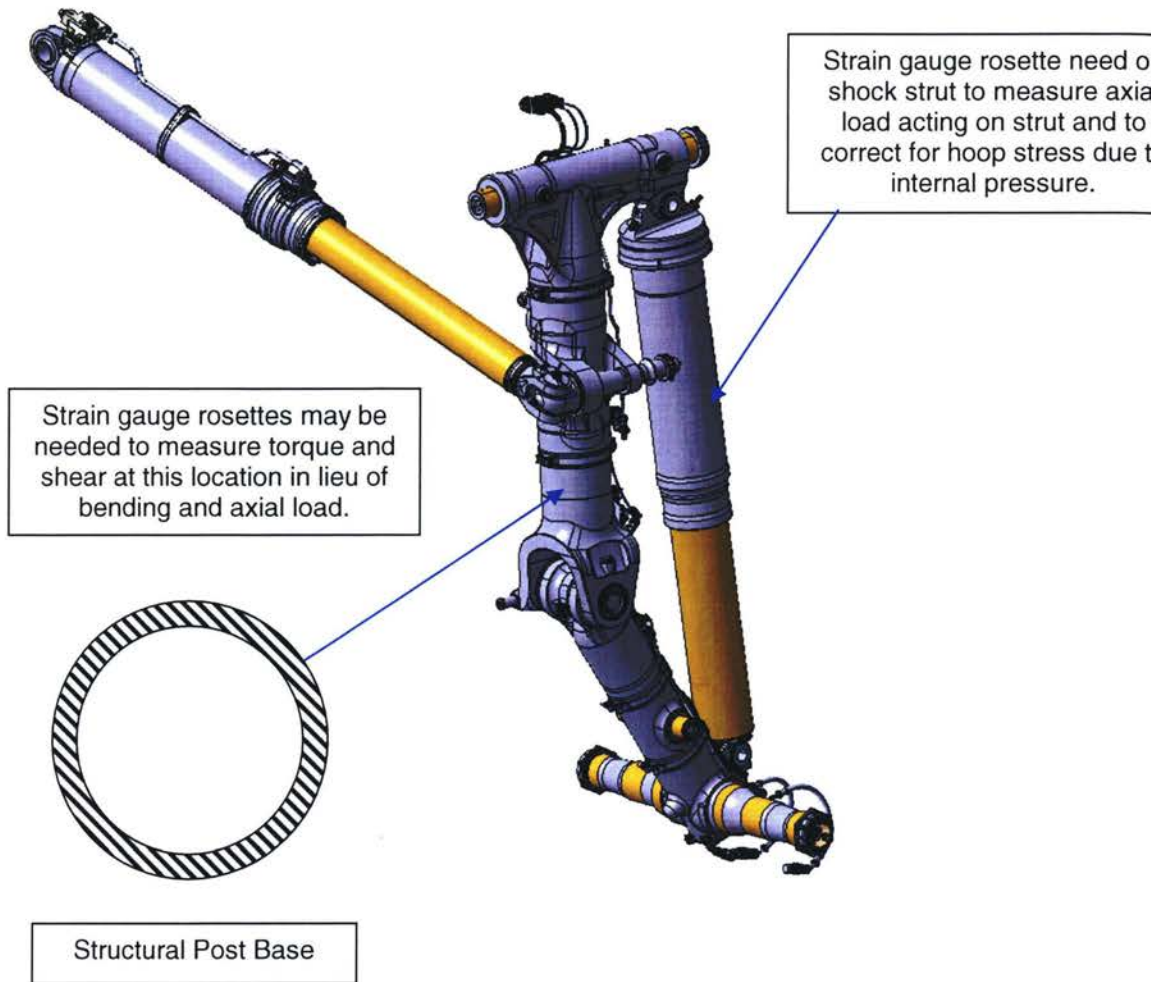


FIGURE 3-3: POST LOAD MONITORING CONFIGURATION – AFT ARTICULATED TYPE

Strain Gauge Attachment to Structure

Generally speaking, there are three ways that strain gauges can be attached to structure:

- Adhesive bonding
- Welding
- Mechanical means

All three methods each have benefits and consequences:

TABLE 3-1: PROS AND CONS OF STRAIN GAUGE ATTACHMENT METHODS

| | Adhesive | Welding | Mechanical |
|-------------|---|---|---|
| Benefit | - does not produce stress concentration - flight test programs for many aircraft have successfully used adhesives to bond strain gauges to components | - does not produce stress concentration - creates a permanent bond between the strain gauge and component | - strain gauge permanently fixed to the part without the need to bond |
| Consequence | - substrate cannot have any protective coatings in region of bond (i.e. can introduce region prone to corrosion) - bond can slowly degrade over time due to fatigue and environmental conditions | - can adversely affect the mechanical properties of the component in the region of the weld | - introduces stress concentration to part |

Chapter 4: Landing Gear Analysis Theory

4.1 Landing Gear Structural Modelling

Traditionally, landing gear structural modeling has entailed idealizing the complete structure as a series of beam and shell elements (see below):

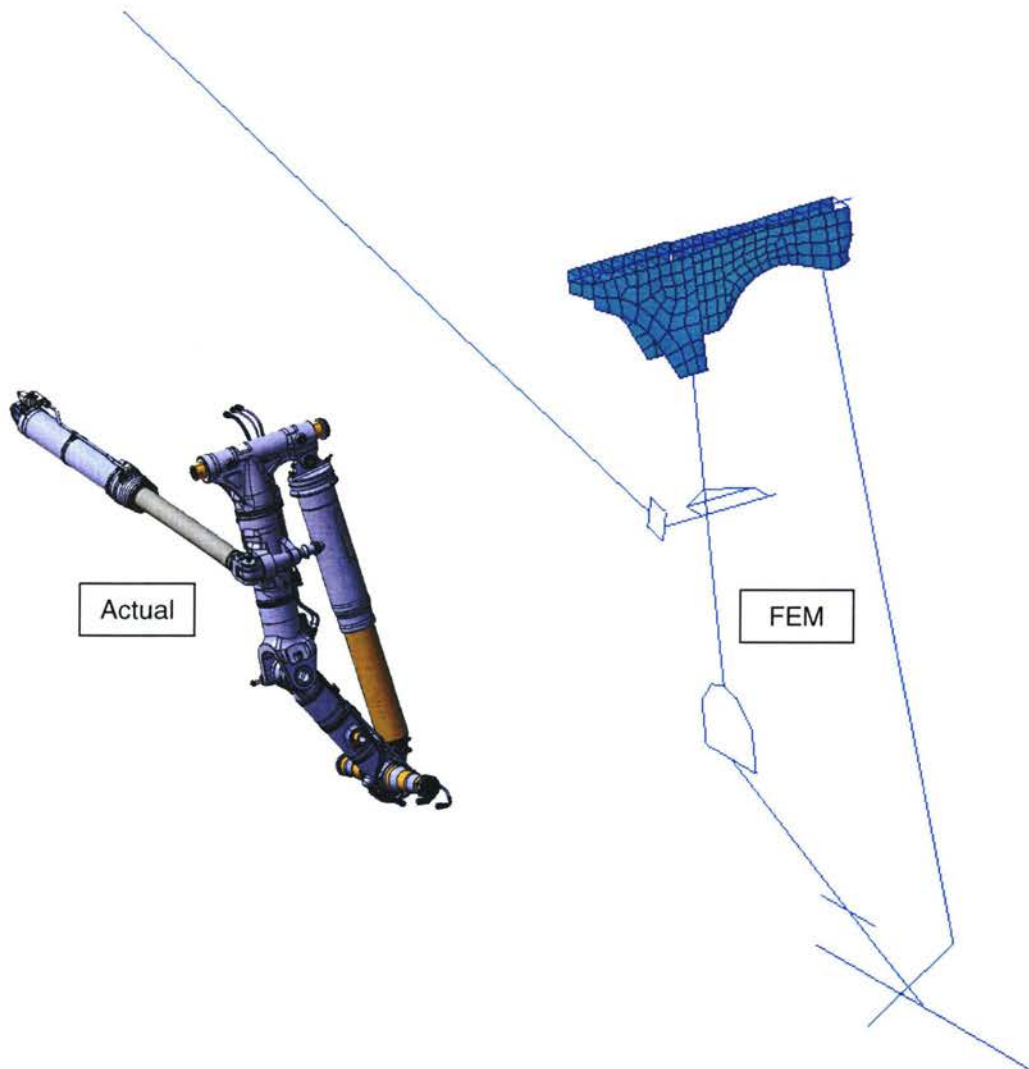


FIGURE 4-1: AN EXAMPLE OF A STRUCTURAL BEAM MODEL

Creating a beam model of the landing gear allows stress/fatigue engineers to determine the internal forces and moments acting at any given point on the landing gear. This type of model also allows the use of large displacement theory which considers secondary loading effects due to structural deflections.

The internal loads predicted by the beam model can then be used to both size and analyze the landing gear components that have been represented in the model. The process is iterative in nature – once the internal forces are used to size components, the new section properties are then applied to the beam model. Once the properties are updated, all load cases are rerun since the stiffness of the beam model has changed due to the new section properties. Typically, a beam model is updated five to ten times over the development period of a landing gear design (approximately three years).

4.2 Superposition Principle

The principle of superposition states that the deflections at any point in a structure is equal to the sum of the deflections caused by each load acting separately. This principle also applies to internal loads, stresses, strains, etc. For the principle of superposition to apply to a structure, the following assumptions are made:

- Small displacement
- Small strain
- Linear elastic material behaviour

For landing gear structures, it can be argued that, under cyclic fatigue loading conditions, the majority of the applied loads will not violate the assumptions stated above. For overload and limit load conditions, the superposition principle may not be valid. In fact, this assumption may be optimistic since the effects of secondary loading will not be taken into account using the superposition principle.

Regardless of the shortcomings of the superposition principle for overload and limit load conditions, this thesis makes use of this principle for internal loads prediction for both overload and fatigue. This assumption must be viewed as an initial indicator of overload only. Once an overload condition has been predicted, detailed engineering analysis may be required to further refine the analysis.

4.3

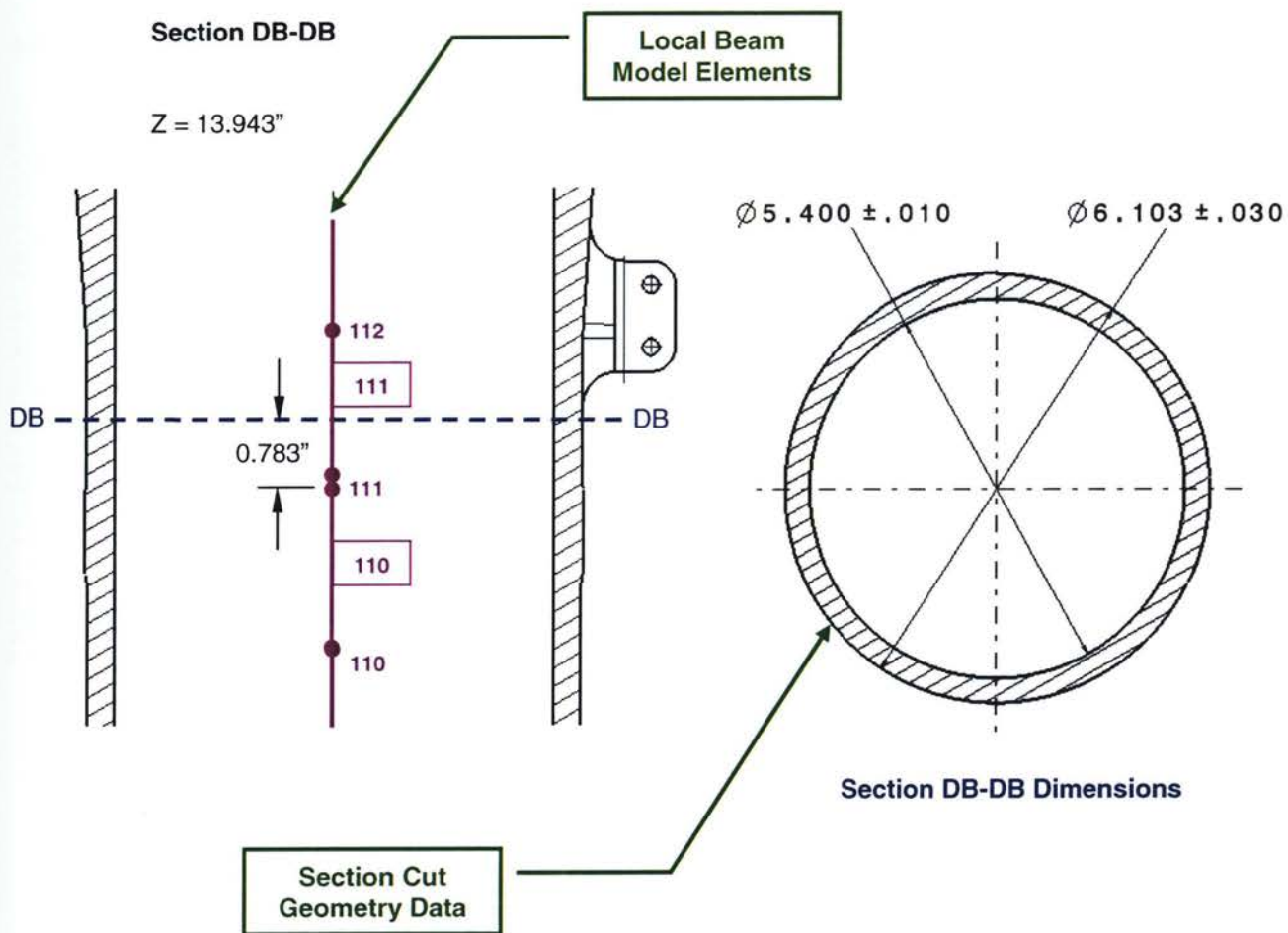
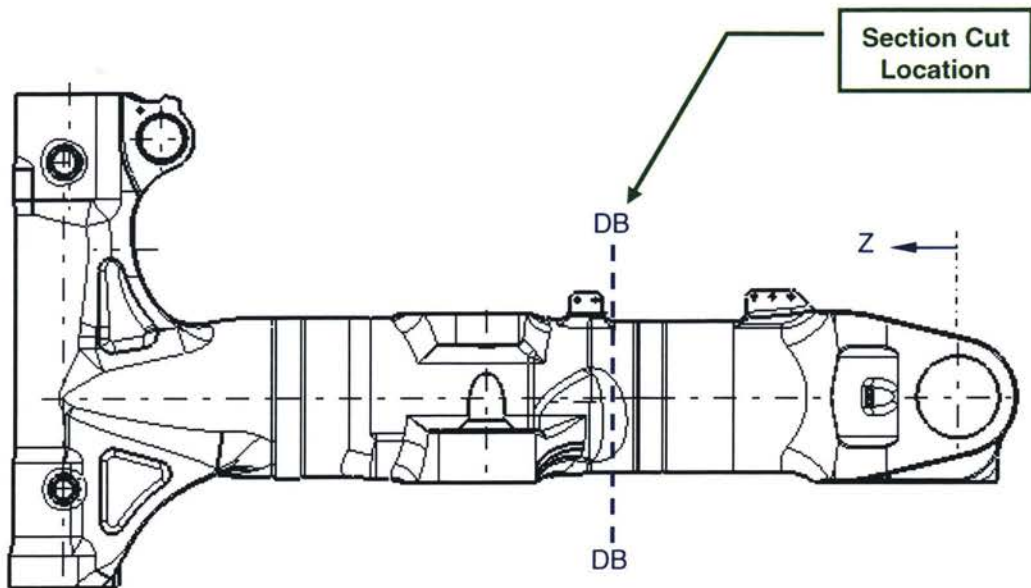
Discrete Section Analysis

Traditionally, landing gear components have been analyzed for both static strength and fatigue life based on discrete section analysis. Discrete section analysis is the process whereby an engineer cuts a cross-section at key locations on a component and completes the following steps:

1. Calculate section properties (i.e. area, moment of inertia, bending modulus, etc.)
2. Calculate the applied loads at the section (i.e. bending, shear, internal pressure, etc.).
This step is typically done by referencing the beam model internal loads.
3. Calculate the resulting stresses based on the calculations completed in step 1 and 2
4. For fatigue, calculate the equivalent uniaxial stress (Von Mises or Principal Stress)
For static strength, compare the individual stresses to the appropriate allowable (i.e. bending, shear, etc.).

Discrete section analysis is a very powerful tool to be used with the beam model finite element results for both static and fatigue analysis. It is relatively quick to complete and it also provides insight to the engineer as to what types of load are driving the stress levels at the discrete section.

An example discrete section analysis is provided on the following pages. The analysis output is based on a GLG proprietary software named 'Stress Tools.'



PART: Structural Post P/N C1M5300LA001
CASE: 2011
SECTION: DB-DB 13.943in from Pivot CL

MATERIAL ALLOWABLES FOR 300M STL HT 280-300 KSI PER AR-MMPDS-01 page 2-239

| | | | | |
|---------|---|----------|-----|---|
| FTU | = | 280. | ksi | - Ultimate tension strength |
| FCU | = | 280. | ksi | - Ultimate compression strength |
| FTY | = | 230. | ksi | - Yield tension strength |
| FCY | = | 230. | ksi | - Yield compression strength |
| FSU | = | 168. | ksi | - Ultimate shear strength |
| FST | = | 168. | ksi | - Ultimate torsion strength |
| FTP | = | 201. | ksi | - Tensile proportional limit stress |
| FSL | = | 138. | ksi | - Yield shear strength |
| FSTY | = | 138. | ksi | - Yield torsion strength |
| POISSON | = | 0.32 | | - Poisson ratio |
| eu | = | 0.07 | | - Ultimate plastic strain |
| nt | = | 17.31952 | | - Ultimate range shape factor |
| E | = | 29000. | ksi | - Elastic modulus |
| G | = | 11000. | ksi | - Modulus of rigidity |
| FOU | = | 247. | ksi | - Ultimate intercept stress in Cozzzone trapezoidal stress distribution |
| FOY | = | 71. | ksi | - Yield intercept stress in Cozzzone trapezoidal stress distribution |

APPLIED LOADS

| | | | | |
|-----------------|-----------------------------|---------------------------------------|-----------------|--|
| Ultimate | | | | |
| PSX | = | -1*FY (M111J111) | = | -84.356 kip |
| PSY | = | 1*FZ (M111J111) | = | 35.161 kip |
| Axial | = | -1*FX (M111J111) | = | 0.688 kip |
| MBX | = | -1*MY (M111J111) -0.783*FZ (M111J111) | = | -1096.995 kip.in |
| MBY | = | 1*MZ (M111J111) -0.783*FY (M111J111) | = | -1523.655 kip.in |
| Torque | = | 1*MX (M111J111) | = | 1545.668 kip.in |
| FORCE FILE: | GVI_MLG_M7L1.2U_COMBINE.DIR | | | Internal Loads within Beam Model |
| Limit | | | | |
| PSX | = | PSX_ult/1 = | -52.516 kip | |
| PSY | = | PSY_ult/1 = | 19.663 kip | |
| Axial | = | Axial_ult/1 = | 0.825 kip | |
| MBX | = | MBX_ult/1 = | -685.352 kip.in | |
| MBY | = | MBY_ult/1 = | -974.865 kip.in | |
| Torque | = | Torque_ult/1 = | 970.711 kip.in | |
| FORCE FILE: | GVI_MLG_M7L1.2L_COMBINE.DIR | | | |

DIMENSIONS OF TUBE SECTION

| | | |
|----------------------|---|----------|
| OD _{NOM} | = | 6.103 in |
| ID _{NOM} | = | 5.400 in |
| OD _{REW} | = | 0.000 in |
| ID _{REW} | = | 0.000 in |
| OD _{OTHER} | = | 0.030 in |
| ID _{OTHER} | = | 0.010 in |
| OD | = | 6.073 in |
| ID | = | 5.410 in |
| L _{BEARING} | = | 1.000 in |
| ecc _x | = | 0.000 in |
| ecc _y | = | 0.000 in |

PART: Structural Post P/N C1M5300LA001
CASE: 2011
SECTION: DB-DB 13.943in from Pivot CL

SECTION PROPERTIES

**Geometric
Properties**

AREA = 5.97942 in² - area of cross section
XBAR = 0.00000 in - x coordinate of centroid
YBAR = 1.82961 in - y coordinate of centroid
QXX = 5.46999 in³ - semi-area static moment for x-axis
QYY = 5.470 in³ - semi-area static moment for y-axis
IXX = 24.721 in⁴ - moment of inertia for x-axis
IYY = 24.721 in⁴ - moment of inertia for y-axis
ZX1 = 8.141 in³ - resisting moment of section for max y
ZX2 = 8.141 in³ - resisting moment of section for min y
ZY1 = 8.141 in³ - resisting moment of section for max x
ZY2 = 8.141 in³ - resisting moment of section for min x
D/T = 18.320 - ratio of outer diameter and tube thickness
KX1 = 1.344 - (2*QXX/ZX1)
KX2 = 1.344 - (2*QXX/ZX2)
KY1 = 1.344 - (2*QYY/ZY1)
KY2 = 1.344 - (2*QYY/ZY2)
Kshrx = 1.996 - max shear coefficient for x-axis
Kshry = 1.996 - max shear coefficient for y-axis
RHOXX = 2.033 in - radius of gyration for x-axis
RHOYY = 2.033 in - radius of gyration for y-axis
TX = 0.663 in - thickness of tube in y-axis
TY = 0.663 in - thickness of tube in x-axis
TORZ = 16.283 in³ - torsional static moment of section

Allowable Bending Moments

| X - axis | | Y - axis | |
|--------------------------------|------------------------|--------------------------------|------------------------|
| C1 | = 3.037 in | C3 | = 3.037 in |
| Q1x | = 5.5 in ³ | Q1y | = 5.5 in ³ |
| I1x | = 24.7 in ⁴ | I1y | = 24.7 in ⁴ |
| Z1x = I1x/C1 | = 8.1 in ³ | Z1y = I1y/C3 | = 8.1 in ³ |
| Kb1x = 2*Q1x/Z1x | = 1.34380 | Kb1y = 2*Q1y/Z1y | = 1.34380 |
| C2 | = 3.036 in | C4 | = 3.036 in |
| Q2x | = 5.5 in ³ | Q2y | = 5.5 in ³ |
| I2x | = 24.7 in ⁴ | I2y | = 24.7 in ⁴ |
| Z2x = I2x/C2 | = 8.1 in ³ | Z2y = I2y/C4 | = 8.1 in ³ |
| Kb2x = 2*Q2x/Z2x | = 1.34380 | Kb2y = 2*Q2y/Z2y | = 1.34380 |
| Ultimate | | Ultimate | |
| Strain1 | = 0.070 | Strain3 | = 0.070 |
| FBU1 = FBU(D/T) | = 343.8 ksi | FBU3 = FBU(D/T) | = 343.8 ksi |
| Mrx1 = FBU1*Z1x | = 2798.9 kip.in | Mry1 = FBU3*Z1y | = 2798.9 kip.in |
| Strain2 | = 0.070 | Strain4 | = 0.070 |
| FBU2 = FBU(D/T) | = 343.8 ksi | FBU4 = FBU(D/T) | = 343.8 ksi |
| Mrx2 = FBU2*Z2x | = 2798.9 kip.in | Mry2 = FBU4*Z2y | = 2798.9 kip.in |
| Mallx = 0.5*(Mrx1+Mrx2) | = 2798.9 kip.in | Mally = 0.5*(Mry1+Mry2) | = 2798.9 kip.in |
| Limit | | Limit | |
| Strain1_1 | = 0.010 | Strain3_1 | = 0.010 |
| Stress1_1 | = 230.0 ksi | Stress3_1 | = 230.0 ksi |
| FOY1 | = 71.0 ksi | FOY3 | = 71.0 ksi |
| FBY1 = Stress1_1+FOY1*(Kb1x-1) | = 254.4 ksi | FBY3 = Stress3_1+FOY3*(Kb1y-1) | = 254.4 ksi |
| Mrx1_1 = FBY1*Z1x | = 2071.3 kip.in | Mry1_1 = FBY3*Z1y | = 2071.3 kip.in |
| Strain2_1 | = 0.010 | Strain4_1 | = 0.010 |
| Stress2_1 | = 230.0 ksi | Stress4_1 | = 230.0 ksi |
| FOY2 | = 71.0 ksi | FOY4 | = 71.0 ksi |
| FBY2 = Stress2_1+FOY2*(Kb2x-1) | = 254.4 ksi | FBY4 = Stress4_1+FOY4*(Kb2y-1) | = 254.4 ksi |
| Mrx2_1 = FBY2*Z2x | = 2071.3 kip.in | Mry2_1 = FBY4*Z2y | = 2071.3 kip.in |
| Mallx_1 = 0.5*(Mrx1_1+Mrx2_1) | = 2071.3 kip.in | Mally_1 = 0.5*(Mry1_1+Mry2_1) | = 2071.3 kip.in |

**Bending Allowables (see
section Error! Reference**

PART: Structural Post P/N C1M5300LA001
CASE: 2011
SECTION: DB-DB 13.943in from Pivot CL

Tension Limit Stress

$$FT = \frac{PTU}{AREA} = 0.138 \text{ ksi}$$

$$RT = \frac{FT}{FTY} = 0.001$$

Yielding Check

Bending Limit Stress

$$RBX = \frac{MBX}{Mall_{XLIMIT}} = -0.331$$

$$RBY = \frac{MBY}{Mall_{YLIMIT}} = -0.471$$

$$RB = \sqrt{RBX^2 + RBY^2} = 0.575$$

Average Shear Limit Stress

$$FSX = \frac{PSX}{AREA} = 8.783 \text{ ksi}$$

$$FSY = \frac{PSY}{AREA} = 3.288 \text{ ksi}$$

$$RSX = \frac{FSX}{FSL} = 0.064$$

$$RSY = \frac{FSY}{FSL} = 0.024$$

$$RS = \sqrt{RSX^2 + RSY^2} = 0.068$$

Max Shear Limit Stress

$$FSX_{MAX} = \frac{PSX * QYY}{TX * IYY} = 17.527 \text{ ksi}$$

$$FSY_{MAX} = \frac{PSY * QXX}{TY * IXX} = 6.562 \text{ ksi}$$

$$RSX_{MAX} = \frac{FSX_{MAX}}{FSL} = 0.127$$

$$RSY_{MAX} = \frac{FSY_{MAX}}{FSL} = 0.048$$

$$RS_{MAX} = \sqrt{RSX_{MAX}^2 + RSY_{MAX}^2} = 0.136$$

Torsion Limit Stress

$$FS_{TORQUE} = \frac{TORQUE}{TORSION} = 59.617 \text{ ksi}$$

$$RST = \frac{FS_{TORQUE}}{FSTY} = 0.432$$

Utilization Factors

$$U1 = \sqrt{(RT + RB)^2 + (RS + RST)^2} = 0.763$$

$$U2 = \sqrt{(RT - RB)^2 + (RS + RST)^2} = 0.762$$

$$U3 = \sqrt{RT^2 + (RS_{MAX} + RST)^2} = 0.568$$

Limit Margin of safety

| Case | MS |
|------|-------|
| 2021 | 0.314 |
| 2012 | 0.422 |
| 2022 | 0.425 |
| 2015 | 0.563 |
| 2025 | 0.579 |

M.S. = 1/MaxU - 1 = 0.311

Analysis Software: Stress Tools V.1 R.11

PART: Structural Post P/N C1M5300LA001
CASE: 2011
SECTION: DB-DB 13.943in from Pivot CL

Tension Stress

$$FT = \frac{FTU}{AREA} = 0.115 \text{ ksi}$$

$$RT = \frac{FT}{FTU} = 0.000$$

Bending Stress

$$RBX = \frac{MBX}{Mall_x} = -0.392$$

$$RBY = \frac{MBY}{Mall_y} = -0.544$$

$$RB = \sqrt{RBX^2 + RBY^2} = 0.671$$

Ultimate/Rupture
Check

Average Shear Stress

$$FSX = \frac{PSX}{AREA} = 14.108 \text{ ksi}$$

$$FSY = \frac{PSY}{AREA} = 5.880 \text{ ksi}$$

$$RSX = \frac{FSX}{FSU} = 0.084$$

$$RSY = \frac{FSY}{FSU} = 0.035$$

$$RS = \sqrt{RSX^2 + RSY^2} = 0.091$$

Max Shear Stress

$$FSX_{MAX} = \frac{PSX * QYY}{TX * IYY} = 28.153 \text{ ksi}$$

$$FSY_{MAX} = \frac{PSY * QXX}{TY * IXX} = 11.735 \text{ ksi}$$

$$RSX_{MAX} = \frac{FSX_{MAX}}{FSU} = 0.168$$

$$RSY_{MAX} = \frac{FSY_{MAX}}{FSU} = 0.070$$

$$RS_{MAX} = \sqrt{RSX_{MAX}^2 + RSY_{MAX}^2} = 0.182$$

Torsion Stress

$$FS_{TORQUE} = \frac{TORQUE}{TORSION} = 94.928 \text{ ksi}$$

$$RST = \frac{FS_{TORQUE}}{FST} = 0.565$$

Utilization Factors

$$U1 = \sqrt{(RT + RB)^2 + (RS + RST)^2} = 0.939$$

$$U2 = \sqrt{(RT - RB)^2 + (RS + RST)^2} = 0.938$$

$$U3 = \sqrt{RT^2 + (RS_{MAX} + RST)^2} = 0.747$$

Ultimate Margin of safety

M.S. = 1/MaxU - 1 = 0.065

| Case | MS |
|------|-------|
| 2021 | 0.068 |
| 2012 | 0.137 |
| 2022 | 0.140 |
| 2015 | 0.357 |
| 2025 | 0.371 |

Analysis Software: Stress Tools V.1 R.11

4.4

Finite Element Analysis

As both finite element software and computer hardware develops, finite element analysis is becoming more dominant as an analysis tool for engineers designing and analyzing landing gear. The following types of finite element analysis are utilized in landing gear structural analysis:

- Linear Elastic (for static and fatigue)
- Nonlinear Elasto-Plastic
- Nonlinear Buckling/Collapse

Examples of landing gear finite element analysis are provided below:

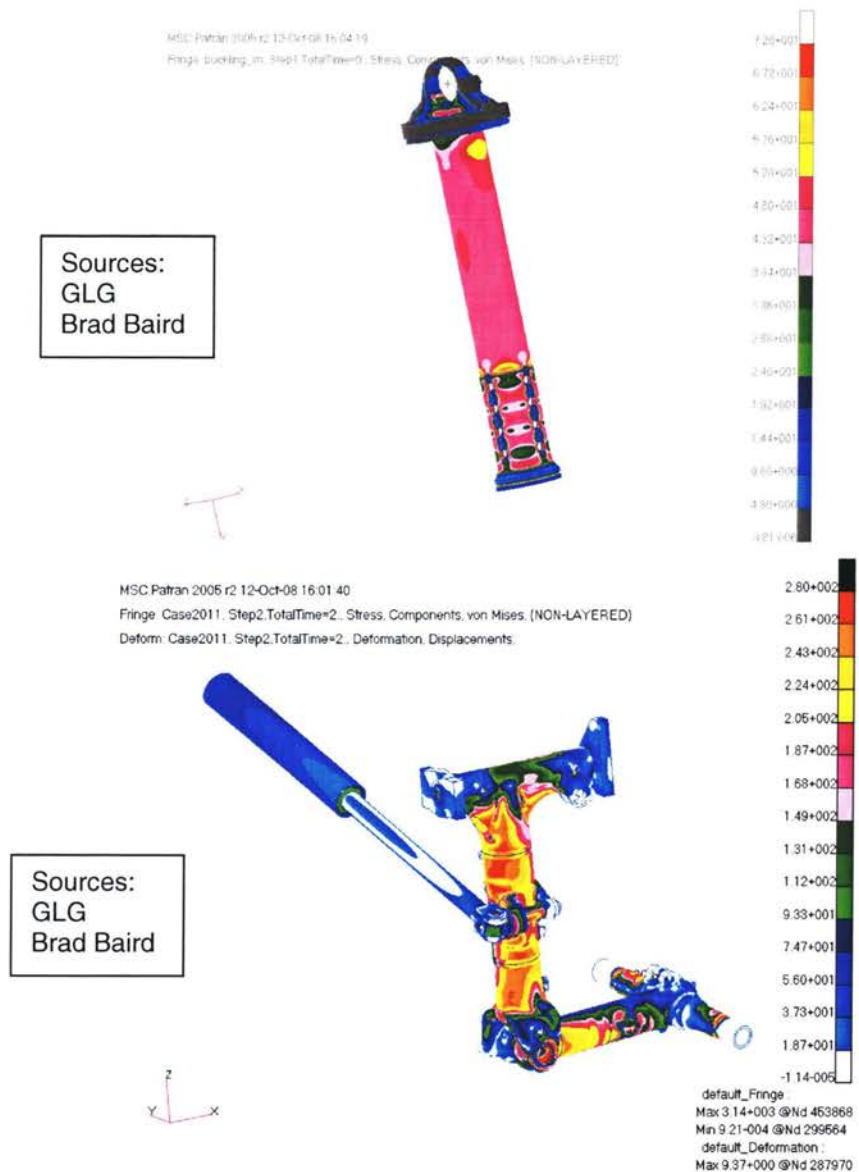


FIGURE 4-2: EXAMPLES OF LANDING GEAR FINITE ELEMENT ANALYSIS

Chapter 5: Static Analysis – Overload Detection

Overload detection can be categorized into two classes:

- Component yielding
- Component failure (i.e. rupture)

For both cases, traditional equations are utilized to predict yield and/or rupture. For the scenario where a component ruptures, visual inspections by maintenance crews will indicate that a component has failed. As a result, the analysis presented in this thesis will focus entirely on predicting the onset of yield in individual components.

5.1 Yielding Criteria

For ductile metals, the Von Mises criterion is typically utilized to predict yielding in a component. This criterion is also known as the Maximum Distortion Energy Criterion. According to this criterion, a given structural component is safe as long as the maximum value of the distortion energy per unit volume in that material remains smaller than the distortion energy per unit volume required to cause yielding in a tensile-test specimen of the same material. The Von Mises equation for a 3D stress state is given below:

$$\sigma_{vm} = \frac{1}{\sqrt{2}} \sqrt{(\sigma_x - \sigma_y)^2 + (\sigma_y - \sigma_z)^2 + (\sigma_x - \sigma_z)^2 + 6(\tau_{xy}^2 + \tau_{yz}^2 + \tau_{xz}^2)} \quad (5.1.1)$$

For a 2D stress state, the Von Mises stress is simplified to the following:

$$\sigma_{vm} = \sqrt{\sigma_x^2 + \sigma_y^2 - \sigma_x \sigma_y + 3\tau_{xy}^2} \quad (5.1.2)$$

In general, if yield checks are completed for finite element results, the stress state will be 3D since the majority of landing gear components are analyzed as 3D solids. On the other hand, traditional discrete section cut analysis is in 2D which allows the use of the simplified Von Mises formula for a 2D stress state. Refer to reference 144, pages 368 to 369 for further details.

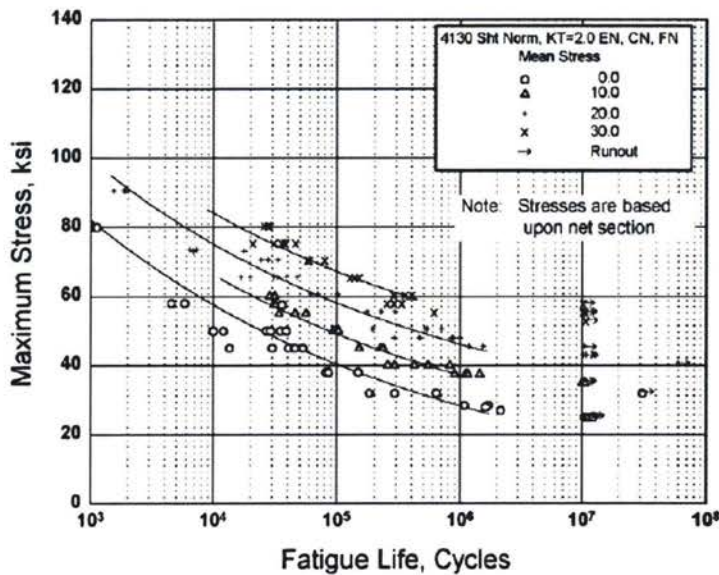


Figure 2.3.1.2.8(c). Best-fit S/N curves for notched, $K_t = 2.0$, AISI 4130 alloy steel sheet, normalized, longitudinal direction.

Correlative Information for Figure 2.3.1.2.8(c)

Product Form: Sheet, 0.075 inch thick

Test Parameters:

Properties:

| TUS, ksi | TYS, ksi | Temp., °F |
|----------|----------|-------------|
| 117 | 99 | RT |
| | | (unnotched) |
| 120 | -- | RT |
| | | (notched) |
| | | K_t 2.0 |

Loading - Axial
 Frequency - 1100-1800 cpm
 Temperature - RT
 Environment - Air

No. of Heats/Lots: Not specified

Specimen Details: Notched, $K_t = 2.0$

| Notch Type | Gross Width | Net Width | Notch Radius |
|------------|-------------|-----------|--------------|
| Edge | 2.25 | 1.500 | 0.3175 |
| Center | 4.50 | 1.500 | 1.500 |
| Fillet | 2.25 | 1.500 | 0.1736 |

Equivalent Stress Equation:
 $\log N_f = 17.1 - 6.49 \log (S_{eq})$
 $S_{eq} = S_{max} (1-R)^{0.86}$
 Std. Error of Estimate, Log (Life) = 0.19
 Standard Deviation, Log (Life) = 0.78
 $R^2 = 94\%$

FIGURE 6-1: SAMPLE S-N CURVE

From the figure above, the following equations are used to calculate the allowable fatigue cycles for a given stress pair:

$$S_{eq} = S_{max} (1 - R)^{0.86} \quad \text{Equivalent Stress} \quad (6.1.4)$$

$$\log N_f = 17.1 - 6.49 \log (S_{eq}) \quad \text{Log Life} \quad (6.1.5)$$

6.2 Strain-Life Theory (E-N)

Strain-Life fatigue is much more robust for predicting fatigue life of components that undergo plasticity during their service life. Currently, the majority of landing gear components use strain-life theory since these components are typically exposed to both HCF and low cycle fatigue (LCF).

6.2.1 Monotonic Stress-Strain Relationship

In general, strain (ϵ) can be separated into its elastic (ϵ_e) and plastic (ϵ_p) components via the following equations:

$$\epsilon = \epsilon_e + \epsilon_p \quad (6.2.1) \quad \epsilon_e = \frac{\sigma}{E} \quad (6.2.2) \quad \epsilon_p = \left(\frac{\sigma}{K} \right)^{1/n} \quad (6.2.3)$$

Where

σ = stress

E = Young's Modulus

K = strength coefficient

n = strain hardening exponent

The monotonic strain-stress relationship can now be written in the following form:

$$\epsilon = \frac{\sigma}{E} + \left(\frac{\sigma}{K} \right)^{1/n} \quad (6.2.4)$$

This equation is often referred to as the Ramberg-Osgood equation.

6.2.2 Cyclic Stress-Strain Relationship

Cyclic stress-strain curves are fundamental to the use of strain-life fatigue theory for determining the durability of structures under cyclic loading. The response of a material subjected to inelastic loading is in the form of a hysteresis loop (shown on the following page).

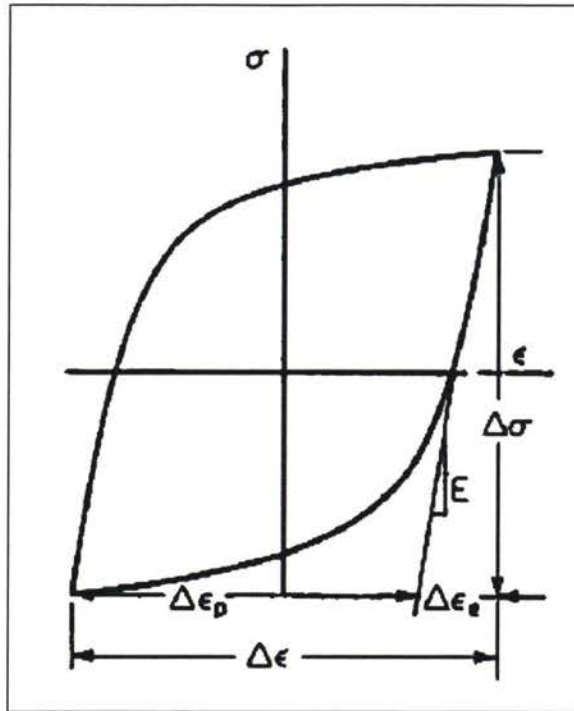


FIGURE 6-2: HYSTERESIS LOOP FOR CYCLIC LOADING

The total width of the loop is $\Delta\epsilon$ (i.e. total strain range) and the total height is $\Delta\sigma$ (i.e. total stress range). These values can be stated in terms of amplitude:

$$\epsilon_a = \frac{\Delta\epsilon}{2} \quad (6.2.5)$$

$$\sigma_a = \frac{\Delta\sigma}{2} \quad (6.2.6)$$

The total strain strain change is a sum of the elastic and plastic components:

$$\Delta\epsilon = \Delta\epsilon_e + \Delta\epsilon_p \quad (6.2.7)$$

In terms of amplitude,

$$\frac{\Delta\epsilon}{2} = \frac{\Delta\epsilon_e}{2} + \frac{\Delta\epsilon_p}{2} \quad (6.2.8)$$

Using Hooke's Law, the elastic term may be replaced by $\Delta\sigma / E$.

$$\frac{\Delta\epsilon}{2} = \frac{\Delta\sigma}{2E} + \frac{\Delta\epsilon_p}{2} \quad (6.2.9)$$

When dealing with cyclical stress-strain histories, the Ramberg-Osgood equation can be modified as follows:

$$\varepsilon = \frac{\sigma}{E} + \left(\frac{\sigma}{K'} \right)^{1/n'} \quad (6.2.10)$$

Where

K' = cyclic strength coefficient

n' = cyclic strain hardening exponent

Based on this equation, the strain-range equation can now be modified as follows:

$$\frac{\Delta\varepsilon}{2} = \frac{\Delta\sigma}{2E} + \left(\frac{\Delta\sigma}{2K'} \right)^{1/n'} \quad (6.2.11)$$

Multiplying both sides by 2 simplifies the equation:

$$\Delta\varepsilon = \frac{\Delta\sigma}{E} + 2 \left(\frac{\Delta\sigma}{2K'} \right)^{1/n'} \quad (6.2.12)$$

The equation above is considered the cyclic stress-strain curve.

6.2.3 Strain-Life Equation Derivation

Basquin was the first to observe that S-N data could be plotted linearly on a log-log scale. Using the stress amplitude, the plot may be linearized by

$$\frac{\Delta\sigma}{2} = \sigma'_f (2N_f)^b \quad (6.2.13)$$

where

$2N_f$ = reversals to failure

σ'_f = fatigue strength coefficient

b = fatigue strength exponent (Basquin's exponent)

Both Coffin and Manson found that plastic strain-life ($\epsilon_p - N$) data could be linearized on log-log coordinates. Plastic strain can be related as a power law function:

$$\frac{\Delta \epsilon_p}{2} = \epsilon'_f (2N_f)^c \quad (6.2.14)$$

where

- $2N_f =$ reversals to failure
- $\epsilon'_f =$ fatigue ductility coefficient
- $c =$ fatigue ductility exponent

Based on equations 6.2.13, 6.2.14, and 6.2.8, the strain-life equation can be written as follows:

$$\frac{\Delta \epsilon}{2} = \frac{\sigma'_f}{E} (2N_f)^b + \epsilon'_f (2N_f)^c \quad (6.2.15)$$

This equation is shown graphically in the figure below:

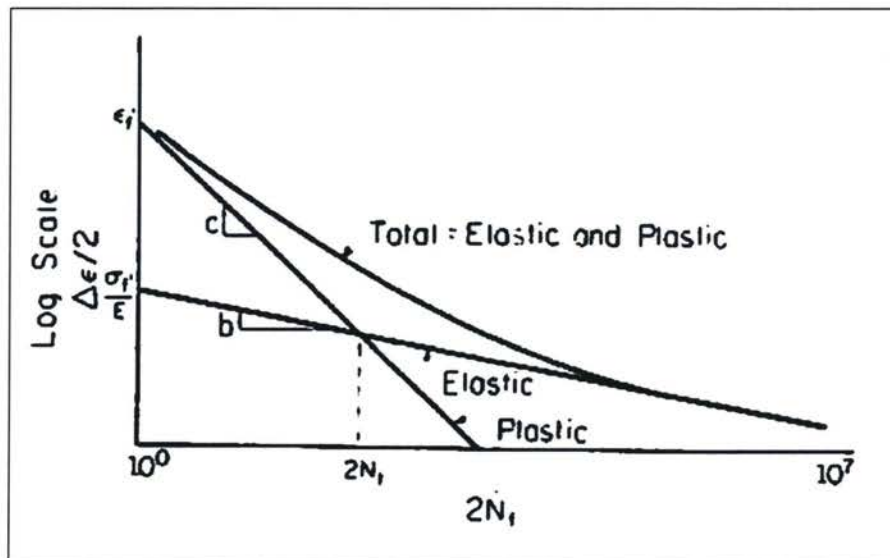


FIGURE 6-3: STRAIN-LIFE CURVE

6.2.4 Strain-Life Equation – Mean Stress Correction

The strain-life equation derived in the previous section does not take into account the effects of mean stress on the fatigue life of a component. Generally speaking, a tensile mean stress will tend to decrease the fatigue life and a compressive mean stress will tend to increase the fatigue life.

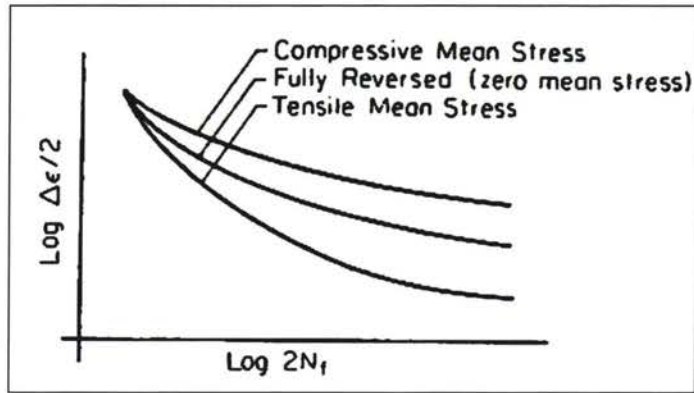


FIGURE 6-4: EFFECT OF MEAN STRESS ON STRAIN-LIFE CURVE

There are two mean stress correction techniques that are used extensively in practice:

- Morrow
- Smith-Watson-Topper (SWT)

Typically, the Morrow is used when the dominant mean stress within a stress history is compressive in nature. The E-N equation is modified as follows for the Morrow correction:

$$\frac{\Delta \epsilon}{2} = \frac{\sigma'_f - \sigma_o}{E} (2N_f)^b + \epsilon'_f (2N_f)^c \quad (6.2.16)$$

where

σ_o = mean stress

The SWT correction is used when the dominant mean stress in within a stress history is tensile in nature. The E-N equation is modified as follows for the SWT correction:

$$\sigma_{\max} \frac{\Delta \epsilon}{2} = \frac{(\sigma'_f)^2}{E} (2N_f)^{2b} + \sigma'_f \epsilon'_f (2N_f)^{b+c} \quad (6.2.17)$$

Notch Correction

For E-N analysis, Neuber's rule is typically used to correct for notches or other geometric features that cause stress concentrations (K_t). Neuber's rule states that the theoretical stress concentration is the geometric mean stress and strain concentration of the square root of the product K_σ and K_ϵ .

The equations for Neuber's rule are:

$$K_t = \sqrt{K_\sigma K_\epsilon} \quad (6.3.1)$$

$$K_t^2 = \frac{\sigma}{S} \frac{\epsilon}{e} \quad (6.3.2)$$

$$K_t^2 S e = \sigma \epsilon \quad (6.3.3)$$

where

S = nominal stress

e = nominal strain

σ = notch stress

ϵ = notch strain

The nominal stress and strain can be related using Hooke's Law to simplify the equation as follows:

$$K_t^2 = \frac{\sigma}{S} \frac{\epsilon E}{S} \quad (6.3.4)$$

$$\frac{(K_t S)^2}{E} = \sigma \epsilon$$

The monotonic stress-strain equation can now be substituted into the Neuber correction:

$$\frac{(K_t S)^2}{E} = \sigma \left[\frac{\sigma}{E} + \left(\frac{\sigma}{K'} \right)^{1/n'} \right] \quad (6.3.5)$$

In the same manner, the cyclic stress-strain curve can be substituted into the Neuber correction:

$$\frac{(K_t \Delta S)^2}{2E} = \frac{\Delta \sigma^2}{2E} + \Delta \sigma \left(\frac{\sigma}{2K'} \right)^{1/n'} \quad (6.3.6)$$

Therefore, for components that are analyzed with stress concentrations, Neuber rule is used to predict the actual stress levels at the concentration, not the linear-elastic prediction based on $K_t S$.

Random Loading History

In general, landing gear components are subjected to random loading histories. As a result, a method must be used to determine the appropriate stress pairs. At the present, it is standard industry practice to use the rainflow method.

The rainflow method attempts to identify closed hysteresis loops in the stress-strain response of a material subjected to cyclic loading. The first step in rainflow counting is to draw the stress-strain history so that the time axis is vertical with increasing time downward. The strain history is then imagined as a series of "pagoda roofs." Cycles are then identified by the manner in which rain is allowed to drip or fall down the roofs. A number of rules have been established to identify closed hysteresis loops and are provided below:

1. To eliminate the counting of half cycles, the strain-time history is drawn so as to begin and end at the strain value of greatest magnitude.
2. A flow of rain is begun at each strain reversal in the history and is allowed to continue to flow unless;
 - a. The rain began at a local maximum point (peak) and falls opposite a local maximum point greater than that from which it came.
 - b. The rain began at a local minimum point (valley) and falls opposite a local minimum point greater (in magnitude) than that from which it came.
 - c. It encounters a previous rainflow.

A sample rainflow count example is provided below along with the resulting hysteresis loop:

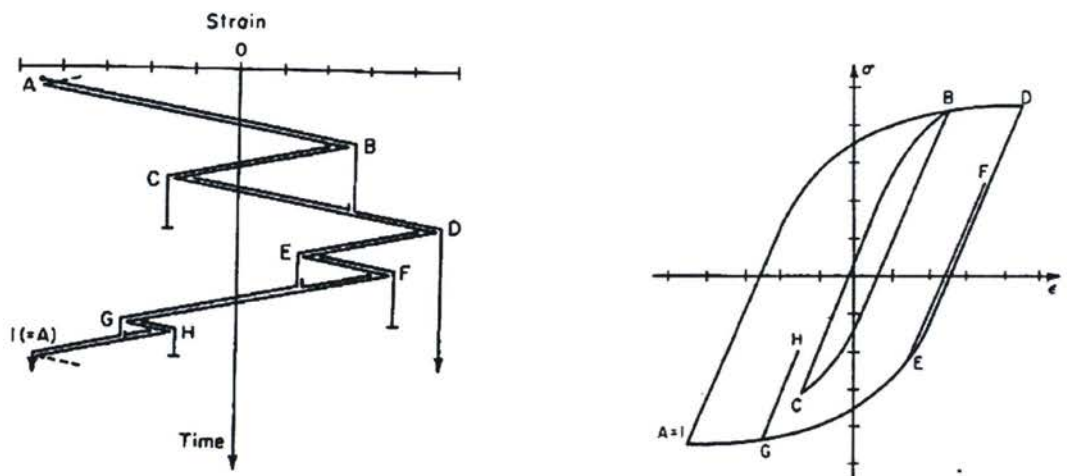


FIGURE 6-5: SAMPLE RAINFLOW COUNTING EXAMPLE AND RESULTING HYSTERESIS LOOP

6.5

Miner's Rule

The damage fraction, D , is defined as the fraction of life used up by an event or series of events. Miner's Rule states that, when the summation of damages reaches a value of 1.0, the component has used up its life and crack initiation will begin.

In mathematical terms, Miner's Rule can be equated as follows:

$$\sum D \geq 1 \quad (6.5.1)$$

In the aerospace industry, Miner's rule is used extensively to predict the onset of crack initiation. All fatigue damage/life predictions provided by the software presented in section 8.5 is based on Miner's rule.

Chapter 7: Load Prediction Algorithm Development

Load prediction algorithms have been developed for two potential load monitoring locations:

- Axle Root
- Post

7.1 Axle Equations

This section outlines the governing equations for predicting ground loads acting on landing gear by placing uniaxial strain gauges on the landing gear axles.

In order to predict the ground loads acting on a landing gear, the ideal strain gauge installation locations are at the axles. The axle root is the theoretically most ideal location for strain gauge placement because it is directly adjacent to the load application point (i.e. the wheel and tire).

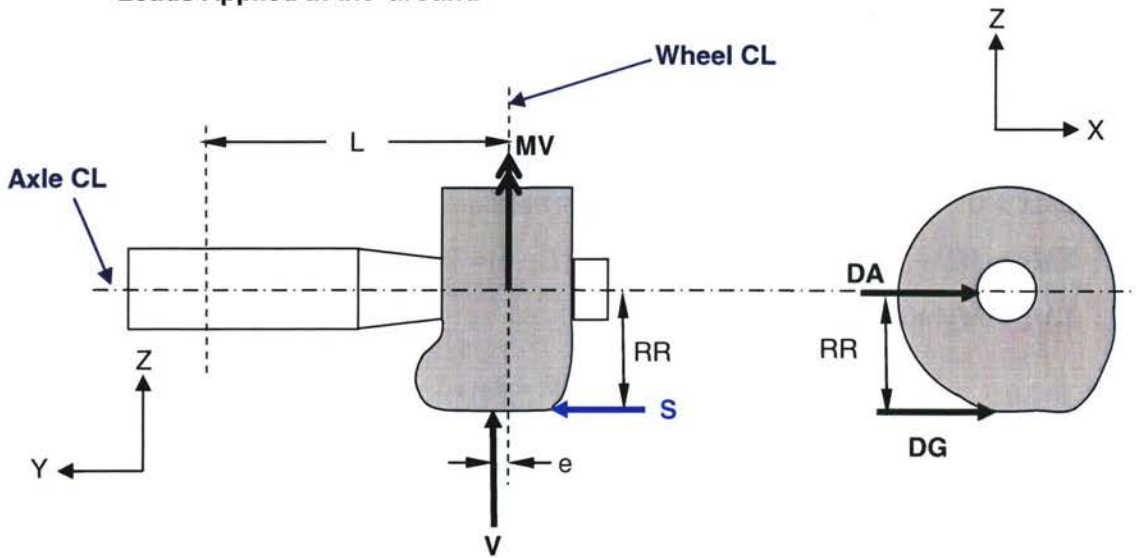
The strain gauges must be placed on the interior surface of the axles in order to protect the gauges from runway debris and harsh environments. Landing gear axles are exposed to four main types of stress:

- Bending
- Axial
- Shear
- Hoop

The bending, axial, and shear stresses are a direct result of the loads being applied to the landing gear via the landing gear tires. The hoop stresses acting on an axle are due to the contact between the wheel bearing and the axle and the mating part with the axle (typically a piston or bogie beam). This contact produces a compressive hoop pressure on the axle which, in turn, causes hoop stress in the axles. Any strain measurements that are taken at the axle must take this hoop stress into account in order to correctly predict the loads being applied to the landing gear.

7.1.1 Governing Equations:

Loads Applied at the Ground



Loads Applied at the Axle

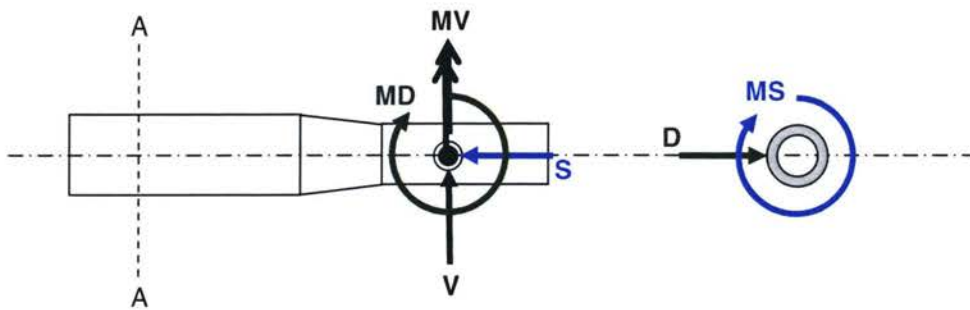


FIGURE 7-1: APPLIED LOADS AT WHEEL CENTRELINE

where

- | | | |
|-------------------------|--|---------|
| $D = DA$ | Drag force acting on axle centreline when brakes inactive | (7.1.1) |
| $D = DG$ | Drag force acting at the ground when brakes are active | (7.1.2) |
| $S =$ | Applied side load at the ground | (7.1.3) |
| $V =$ | Applied vertical load at the ground | (7.1.4) |
| $MD = Ve + S \times RR$ | Applied moment about the global X-axis | (7.1.5) |
| $MS = -DG \times RR$ | Applied moment about the global Y-axis (brake torque) | (7.1.6) |
| $MV \approx 0$ | Applied moment about the global Z-axis (typically assumed to be zero) | (7.1.7) |

Loads at Section A-A

At section A-A, the equations of equilibrium are as follows:

$$\Sigma F_x = S \quad (7.1.8)$$

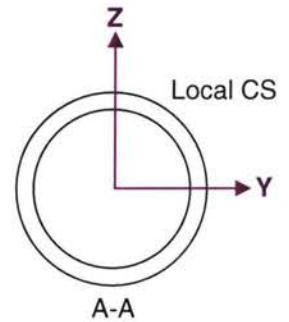
$$\Sigma F_y = D \quad (7.1.9)$$

$$\Sigma F_z = V \quad (7.1.10)$$

$$\Sigma M_x = 0 \quad (\text{any torque due to braking is not transferred to the axle}) \quad (7.1.11)$$

$$\Sigma M_y = MD - V(L - e) = Ve + S \times RR - V(L - e) = V(2e - L) + S \times RR \quad (7.1.12)$$

$$\Sigma M_z = MV + D(L - e) \quad (7.1.13)$$

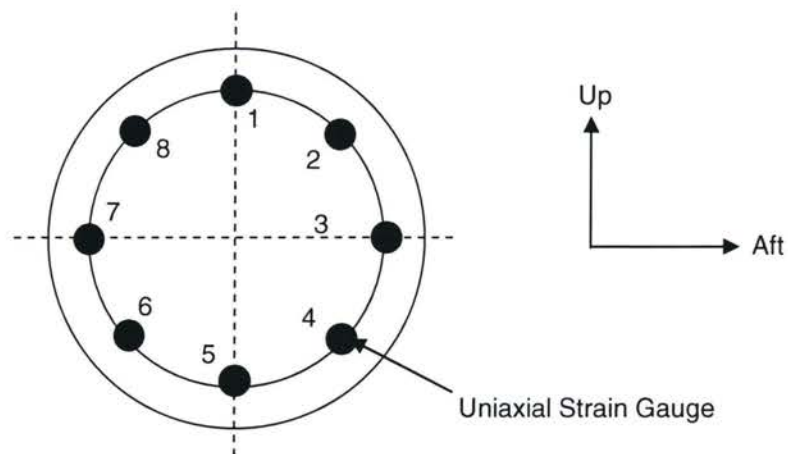


From the equations above, there are 6 unknowns that need to be solved:

D, S, V, MV, RR, e

In order to solve for these unknowns, 6 uniaxial strain measurements are need at various locations on the axle at section A-A. For analysis purposes, 8 strain gauge locations have been chosen at this time. In the future, the 6 best gauge locations will be chosen.

Section A-A



Section A-A Stress Analysis Fundamental Equations

In general, the uniaxial strain gauges will measure strain based on the following types of stress:

Bending

Axial

Hoop

$$\sigma_b = \frac{My}{Z_{yy}} + \frac{Mz}{Z_{zz}} \quad (7.1.13)$$

$$\sigma_a = -\frac{S}{A} \quad (7.1.14)$$

$$\sigma_H \quad (7.1.15)$$

The total stress values are:

$$\sigma_x = \sigma_b + \sigma_a = \left(\frac{V(2e-L) + S \times RR}{Z_{yy}} + \frac{MV + D(L-e)}{Z_{zz}} \right) - \frac{S}{A} \quad (7.1.16)$$

$$\sigma_y = \sigma_H$$

The total axial strain is then (from Hooke's Law):

$$\epsilon_x = \frac{1}{E} (\sigma_x - \nu \sigma_y) = \frac{1}{E} \left[\left(\frac{V(2e-L) + S \times RR}{Z_{yy}} + \frac{MV + D(L-e)}{Z_{zz}} - \frac{S}{A} \right) - \nu \sigma_H \right] \quad (7.1.17)$$

In the total axial strain equation above, there are a total of 6 unknowns, therefore six strain gauges are needed to solve for all of the variables. The hoop stress is also an unknown in the equation, but the values of the expected hoop stress at each strain gauge can be determined by relating the applied loads to hoop stress via FEA.

A finite element model of the axle/bogie beam or axle/piston interface with contact can relate the hoop stress levels to the applied load. This analysis is completed in two steps:

- Apply combinations of vertical and drag ground loads to the model
- Apply combinations of MD and MV moments to the model

Using the principal of superposition (see section 4.2), the total axial strain can be related as follows:

$$\sigma_x = \sigma_x(D, V) + \sigma_x(MD, MV) + \sigma_x(S) \quad (7.1.18)$$

$$\sigma_y = \sigma_y(D, V) + \sigma_y(MD, MV) \quad (7.1.19)$$

$$\varepsilon_x = \frac{1}{E}(\sigma_x - \nu\sigma_y) = \frac{1}{E}[(\sigma_x(S) + \sigma_x(D,V) + \sigma_x(MD,MV)) - \nu(\sigma_y(D,V) + \sigma_y(MD,MV))] \quad (7.1.2)$$

In fact, with the use of FEA, there is no need to derive the stress equations based on applied loads and moments. Instead, the FEA results can be used directly.

On the the following pages, I summarize an FEA analysis of the A380-800 PAX WLG Axle that I have completed based on available CATIA models provided by GLG. Various combinations of the following loads were applied to the landing gear:

- vertical and drag loads
- MD and MV moments
- side loads

The finite element analysis was created in MSC.Patran 2005r2 and the solver used was ABAQUS version 6.6-1. In total, the model contains three individual components:

- Axle
- Bogie Beam
- Bushing

The interaction between these three components was modeled using the Hard Contact boundary condition provided in ABAQUS. The loads applied at the journal bearings are based on a cosine pressure distribution to simulate the bearing/axle contact.

Finite Element Model

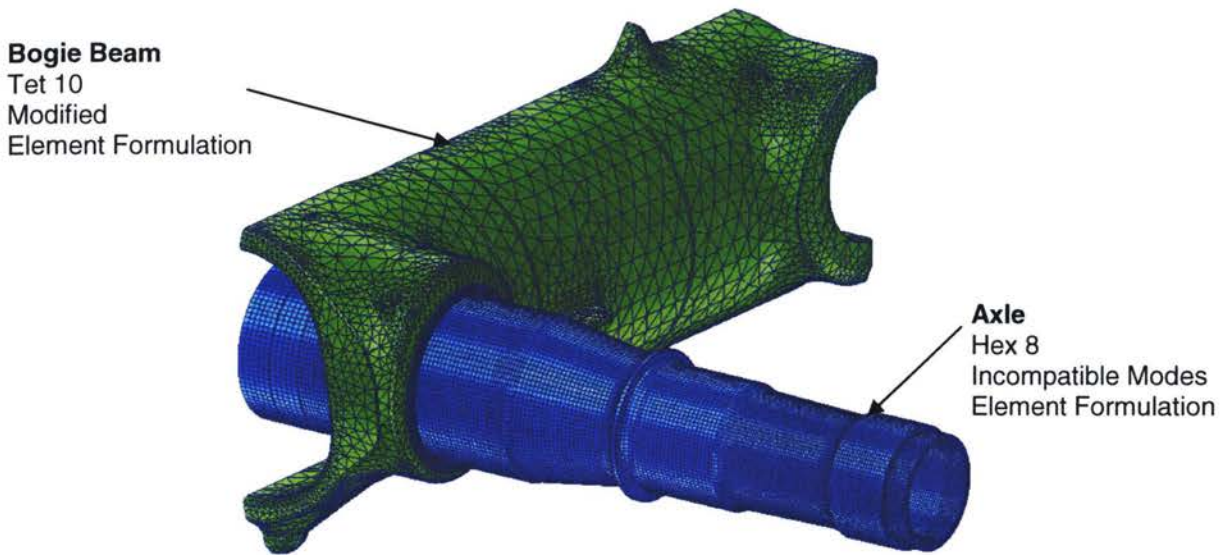


FIGURE 7-2: FINITE ELEMENT MODEL OF AXLE REGION

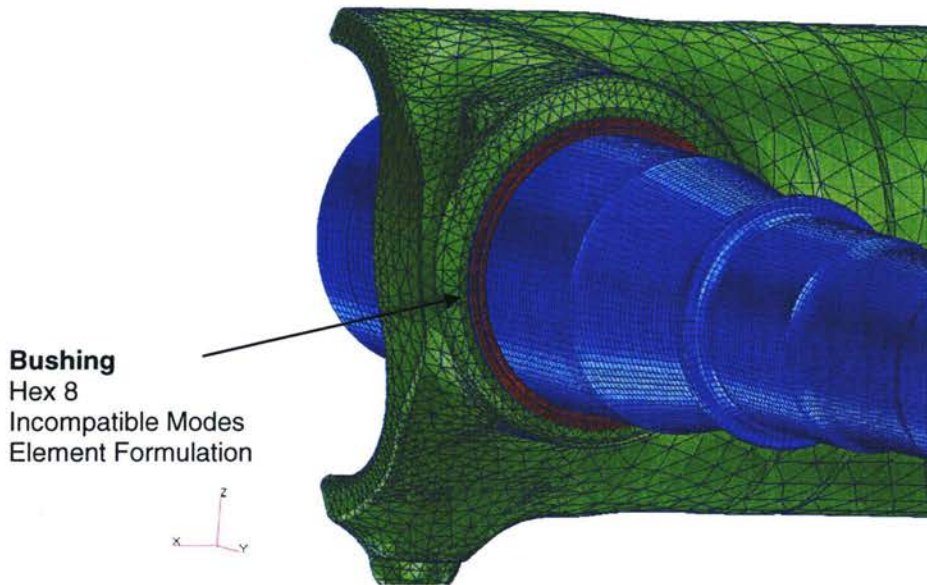


FIGURE 7-3: FINITE ELEMENT CONTACT MODEL OF AXLE INTERFACE

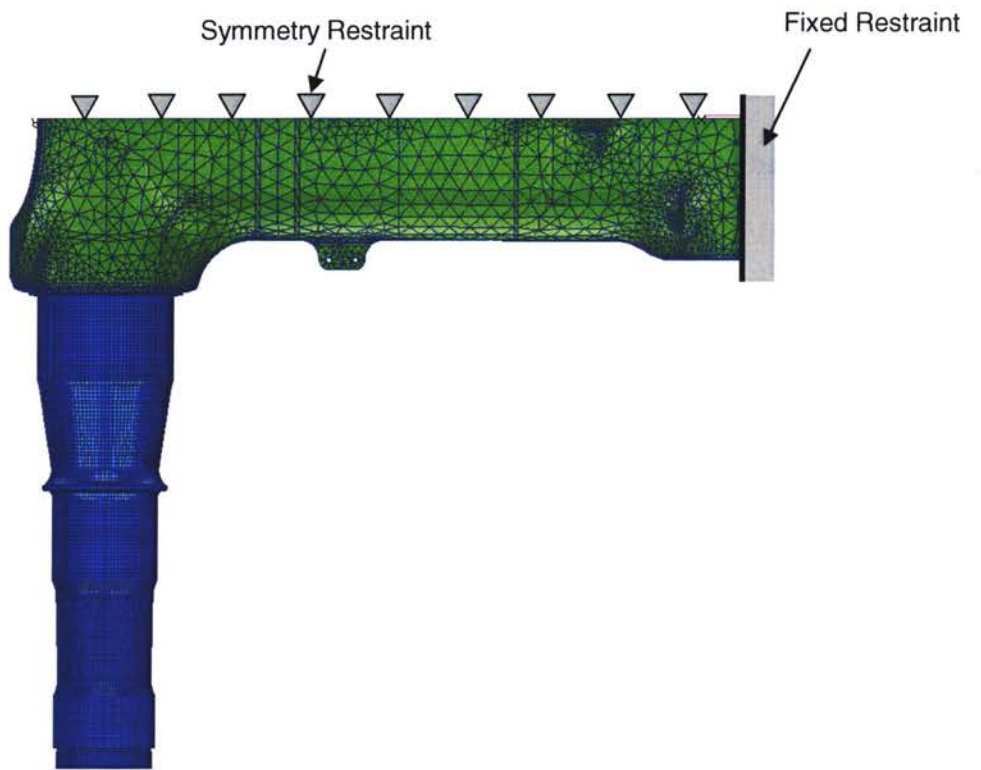


FIGURE 7-4: AXLE INTERFACE SUPPORTS

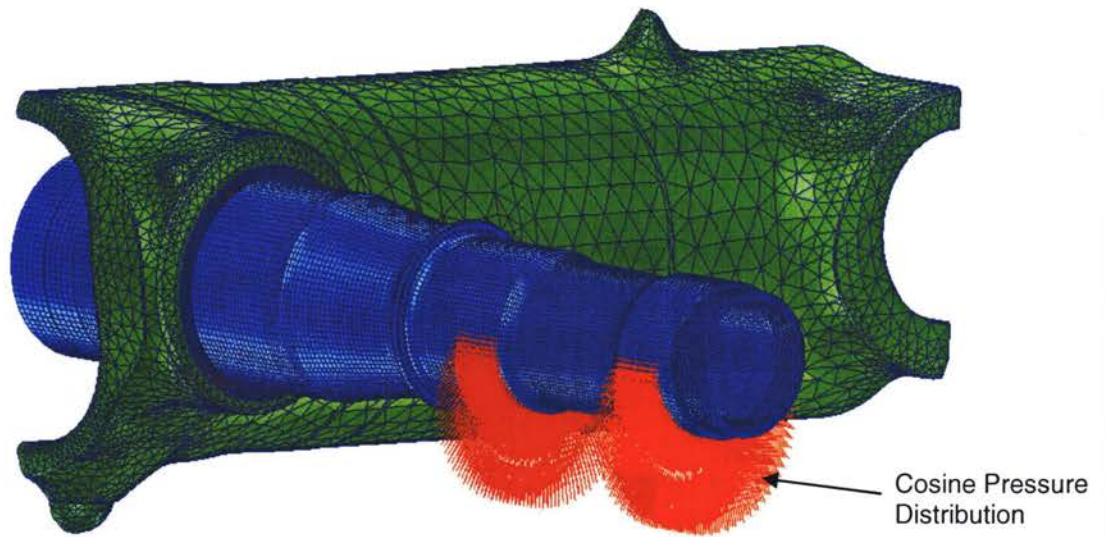
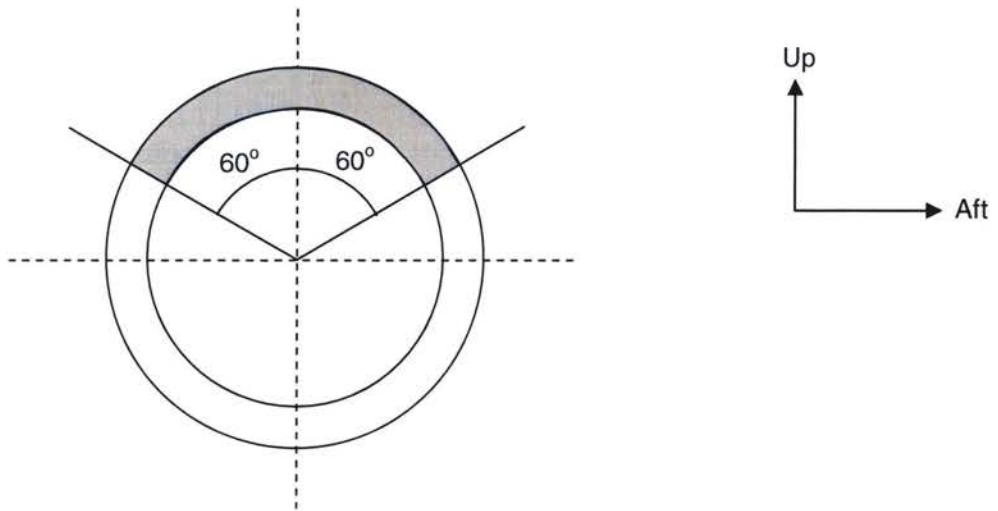


FIGURE 7-5: GROUND LOAD APPLICATION TO AXLE

7.2.1 Drag/Vertical Ground Load Calibration

Combinations of vertical and drag were applied to the WLG axle for the following range:



Since it is not possible to have a significant vertical load in the downwards direction, there is no need to analyze more than the range specified above. All results below are based on an applied ground load of 1 kN and the strains are quoted in microns.

The ground load angle, θ , is in degrees and can be determined via:

$$\theta_{RF} = \tan^{-1}\left(\frac{D}{V}\right) \quad (7.2.1)$$

The resultant ground load, R , is determined via:

$$RF = \sqrt{D^2 + V^2} \quad (7.2.2)$$

After analyzing the strain results, it has been observed that the axial strain can be related to the applied load, RF , and angle, θ_{RF} , via a cosine curve fit.

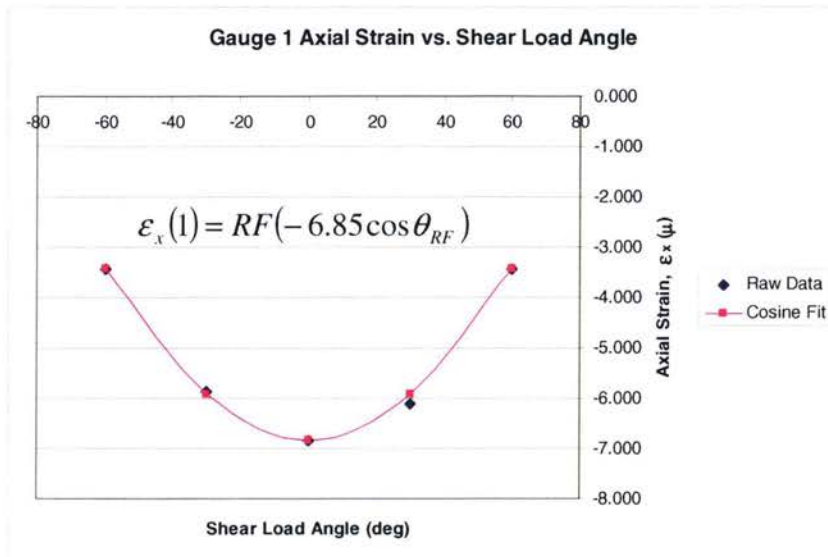


FIGURE 7-6: GAUGE 1 DV RESULTS

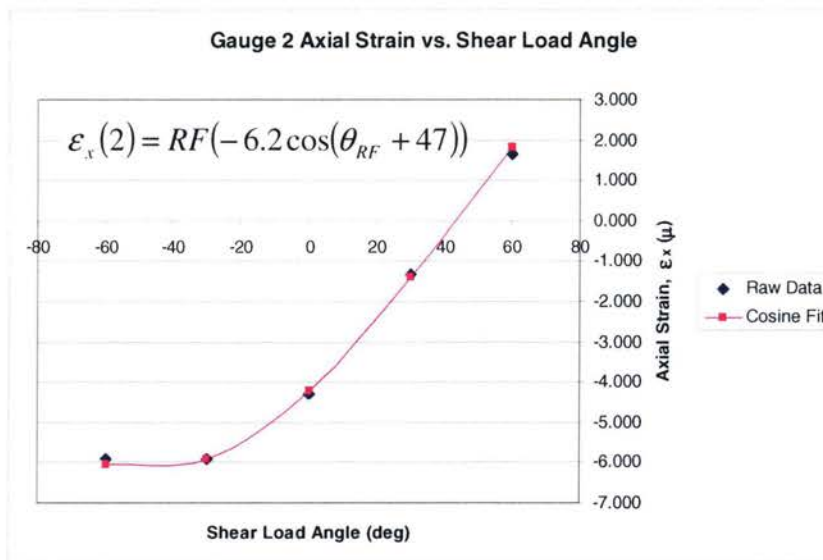


FIGURE 7-7: GAUGE 2 DV RESULTS

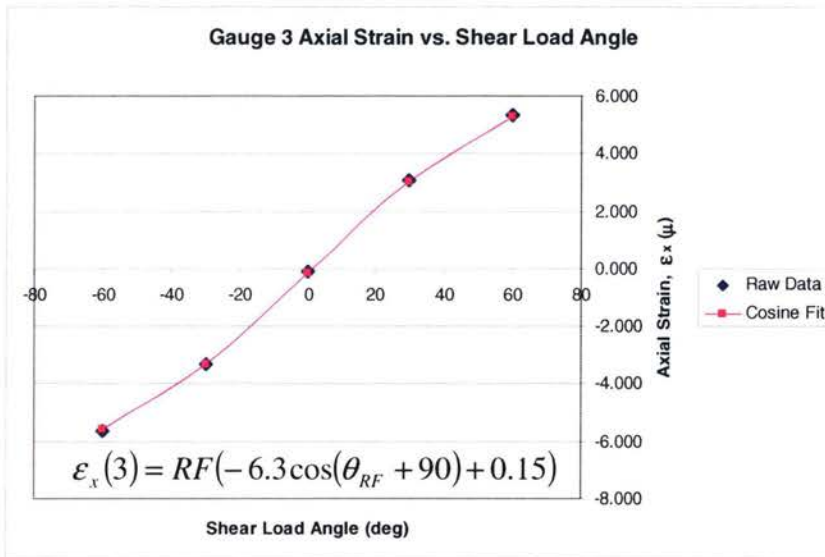


FIGURE 7-8: GAUGE 3 DV RESULTS

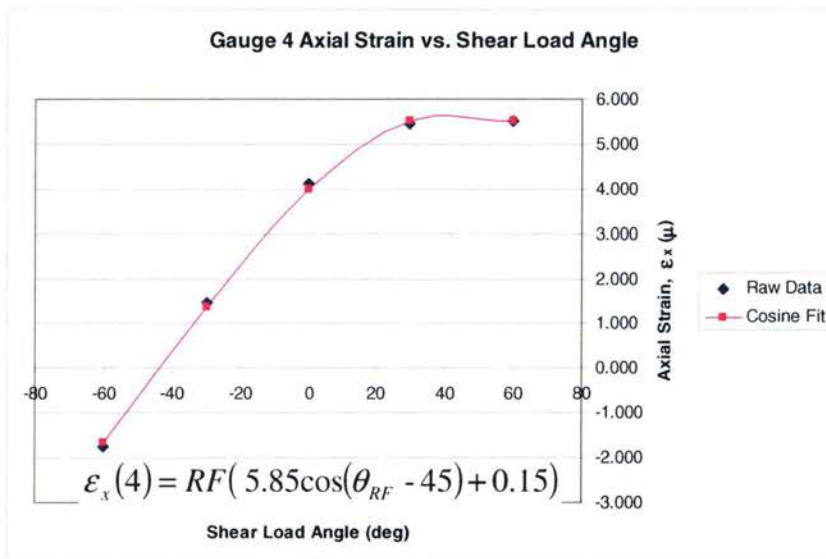


FIGURE 7-9: GAUGE 4 DV RESULTS

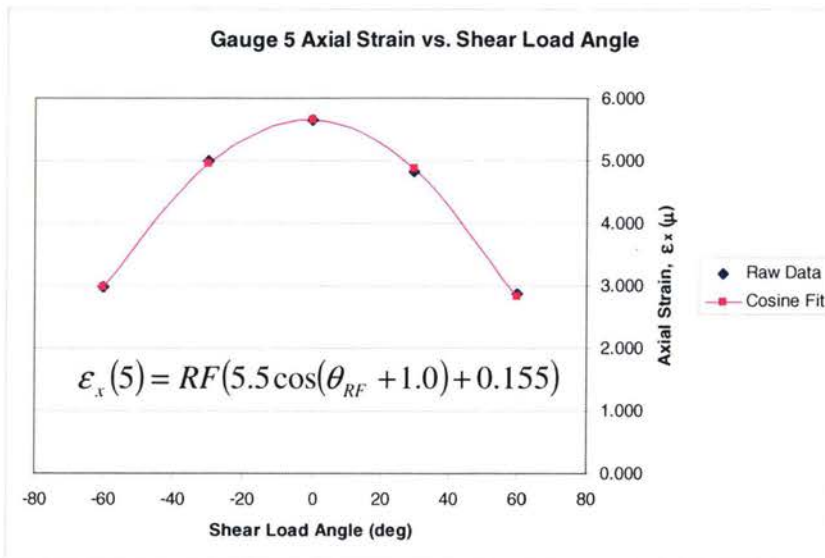


FIGURE 7-10: GAUGE 5 DV RESULTS

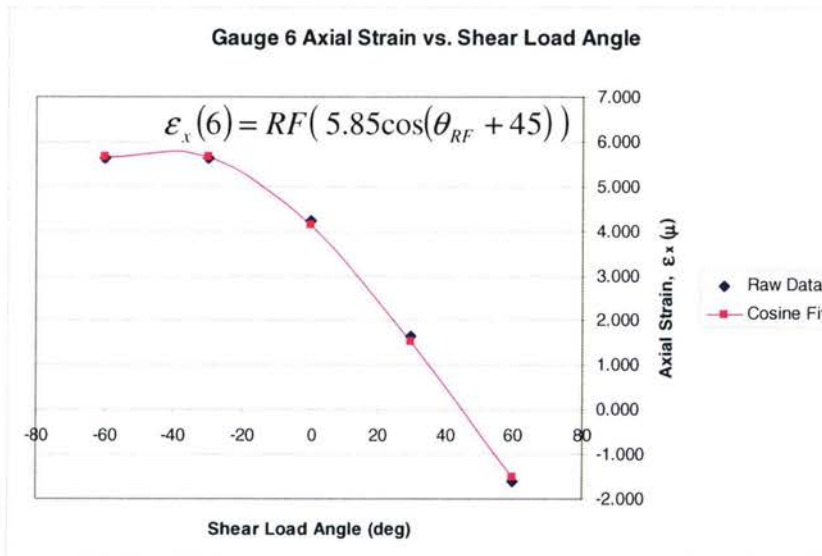


FIGURE 7-11: GAUGE 6 DV RESULTS

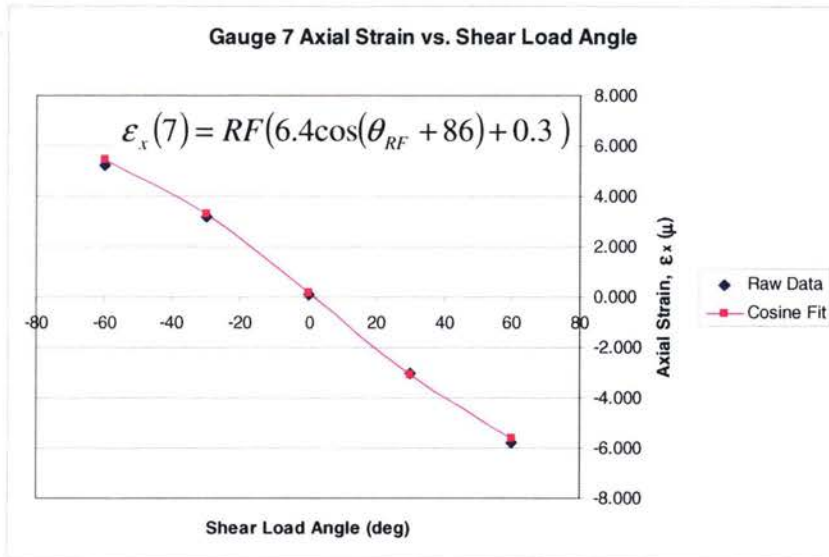


FIGURE 7-12: GAUGE 7 DV RESULTS

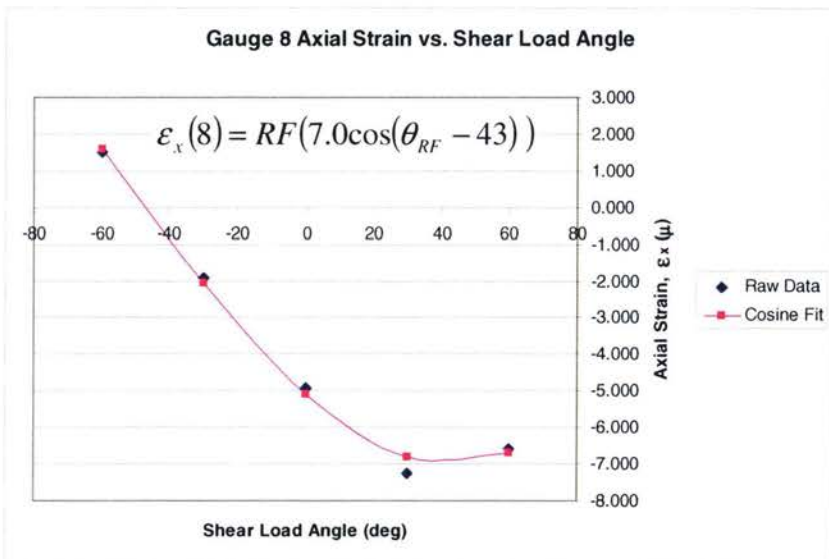


FIGURE 7-13: GAUGE 8 DV RESULTS

Based on the observation that the uniaxial strain readings at each gauge can be related to the applied ground forces with a cosine curve fit, the cosine equation has the general form:

$$\varepsilon'_x = RF(A \cos(\theta_{RF} + \phi_{RF}) + B) \quad (7.2.3)$$

Where

A = strain amplitude in microns

Φ_{RF} = phase angle in degrees

B = mean strain in microns

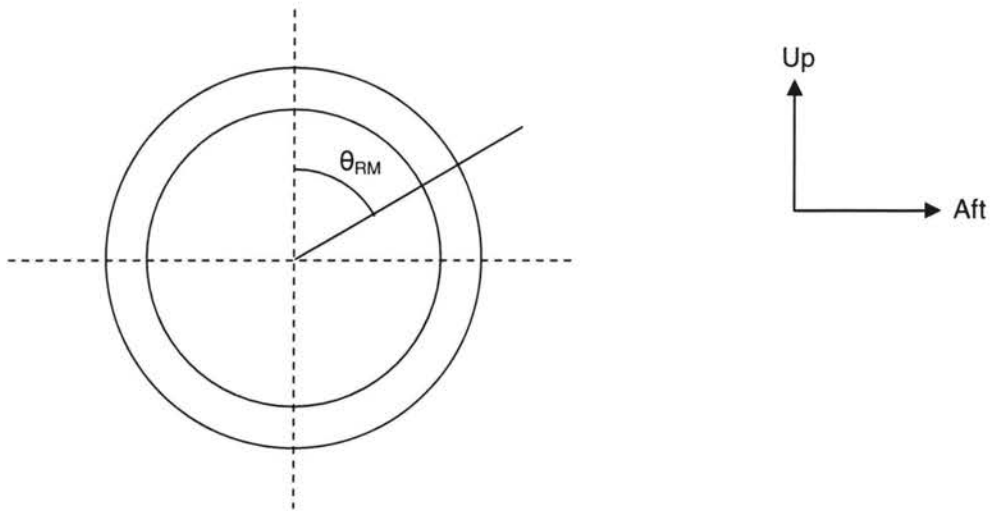
For the eight possible strain gauge locations, the coefficients for A, Φ_R , and B are:

$$A = \begin{bmatrix} -6.850 \\ -6.200 \\ -6.300 \\ 5.850 \\ 5.500 \\ 5.850 \\ 6.400 \\ -7.000 \end{bmatrix} \quad \phi_{RF} = \begin{bmatrix} 0.000 \\ 47.000 \\ 90.000 \\ -45.000 \\ 1.000 \\ 45.000 \\ 86.000 \\ -43.000 \end{bmatrix} \quad B = \begin{bmatrix} 0.000 \\ 0.000 \\ 0.150 \\ 0.150 \\ -0.155 \\ 0.000 \\ 0.300 \\ 0.000 \end{bmatrix}$$

7.2.2

MX / MZ Ground Load Calibration

Combinations of vertical and drag were applied to the WLG axle for the following range:



It is possible that the resultant moment is applied at any orientation. All results below are based on an applied ground load of 1 kN-mm and the strains are quoted in microns.

The ground load angle, θ , is in degrees and can be determined via:

$$\theta_{RM} = \tan^{-1}\left(\frac{MZ}{MX}\right) \quad (7.2.4)$$

The resultant ground load, R, is determined via:

$$RM = \sqrt{MX^2 + MZ^2} \quad (7.2.5)$$

After analyzing the strain results, it has been observed that the axial strain can be related to the applied load, RM, and angle, θ_{RM} , via a cosine curve fit.

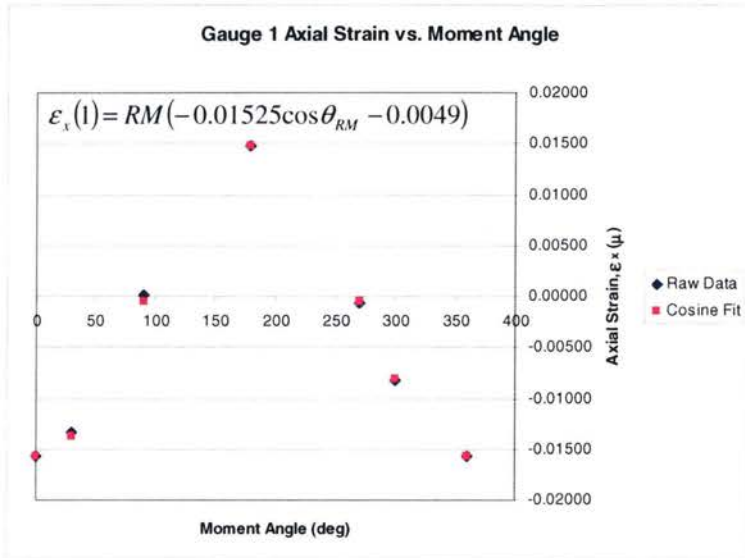


FIGURE 7-14: GAUGE 1 RM RESULTS

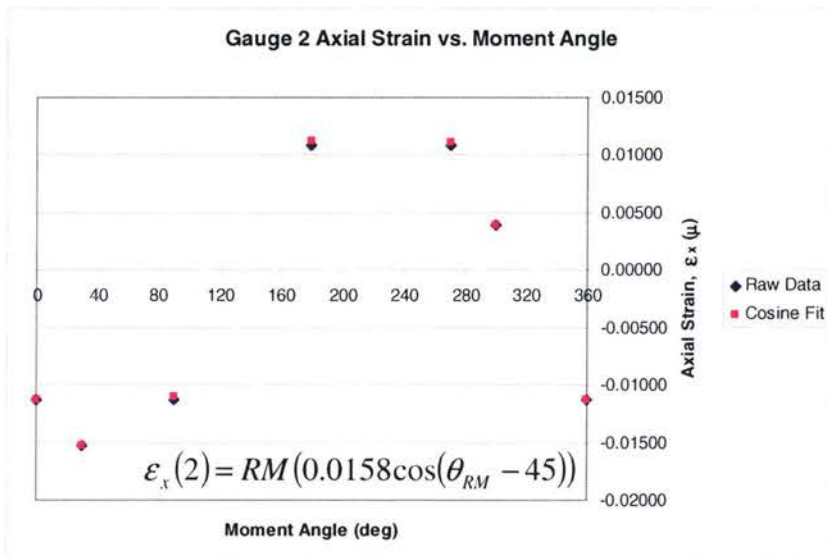


FIGURE 7-15: GAUGE 2 RM RESULTS

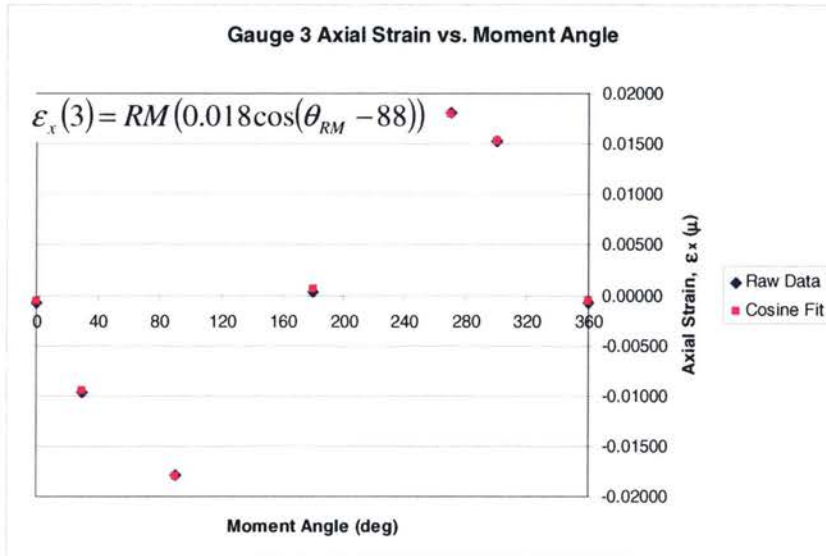


FIGURE 7-16: GAUGE 3 RM RESULTS

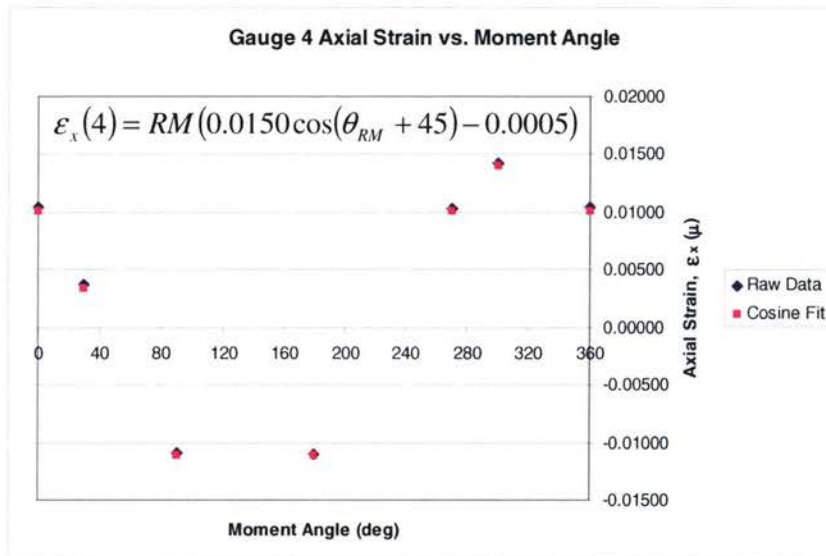


FIGURE 7-17: GAUGE 4 RM RESULTS

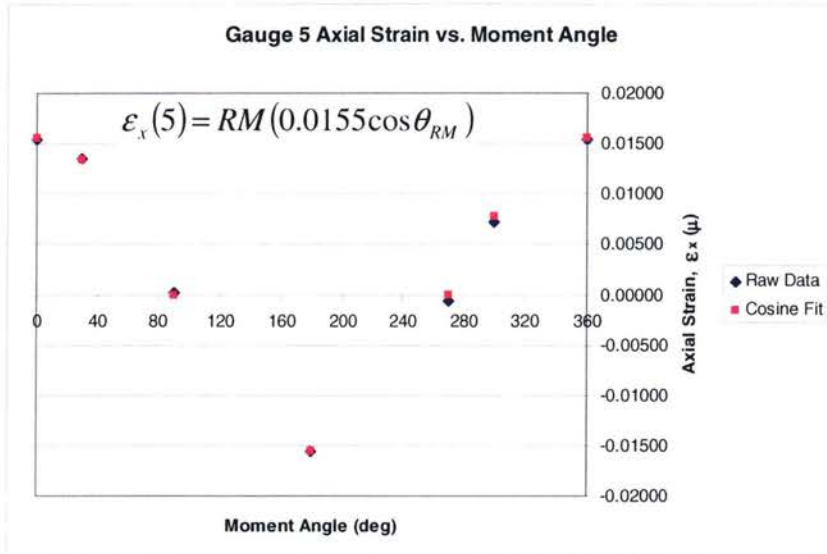


FIGURE 7-18: GAUGE 5 RM RESULTS

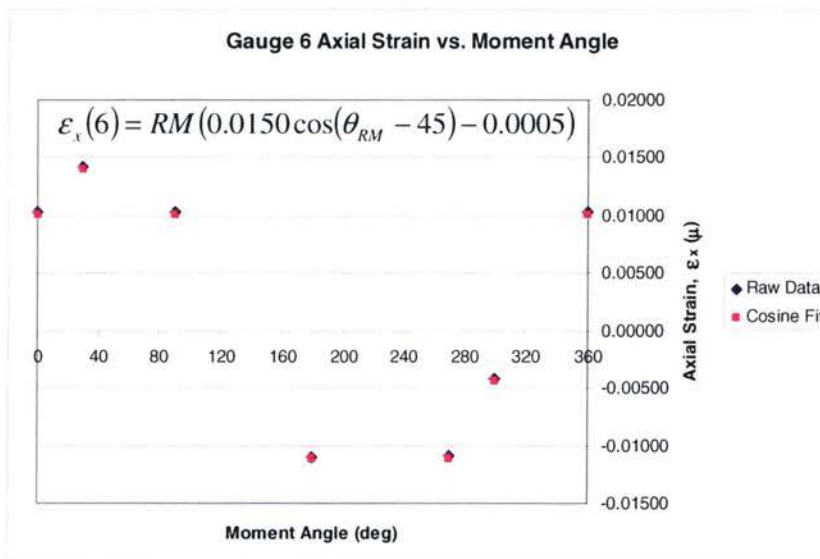


FIGURE 7-19: GAUGE 6 RM RESULTS

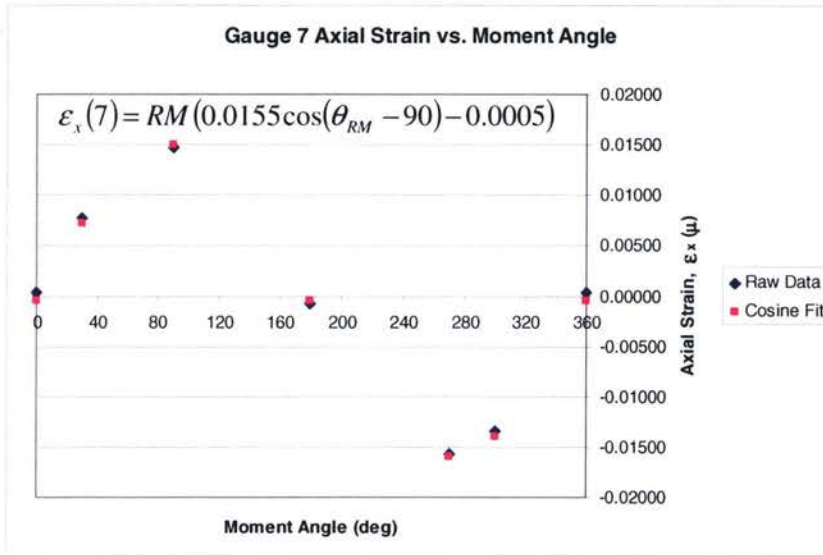


FIGURE 7-20: GAUGE 7 RM RESULTS

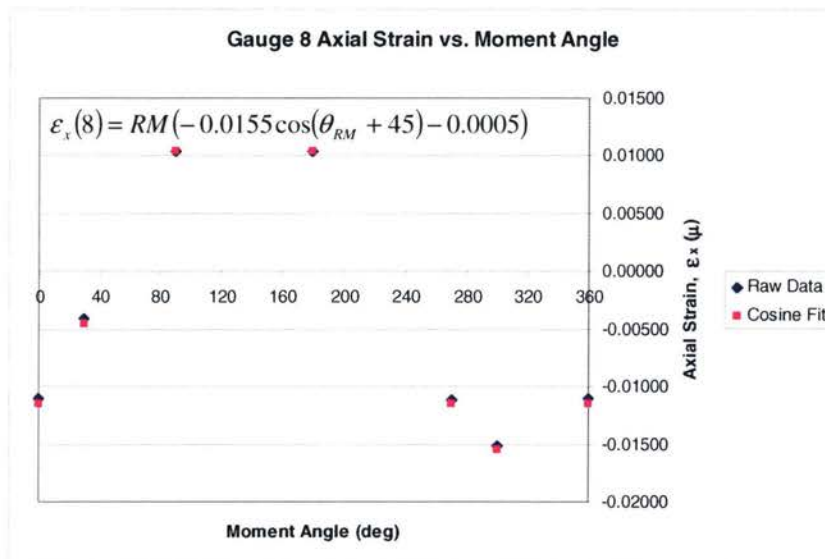


FIGURE 7-21: GAUGE 8 RM RESULTS

Based on the observation that the uniaxial strain readings at each gauge can be related to the applied ground moments with a cosine curve fit, the cosine equation has the general form:

$$\varepsilon_x^g = RM(C \cos(\theta_{RM} + \phi_{RM}) + D) \quad (7.2.6)$$

Where

C = strain amplitude in microns

Φ_{RM} = phase angle in degrees

D = mean strain in microns

For the eight possible strain gauge locations, the coefficients for A, Φ_R , and B are:

$$C = \begin{bmatrix} -0.01525 \\ -0.01580 \\ -0.01800 \\ 0.01500 \\ 0.01550 \\ 0.01500 \\ 0.01550 \\ -0.01550 \end{bmatrix} \quad \phi_{RM} = \begin{bmatrix} 0.000 \\ 0.000 \\ -44.500 \\ -88.000 \\ 45.000 \\ 0.000 \\ -45.000 \\ -90.000 \end{bmatrix} \quad D = \begin{bmatrix} -0.00049 \\ 0.00000 \\ 0.00000 \\ 0.00000 \\ -0.00050 \\ 0.00000 \\ -0.00050 \\ -0.00050 \end{bmatrix}$$

7.2.3 Side Load Results

The applied side load to the axle produces a moment and an axial load in the axle. The moment portion of the side load is included in the MX moment calculation. The axial portion of the side load can be written as follows based on the FEM calibration results:

$$\varepsilon_x''' = SE \quad \text{where } E = \text{axial strain coefficient} \quad (7.2.7)$$

$$E = \begin{bmatrix} -0.670 \\ -0.693 \\ -0.796 \\ -0.670 \\ -0.693 \\ -0.670 \\ -0.670 \\ -0.670 \end{bmatrix}$$

7.2.4 Calculating Ground Loads Based on Calibration Equations

$$\varepsilon_{.x} = \varepsilon'_{.x}(RF, \phi_{RF}) + \varepsilon''_{.x}(RM, \phi_{RM}) + \varepsilon'''_{.x}(S) \quad (7.2.8)$$

Since there are 5 unknowns in equation 7.2.8, 5 of the six strain gauge equations are needed to solve for RF, θ_{RF} , RM, θ_{RM} , and S. The sixth strain gauge reading is used to solve for either e or RR in equation 6.

In order to solve for RF, θ_R , RM, θ_{RM} , and S, an iterative technique must be used that solves nonlinear systems of equations. Some possible techniques that could be used are as follows:

- Newton's Method
- Quasi-Newton's Methods
- Steepest Descent

For all of the calculations presented in this report, Newton's Method has been utilized.

7.2.5 Newton's Method for Solving Nonlinear Systems of Equations

Source: Reference 4

In order to solve for a nonlinear equation with one variable, the Newton-Rhapson technique is often employed to determine the roots of the equation. The general form of the Newton-Rhapson equation is as follows:

$$g(x) = x - \phi(x)f(x) \quad (7.2.9)$$

where $\phi(x)$ is the inverse of the derivative of $f(x)$ (i.e. $1/f'$).

A similar approach can be used in the n-dimension case which involves the matrix

$$A(x) = \begin{bmatrix} a_{11}(x) & a_{12}(x) & \dots & a_{1n}(x) \\ a_{21}(x) & a_{22}(x) & \dots & a_{2n}(x) \\ \cdot & \cdot & \dots & \cdot \\ a_{n1}(x) & a_{n2}(x) & \dots & a_{nn}(x) \end{bmatrix} \quad (7.2.10)$$

where each of the entries $a_{ij}(x)$ is a function from R^n into R-Space. This requires that $A(x)$ be found so that

$$G(x) = x - A^{-1}(x)F(x) \quad (7.2.11)$$

In final form, Newton's method for nonlinear systems of equations has the following form:

$$x^{(k)} = x^{(k-1)} - J(x^{(k-1)})^{-1}F(x^{(k-1)}) \quad (7.2.12)$$

where

$$J(x) = \begin{bmatrix} \frac{\partial f_1}{\partial x_1} & \frac{\partial f_1}{\partial x_2} & \dots & \frac{\partial f_1}{\partial x_n} \\ \frac{\partial f_2}{\partial x_1} & \frac{\partial f_2}{\partial x_2} & \dots & \frac{\partial f_2}{\partial x_n} \\ \cdot & \cdot & \dots & \cdot \\ \frac{\partial f_n}{\partial x_1} & \frac{\partial f_n}{\partial x_2} & \dots & \frac{\partial f_n}{\partial x_n} \end{bmatrix} \quad (7.2.13)$$

For the equations developed in sections 7.2.1 to 7.2.3, I have calculated the resulting partial derivatives required for the J matrix:

$$f = RF(A \cos(\theta_{RF} + \phi_{RF}) + B) + RM(C \cos(\theta_{RM} + \phi_{RM}) + D) + SE \quad (7.2.14)$$

$$\frac{\partial f_i}{\partial RF} = A_i \cos(\theta_{RF} + \phi_{RFi}) + B \quad (7.2.15)$$

$$\frac{\partial f_i}{\partial \theta_{RF}} = -RF \cdot A_i \sin(\theta_{RF} + \phi_{RFi}) \quad (7.2.16)$$

$$\frac{\partial f_i}{\partial RM} = C_i \cos(\theta_{RM} + \phi_{RMi}) + D \quad (7.2.17)$$

$$\frac{\partial f_i}{\partial \theta_{RM}} = -RM \cdot C_i \sin(\theta_{RM} + \phi_{RMi}) \quad (7.2.18)$$

$$\frac{\partial f_i}{\partial S} = E_i \quad (7.2.19)$$

where $1 \leq i \leq 5$.

The inverse of the J-Matrix can be solved by using Gaussian elimination techniques. Once the J-Matrix is solved, iterative techniques via computer code can be used to determine the roots of the nonlinear system of equations.

Once RF, RM, θ_{RF} , θ_{RM} , and S are known, then D, V, MD, and MV can be determined:

$$D = RF \sin \theta_{RF} \quad (7.2.20)$$

$$V = RF \cos \theta_{RF} \quad (7.2.21)$$

$$MD = RM \sin \theta_{RM} \quad (7.2.22)$$

$$MV = RM \cos \theta_{RM} \quad (7.2.23)$$

Thus, Newtons method involves a linearization of the nonlinear system of equations. To assure convergence, it requires an initial guess which is close enough to the desired solution, and a step size which is small enough. For landing gear applications, it may be sufficient to assume an initial value of applied vertical force since this force is always present when the aircraft is on the ground.

Post Equations

Another more simplified means of measuring the ground loads applied to the landing gear structure is to measure the strain levels at the piston and torque links. In general, all applied loads acting at the wheels will be transferred to the remaining landing gear structure via the piston and torque links. By placing strain gauges at these two strategic locations, the post loads applied to the landing gear can be measured.

The post is defined as the equivalent single ground reaction point for the entire landing gear. This point is typically defined as the intersection point between the axle and shock strut centrelines. In total, there can be six components of post loads:

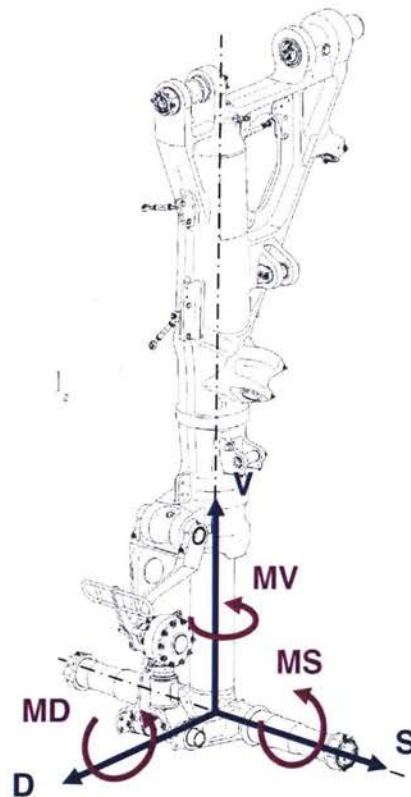


FIGURE 7-22: DEFINITION OF POST LOADS

where

D = Drag force (fore/aft acting load)

S = Side force (Inboard/Outboard acting load)

V = Vertical force (Upward acting load)

MD = Moment acting about the fore/aft axis

MS = Moment acting about the inboard/outboard axis (due to brake torque)

MV = Moment acting about the vertical axis

The following table summarizes the type of internal loads that each load component generates at the piston barrel strain gauge locations (indicated in blue):

TABLE 7-1: INTERNAL LOAD TYPES GENERATED AT PISTON

| Post Load | Axial | Shear X | Shear Y | MBX | MBY |
|-----------|-------|---------|---------|-----|-----|
| D | | | | | |
| S | | | | | |
| V | | | | | |
| MD | | | | | |
| MS | | | | | |

Note: this table assumes that the landing gear has no rake angle *or* that the vertical load axis is parallel with the shock strut axis

Table 7-1 indicates that all five components of load will generate an axial strain at the piston location chosen (either through bending or direct axial loading). As a result, it is theoretically possible to predict these five components of post loads by strategically placing five uniaxial strain gauges at this location (see below).

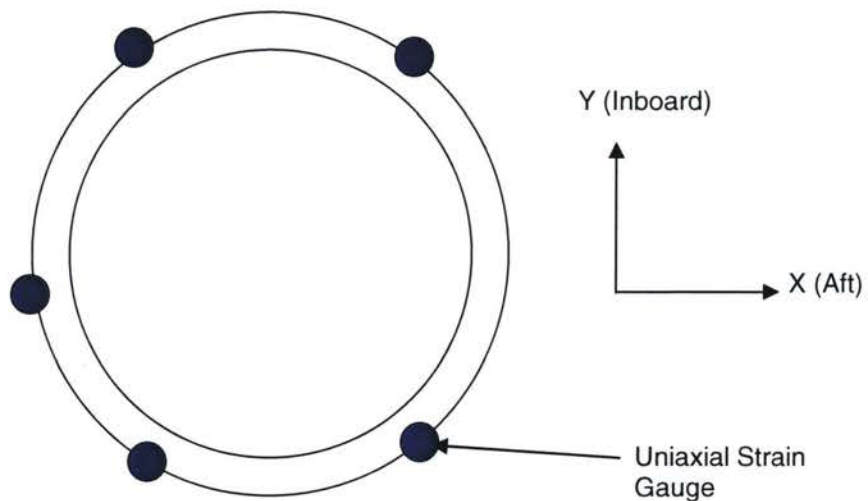


FIGURE 7-24: POTENTIAL STRAIN GAUGE ARRANGEMENT AT PISTON

7.3.1 Torque Link Strain Measurement

Any moment acting about the shock strut axis (MV) is transferred to the outer cylinder (and, consequently, the airframe) via the torque links. The torque links react this moment in shear. This shear load produces high bending loads on the torque links (see below).

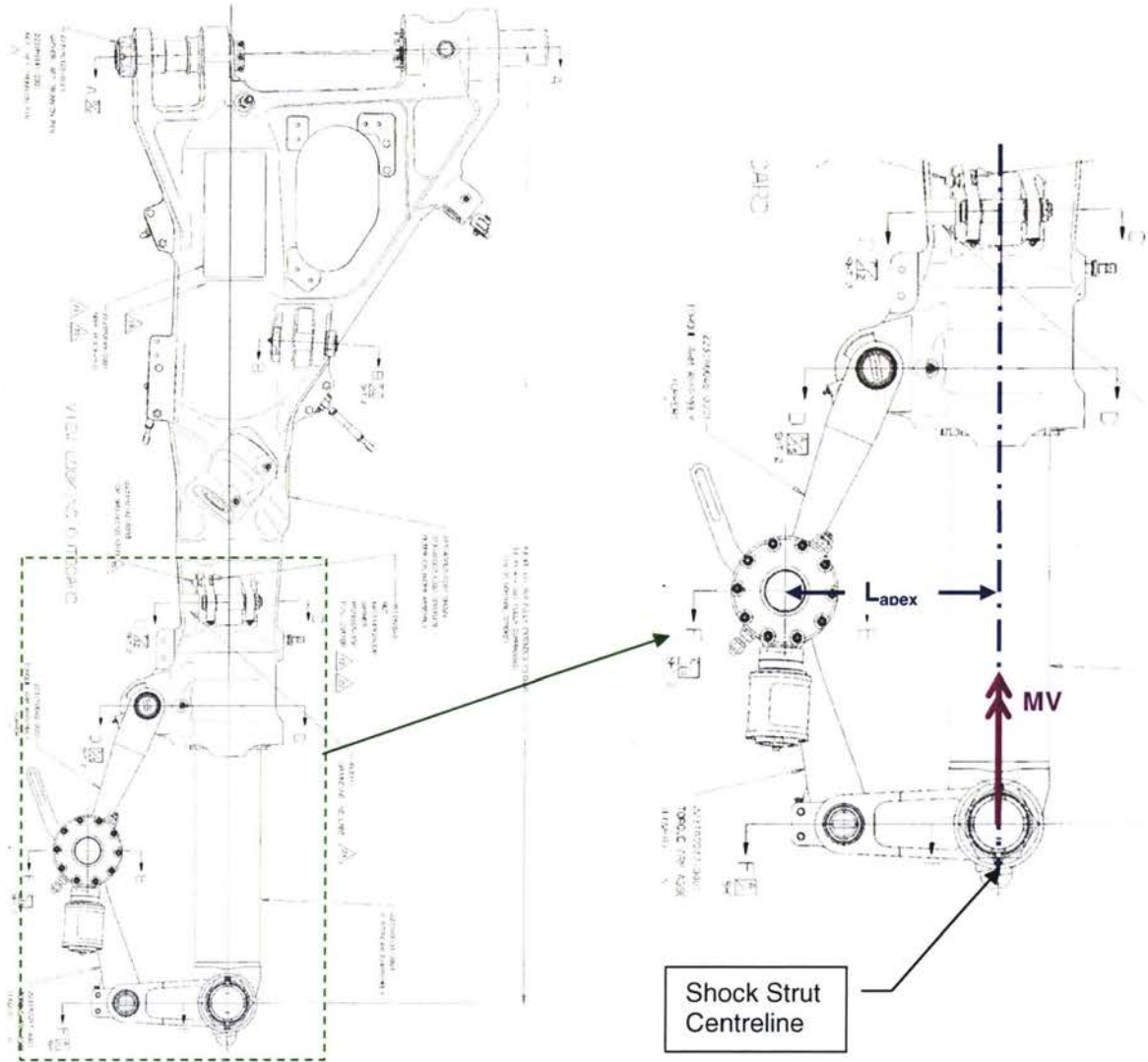


FIGURE 7-25: RELATING TORQUE LINK APEX LOADS TO MV MOMENT

By placing a uniaxial strain gauge at a strategic location on either the upper or lower torque link, the shear load (P_{apex}) acting at the torque link apex can be determined (see following page for details). Furthermore, this shear load can then be related to the MV moment via statics:

$$MV = P_{apex} L_{apex} \quad (7.3.1)$$

Note that, in order to determine the value of L_{apex} , the stroke of the shock strut must be known.

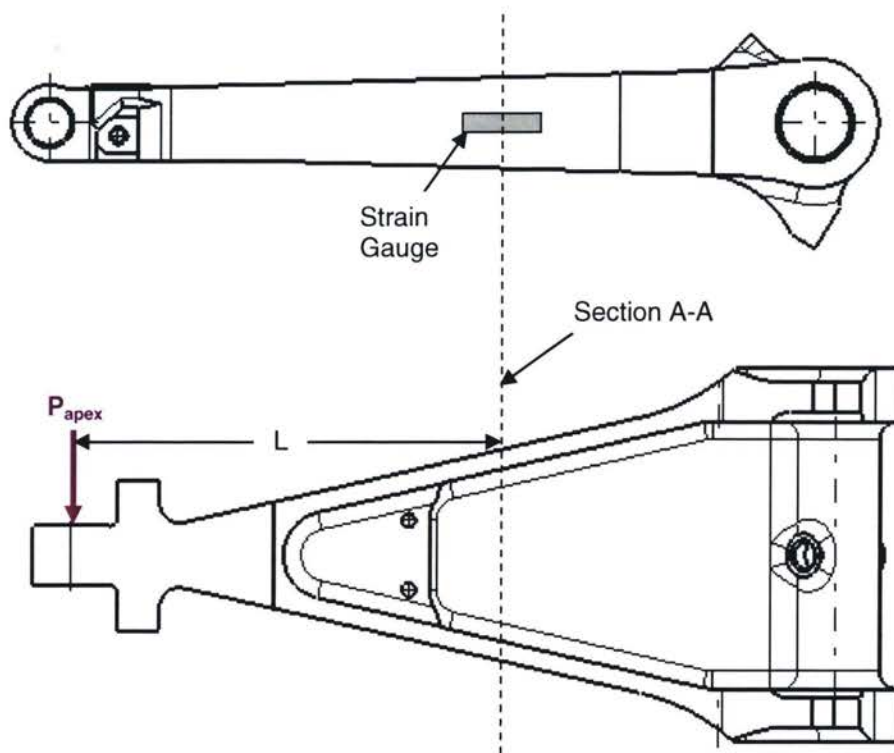


FIGURE 7-26: CALIBRATING STRAIN GAUGE RESULTS TO APEX FORCE

From the figure above, the following applied loads result at section A-A (note: tapered beam theory has been neglected in the equations below):

$$MBX = P_{apex} L \quad (7.3.2)$$

$$PSY = P_{apex} \quad (7.3.3)$$

Since there is moment applied to the torque link, the uniaxial strain gauge data can be calibrated to the applied apex force. This calibration can initially be completed via finite element analysis and then verified during static testing.

7.3.2 Governing Equations

Post Load Equations

The loads applied at the post are a summation of the ground loads applied at the individual wheels. For equation derivations, assume that the landing gear design includes two wheels. Typically, the wheels are referenced as the inboard and outboard wheels (denoted with a subscript i and o respectively). Referring to the axle diagram presented in Figure 7-1 on page 51:

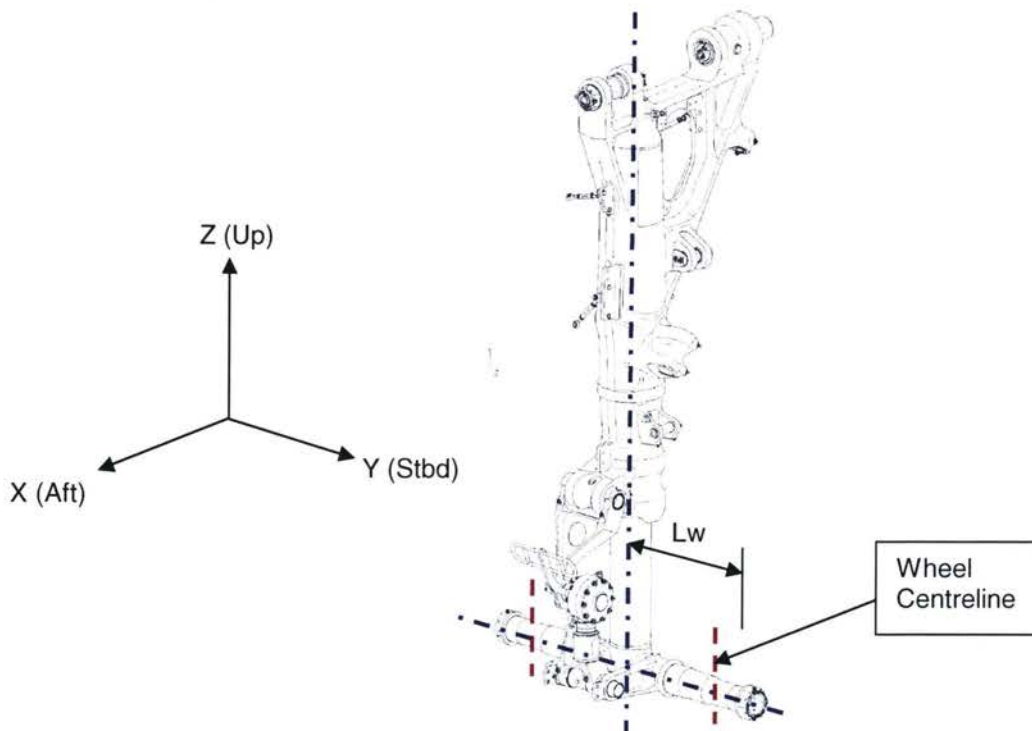


FIGURE 7-27: DEFINITION OF WHEEL CENTRELINE

$$\sum F_x = D = DA_i(\text{or}DG_i) + DA_o(\text{or}DG_o) \quad (7.3.4)$$

$$\sum F_y = S = S_i + S_o \quad (7.3.5)$$

$$\sum F_z = V = V_i + V_o \quad (7.3.6)$$

$$\sum M_x = MD = MD_i + MD_o + (V_i - V_o)Lw \quad (7.3.7)$$

$$\sum M_y = MS = -(DG_i + DG_o)RR \quad (7.3.8)$$

$$\sum M_z = MV = (S_o - S_i)Lw \quad (7.3.9)$$

Notes:

RR = Tire Rolling Radius (i.e. distance from axle centreline to tire contact point)

Lw = distance from shock strut centreline to the wheel centreline

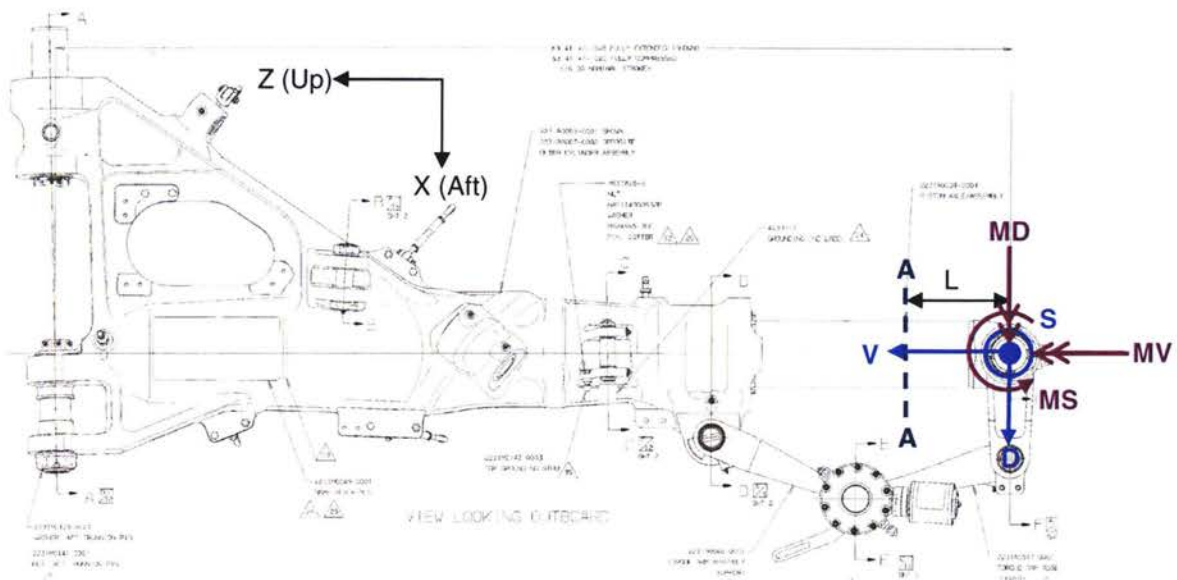


FIGURE 7-28: FREE BODY DIAGRAM FOR LOADS AT SECTION A-A

From the free body diagram above:

$$\sum F_x = D \quad (7.3.10)$$

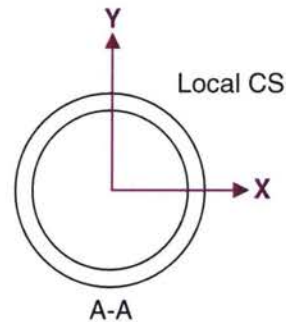
$$\sum F_y = S \quad (7.3.11)$$

$$\sum F_z = V \quad (7.3.12)$$

$$\sum M_x = MD + SL \quad (7.3.13)$$

$$\sum M_y = MS - DL \quad (7.3.14)$$

$$\sum M_z = 0 \quad (\text{MV moment is reacted by the torque links}) \quad (7.3.15)$$



Note that, for some landing gear designs, the oil in the shock strut is throughout the entire length of the piston barrel. If there is oil present at the region where the strain gauges are placed on the barrel, hoop stresses will be present. Due to Hooke's Law, this hoop stress will affect the strain uniaxial strain gauge readings. As a result, an additional strain gauge will be required to monitor the hoop stress at the strain gauge locations. If this stress can be determined, the uniaxial strain gauges can be corrected for the hoop stress.

Section A-A Stress Analysis Fundamental Equations

In general, the uniaxial strain gauges will measure strain based on the following types of stress:

Bending

Axial

Hoop

$$\sigma_b = \frac{My}{Z_{xx}} + \frac{Mz}{Z_{yy}} \quad (7.3.16) \quad \sigma_a = -\frac{V}{A} \quad (7.3.17) \quad \sigma_H = f(V) \quad (7.3.18)$$

The total stress values are:

$$\sigma_x = \sigma_b + \sigma_a = \left(\frac{MD + SL}{Z_{xx}} + \frac{MS - DL}{Z_{yy}} \right) - \frac{V}{A} \quad (7.3.19)$$

$$\sigma_y = \sigma_H = f(V) \quad (7.3.20)$$

The total axial strain is then (from Hooke's Law):

$$\varepsilon_x = \frac{1}{E} (\sigma_x - \nu \sigma_y) = \frac{1}{E} \left[\left(\frac{MD + SL}{Z_{xx}} + \frac{MS - DL}{Z_{yy}} - \frac{V}{A} \right) - \nu \sigma_H \right] \quad (7.3.21)$$

In the total axial strain equation above, there are a total of 5 unknowns, therefore five strain gauges are needed to solve for all of the variables. An additional unknown could be the hoop stress if the shock strut design is such that there is internal pressure at the strain gauge measurement locations. If internal pressure is present, then an additional strain gauge is required to account for x-component of strain caused by the hoop stress

Using the principal of superposition (see section 4.2), the total axial strain can be related as follows:

$$\sigma_x = \sigma_x(D, S) + \sigma_x(MD, MS) + \sigma_x(V) \quad (7.3.22)$$

$$\sigma_y = \sigma_y(V) \quad (7.3.23)$$

$$\varepsilon_x = \frac{1}{E} (\sigma_x - \nu \sigma_y) = \frac{1}{E} \left[(\sigma_x(D, S) + \sigma_x(MD, MS) + \sigma_x(V)) - \nu \sigma_y(V) \right] \quad (7.3.24)$$

In fact, with the use of FEA, there is no need to derive the stress equations based on applied loads and moments. Instead, the FEA results can be used directly.

Torque Link Stress Analysis Fundamental Equations

From section 7.3.1, the basic equations relating the MV moment to the apex load acting on the torque link assembly are as follows:

$$MBX = P_{apex} L \quad (7.3.2) \quad \Rightarrow \quad P_{apex} = \frac{MBX}{L}$$

$$MV = P_{apex} L_{apex} \quad (7.3.1) \quad \Rightarrow \quad MV = \frac{L_{apex}}{L} MBX \quad (7.3.25)$$

From Figure 7-26, the bending stress and strain at section A-A are:

$$\sigma_x = \frac{MBX}{Z_{xx}} \quad (7.3.26)$$

$$\epsilon_x = \frac{\sigma_x}{E} \quad (\text{assuming that the } \sigma_y \text{ component of stress is negligible}) \quad (7.3.27)$$

Combining equations 7.3.26 and 7.3.27 above:

$$\epsilon_x = \frac{MBX}{Z_{xx}E} \quad \Rightarrow \quad MBX = Z_{xx}E\epsilon_x \quad (7.3.28)$$

Therefore, the measured strain can now be related to the MV moment:

$$MV = MBX \frac{L_{apex}}{L} = Z_{xx}E\epsilon_x \frac{L_{apex}}{L} \quad (7.3.29)$$

The following pages complete an FEA analysis of the G650 NLG Piston and torque link assembly. Various combinations of the following loads were applied to the landing gear:

- vertical and drag loads
- MD and MV moments
- side loads

Generally speaking, NLG designs do not include brake installations. As a result, there is no need to measure MS moment since this moment is caused by braking events.

7.4

G650 NLG Study

As part of the technology demonstration plan for the proposed ODHMS system, the post strain gauge configuration (see section 7.3) will be placed on the G650 NLG static, fatigue, and drop test units. In all cases, the test unit is a fully assembled landing gear that is very similar to the landing gear that will be in used on in-service aircraft. For initial calibration of the strain gauges to be used in the test, a finite element model has been created to simulate the loads and supports in the region of the piston and torque links.

7.4.1 Finite Element Model of G650 Piston and Torque Links

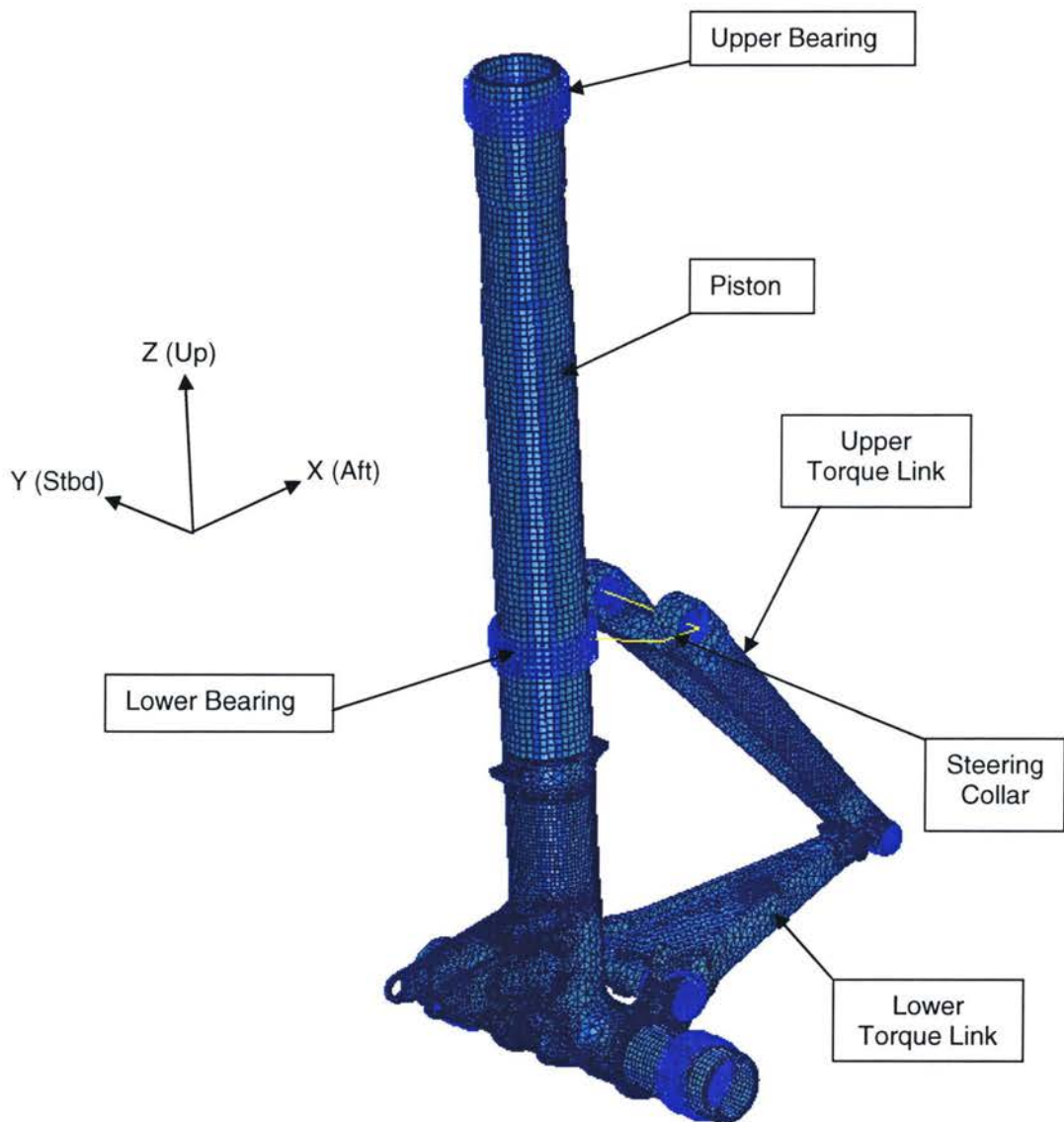


FIGURE 7-29: G650 NLG FE MODEL FOR STRAIN GAUGE CALIBRATION

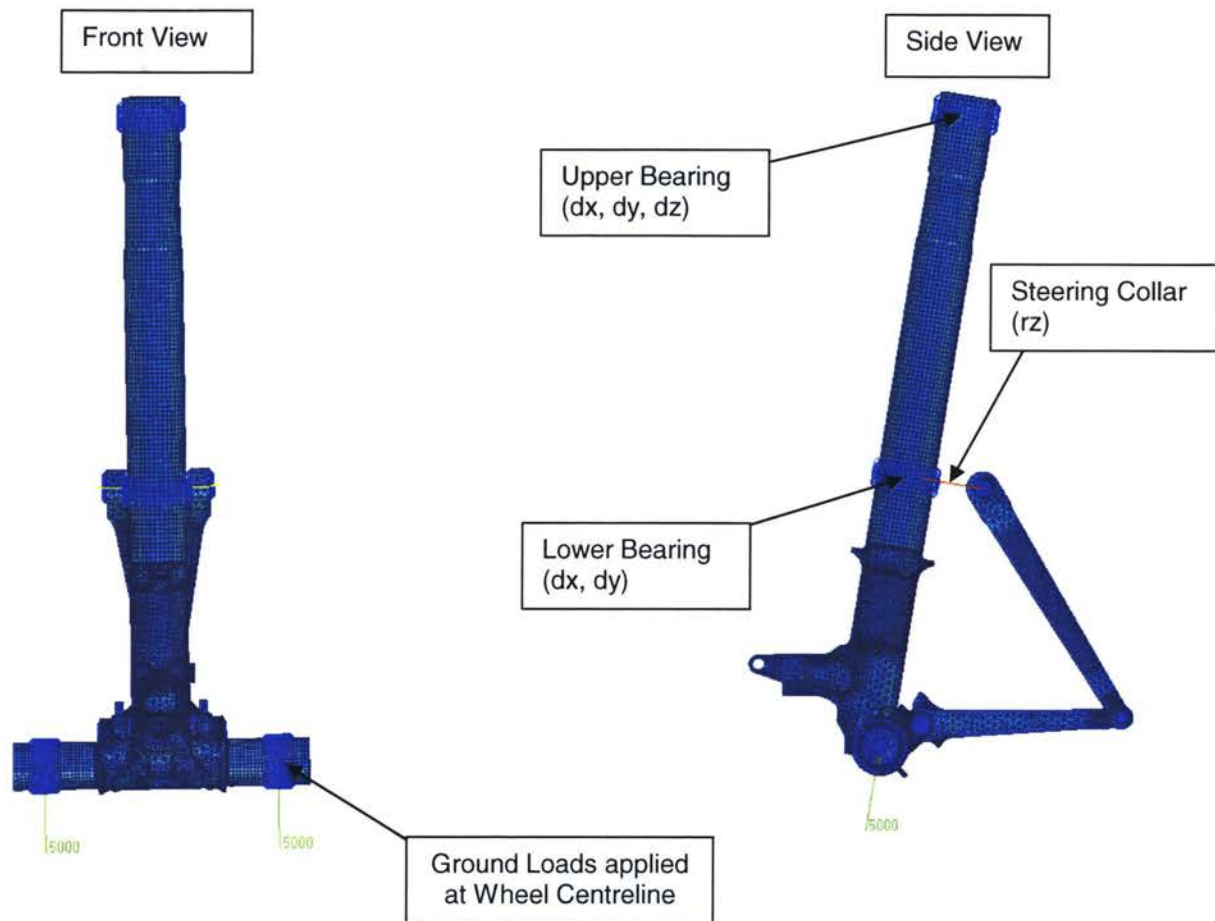


FIGURE 7-30: APPLIED LOADS AND BOUNDARY CONDITIONS

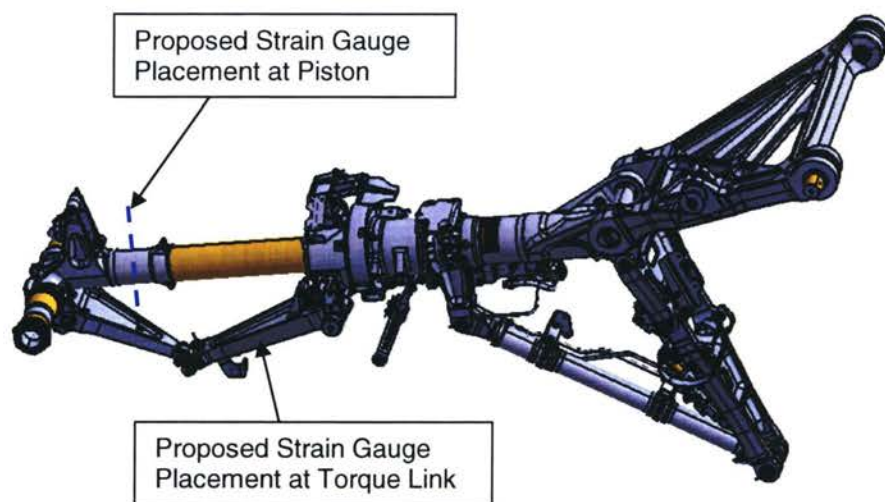


FIGURE 7-31: PROPOSED STRAIN GAUGE LOCATIONS

In total, five individual unit load cases were applied to the finite element model of the G650 NLG:

- Unit Drag 10 kips
- Unit Side 10 kips
- Unit Vertical 10 kips
- Unit MD 100 kips-in
- Unit MV 100 kips-in

A sample Von Mises stress plot for each case is given below:

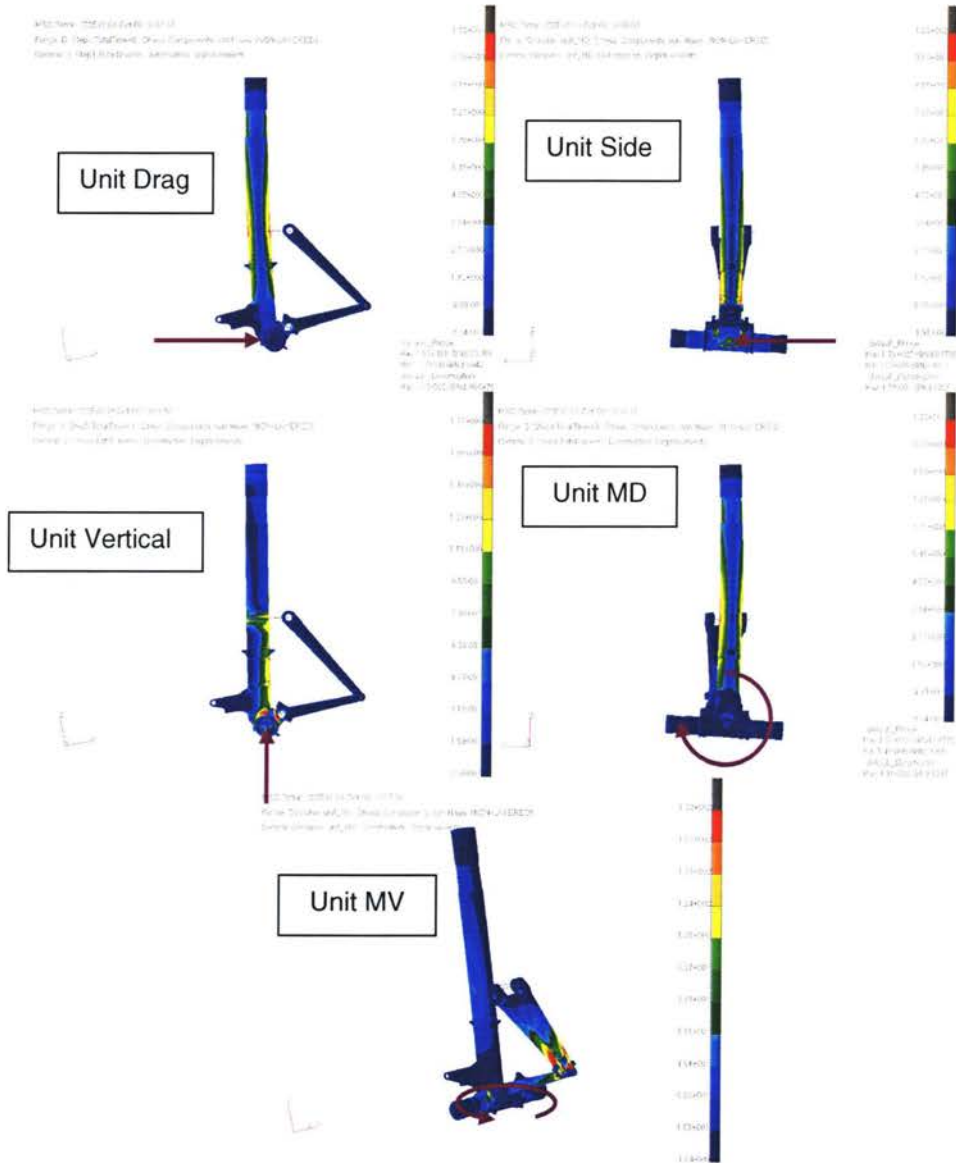


FIGURE 7-32: VON MISES STRESS PLOTS FOR UNIT CASES

Since the finite element model is 3D in nature, it is necessary to skin the outer surface of the the model with 2D elements in the two regions where the strain gauges will be placed. Since strain gauges are only capable of measuring planar strain levels, the stress data extracted from the finite element model must be planar as well. By placing 2D membrane elements on the surface of the model, the finite element model is able to output the planar stress levels. See below for a plot of the 2D elements used in the model:

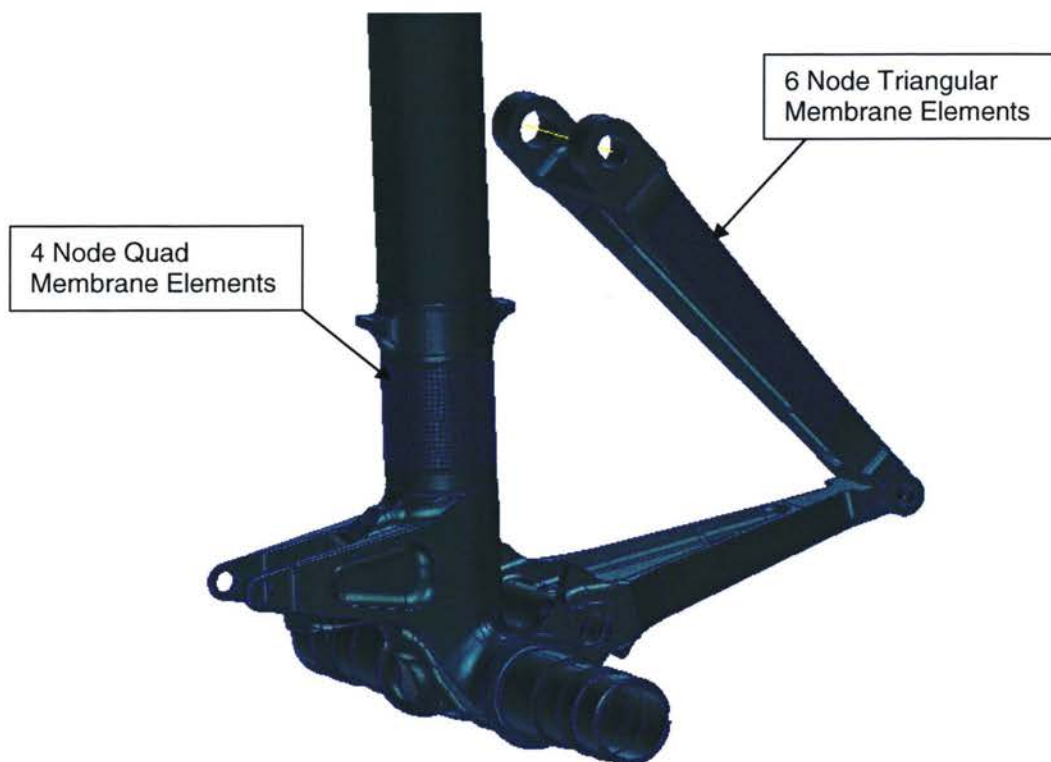


FIGURE 7-33: SKINNING OF PISTON AND TORQUE LINK

7.4.2 Unit Load Results

For analysis purposes, it has been assumed that the strain gauge locations on the piston are at the following locations:

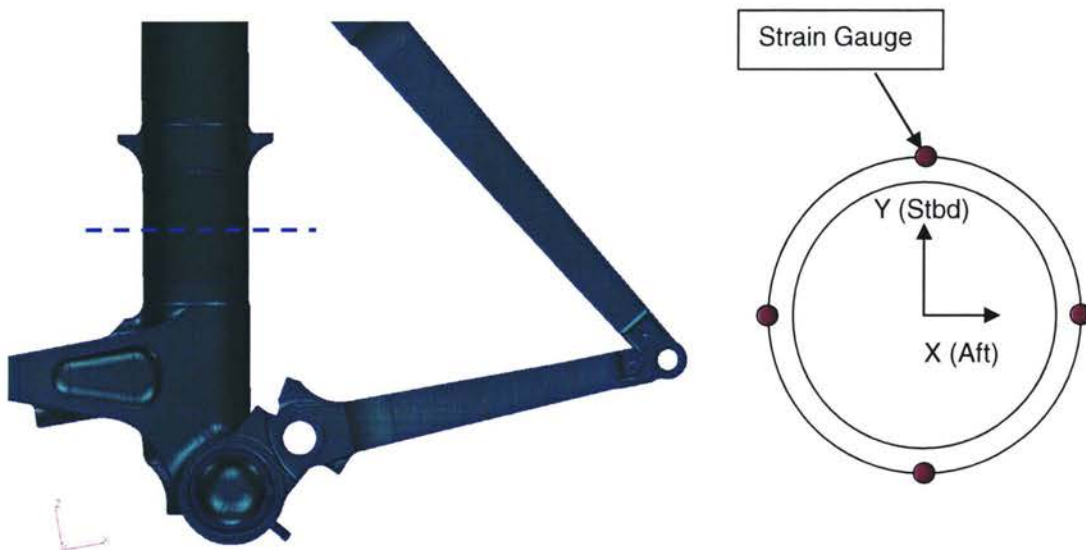


FIGURE 7-34: SAMPLE LOCATIONS FOR PISTON BARREL

Note: referring to section 7.7, the locations quoted above may not be the ideal location for accurate readings.

The upper torque link has been chosen as the location for reading strain levels on the torque link assembly:



FIGURE 7-35: STRAIN GAUGE LOCATION ON TORQUE LINK ASSY

From the finite element model that I have created, the following raw data for the chosen strain gauge locations is provided below. The stress data is outputted from MSC.Patran 2005r2 based on the 2D membrane elements used to skin the piston barrel and lower torque link.

TABLE 7-2: RAW FEM STRESS RESULTS

| Element | Location | Case | Stress (ksi) | | |
|---------|-------------|------|--------------|------------|-------------|
| | | | σ_x | σ_y | τ_{xy} |
| 201389 | Outboard | D | -0.666 | 0.303 | -1.023 |
| | | S | 0.146 | 6.102 | 1.078 |
| | | V | -0.080 | -0.557 | -0.081 |
| | | MD | 1.383 | 84.251 | 15.537 |
| | | MV | -0.710 | -21.807 | -3.810 |
| 200589 | Forward | D | 6.524 | 0.518 | 0.003 |
| | | S | 0.088 | 0.010 | -1.009 |
| | | V | 0.238 | 0.085 | 0.000 |
| | | MD | 0.927 | 0.105 | 1.439 |
| | | MV | 0.259 | 0.019 | 7.449 |
| 202189 | Aft | D | -5.492 | -0.340 | -1.556 |
| | | S | -0.416 | 0.604 | 1.011 |
| | | V | -1.333 | -0.081 | -0.397 |
| | | MD | 1.537 | 1.271 | 2.460 |
| | | MV | 2.923 | -4.128 | -6.812 |
| 199789 | Inboard | D | -0.669 | 0.143 | 1.052 |
| | | S | -0.157 | -6.109 | 1.077 |
| | | V | -0.080 | -0.576 | 0.084 |
| | | MD | -1.511 | -84.328 | 15.524 |
| | | MV | 0.680 | 21.782 | -3.814 |
| 157225 | Torque Link | D | -0.017 | -0.046 | 0.029 |
| | | S | -0.500 | -0.516 | 0.566 |
| | | V | -0.002 | -0.006 | 0.004 |
| | | MD | -0.938 | -0.581 | 0.937 |
| | | MV | -36.376 | -43.054 | 42.975 |

Based on the data above, the stress data is factored such that the force cases (D, S, V) are based on a 1 kip applied force and the moment cases (MD, MV) are based on a 1 kip-in moment. Based on Hooke's Law, the stress levels can then be converted into strain (see following page for the calculations).

TABLE 7-3: UNIT STRESS/STRAIN DATA

| Element | Location | Case | Stress (ksi) | | | Strain (μ) | | |
|---------|-------------|------|--------------|------------|-------------|------------------|--------------|---------------|
| | | | σ_x | σ_y | τ_{xy} | ϵ_x | ϵ_y | γ_{xy} |
| 201389 | Outboard | D | -0.317 | -0.046 | -1.124 | -10.4 | 1.9 | -102.3 |
| | | S | 6.290 | -0.043 | 0.079 | 217.4 | -70.9 | 7.2 |
| | | V | -0.570 | -0.066 | -0.001 | -18.9 | 4.0 | -0.1 |
| | | MD | 0.870 | -0.014 | 0.016 | 30.2 | -10.1 | 1.5 |
| | | MV | -0.225 | 0.000 | -0.003 | -7.7 | 2.5 | -0.2 |
| 200589 | Forward | D | 6.524 | 0.518 | -0.003 | 219.2 | -54.1 | -0.2 |
| | | S | 0.088 | 0.010 | 1.009 | 2.9 | -0.6 | 91.8 |
| | | V | 0.238 | 0.085 | 0.000 | 7.3 | 0.3 | 0.0 |
| | | MD | 0.009 | 0.001 | -0.014 | 0.3 | -0.1 | -1.3 |
| | | MV | 0.003 | 0.000 | -0.074 | 0.1 | 0.0 | -6.8 |
| 202189 | Aft | D | -5.924 | 0.093 | -0.061 | -205.3 | 68.6 | -5.6 |
| | | S | 0.203 | -0.015 | -1.127 | 7.1 | -2.7 | -102.6 |
| | | V | -1.448 | 0.034 | 0.001 | -50.3 | 17.2 | 0.1 |
| | | MD | 0.028 | 0.000 | -0.020 | 1.0 | -0.3 | -1.8 |
| | | MV | -0.013 | 0.001 | 0.076 | -0.4 | 0.2 | 7.0 |
| 199789 | Inboard | D | -0.212 | -0.315 | 1.127 | -3.8 | -8.5 | 102.6 |
| | | S | -6.297 | 0.031 | 0.078 | -217.5 | 70.5 | 7.1 |
| | | V | -0.590 | -0.066 | 0.001 | -19.6 | 4.2 | 0.1 |
| | | MD | -0.871 | 0.013 | 0.016 | -30.2 | 10.1 | 1.5 |
| | | MV | 0.224 | 0.000 | -0.003 | 7.7 | -2.5 | -0.2 |
| 157225 | Torque Link | D | -0.064 | 0.000 | 0.000 | -6.2 | 2.1 | 0.0 |
| | | S | -1.018 | 0.001 | -0.248 | -98.8 | 32.7 | -64.0 |
| | | V | -0.009 | 0.000 | 0.000 | -0.8 | 0.3 | 0.0 |
| | | MD | -0.015 | 0.000 | -0.006 | -1.5 | 0.5 | -1.5 |
| | | MV | -0.796 | 0.002 | -0.164 | -77.3 | 25.7 | -42.2 |

7.4.3 Post Load Equation Development for G650

From section 7.3.2, the basic equation for strain at the piston barrel is:

$$\epsilon_x = \frac{1}{E}(\sigma_x - \nu\sigma_y) = \frac{1}{E}[(\sigma_x(D,S) + \sigma_x(MD,MS) + \sigma_x(V)) - \nu\sigma_y(V)] \tag{7.3.24}$$

As a result of this equation, the following system of linear equations can be derived:

$$[A] \begin{Bmatrix} D \\ S \\ V \\ MD \\ MV \end{Bmatrix} = \begin{Bmatrix} \epsilon_{OUTBD} \\ \epsilon_{FWD} \\ \epsilon_{AFT} \\ \epsilon_{INBD} \\ \epsilon_{TIL} \end{Bmatrix} \tag{7.4.1}$$

From the data provided in Table 7-3, the system of linear equations is as follows:

$$\begin{pmatrix} -10.4 & 217.4 & -18.9 & 30.2 & -7.7 \\ 219.2 & 2.9 & 7.3 & 0.3 & 0.1 \\ -205.3 & 7.1 & -50.3 & 1.0 & -0.4 \\ -3.8 & -217.5 & -19.6 & -30.2 & 7.7 \\ -6.2 & -98.8 & -0.8 & -1.5 & -77.3 \end{pmatrix} \begin{Bmatrix} D \\ S \\ V \\ MD \\ MV \end{Bmatrix} = \begin{Bmatrix} \epsilon_{OUTBD} \\ \epsilon_{FWD} \\ \epsilon_{AFT} \\ \epsilon_{INBD} \\ \epsilon_{T/L} \end{Bmatrix}$$

Since the strain gauge coefficients are constant, the post loads can be solved for any combination of strain readings at the five strain gauge locations via the following equation:

$$\begin{Bmatrix} D \\ S \\ V \\ MD \\ MV \end{Bmatrix} = [A]^{-1} \begin{Bmatrix} \epsilon_{OUTBD} \\ \epsilon_{FWD} \\ \epsilon_{AFT} \\ \epsilon_{INBD} \\ \epsilon_{T/L} \end{Bmatrix} \quad (7.4.2)$$

Solving for the inverse of matrix A:

$$\begin{Bmatrix} D \\ S \\ V \\ MD \\ MV \end{Bmatrix} = \begin{pmatrix} -0.003338 & 0.003843 & 0.000089 & -0.003487 & 0.000038 \\ -0.182146 & -0.076035 & -0.040243 & -0.178716 & -0.003327 \\ 0.117182 & 0.027526 & 0.000400 & 0.116692 & 0.000147 \\ 1.284364 & 0.559409 & 0.296430 & 1.371798 & 0.013164 \\ 0.227684 & 0.094229 & 0.049894 & 0.219639 & -0.041957 \end{pmatrix} \begin{Bmatrix} \epsilon_{OUTBD} \\ \epsilon_{FWD} \\ \epsilon_{AFT} \\ \epsilon_{INBD} \\ \epsilon_{T/L} \end{Bmatrix}$$

As a result of this series of linear equations, the amount of calibration required for this type of strain gauge layout is quite limited. In essence, only 5 load cases may need to be applied to the static test unit to create the strain gauge coefficient matrix A.

It should be noted that the equations derived above assumed that there is no internal pressure at the strain gauge locations on the piston barrel. In reality, there will be internal hoop pressure applied at the strain gauge locations. For the final configuration, an additional strain gauge will be required to measure the strain due to hoop stress. Therefore, the strain gauge readings at the four other locations can be corrected for the hoop stress component.

7.5 **Strain Gauge Data Acquisition**

The equations derived in sections 7.1 and 7.3 are independent of the type of strain gauge chosen for the ODHMS system. The equations only require the strain levels to be output from the strain gauge data acquisition system. For further discussion on the sensing system options, refer to section 3.1.

7.6 **Sensitivity to Temperature**

It will be necessary for the strain monitoring system to correct for temperature. In general, landing gear design requires that the landing gear be able to function between temperatures of -45°C to 70°C . However, in components that are close to the brakes, the temperature requirements may be increased to values of 300°C . Generally speaking, the regions that the strain gauges will be placed on the piston and torque links will not be exposed to the maximum brake temperatures. However, the temperature exposure may be higher than 70°C .

7.7 Strain Gauge Time-Lag

It may be possible that one or more strain gauges may have time lag in reading and outputting data. In other words, it may be possible that one or more strain gauges may not be in the same time sequence as the overall system. As a result of this potential time-lag, it is necessary to investigate the system's sensitivity to time-lag. In this section, the following assumptions are made:

1. 45 degree configuration (see section 7.8.1.3 for definition)
2. Forward-Outboard gauge is out-of-sequence
3. A dynamic landing event has occurred
4. G650 landing simulation results used in analysis

7.7.1 Sample Dynamic Landing Event

The figure below illustrates the predicted shock strut stroke, vertical and drag loads for a dynamic landing event with the following parameters. The simulation results are provided by GLG:

WOG = 12851.5 LB (Weight on Gear)
 Vsink = 10 ft/s (sink/descent speed)
 Vapp = 137.8 kts (aircraft approach speed)

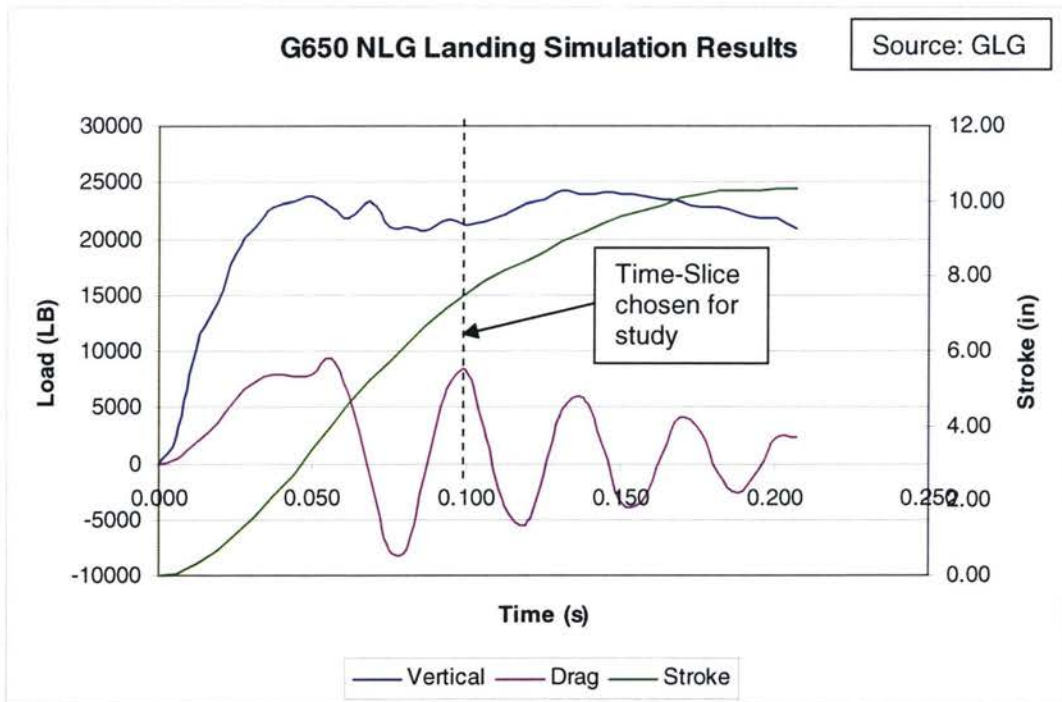


TABLE 7-4: SAMPLE DYNAMIC LANDING EVENT

TABLE 7-5: SENSITIVITY TO STRAIN GAUGE TIME-LAG

| Post Load (kips) | Time-Lag (s) | | | | | |
|------------------|--------------|--------|--------|--------|---------|---------------|
| | 0.003 | 0.001 | 0.0005 | 0.0001 | 0.00005 | 0 |
| D | 5.054 | 6.073 | 6.328 | 6.532 | 6.558 | 6.583 |
| S | -18.410 | -6.137 | -3.068 | -0.614 | -0.307 | 0.000 |
| V | 27.399 | 23.634 | 22.693 | 21.940 | 21.846 | 21.752 |
| MD | 144.927 | 48.309 | 24.155 | 4.831 | 2.415 | 0.000 |
| MV | 20.835 | 6.945 | 3.472 | 0.694 | 0.347 | 0.000 |

From the table above, the time-lag error becomes acceptable at 0.0001 seconds. The error in both side load and MD moment are such that little impact would be seen in terms of yielding and fatigue-life prediction on various components.

7.8 Sensitivity of Load Predictions to Strain Gauge Placement

Based on the equations presented in section 7.4.3, this section investigates the sensitivity of strain gauge placement to the errors in post load prediction. The following strain gauge configurations are investigated at the piston barrel:

- 90 degree configuration (as presented in section 7.4.2)
- 30, 45, and 60 degree configurations

7.8.1 Sensitivity Analysis Results – Vertical and Drag

The sensitivity analysis assumes the following:

- error in strain gauge reading at the most forward strain gauge location
- spin-up load condition (i.e. high drag and vertical load) which is typical for landing scenarios – see section 7.7.1 for the spin-up load case definition)

| | | | |
|------|--------|--------|-------------------------------------|
| Time | 0.094 | s | } Post Loads used for all scenarios |
| D | 6.583 | kips | |
| S | 0.000 | kips | |
| V | 21.752 | kips | |
| MD | 0.000 | kip-in | |
| MV | 0.000 | kip-in | |

7.8.1.1 90 Degree Analysis

Based on the applied loads in section 7.8.1, the predicted strain levels are (see Table 7-3 for unit strain data):

TABLE 7-6: CALCULATED STRAIN LEVELS FOR THE 90 DEG CONFIGURATION

| Time (s) | $\epsilon_x (\mu)$ | | | | |
|----------|--------------------|-------------|-------|---------|-----|
| | Outboard | Forward | Aft | Inboard | T/L |
| 0.094 | -480 | 1601 | -2446 | -452 | -59 |

The resulting error by varying the strain gauge output is:

TABLE 7-7: SIDE LOAD ERROR FOR THE 90 DEG CONFIGURATION

| Strain Ratio | Fwd-Inbd Reading (μ) | Side Load (kips) |
|--------------|----------------------------|------------------|
| 1.10 | 1761 | 173.702 |
| 1.05 | 1681 | 86.851 |
| 1.00 | 1601 | 0.000 |
| 0.95 | 1521 | -86.851 |
| 0.90 | 1441 | -173.702 |

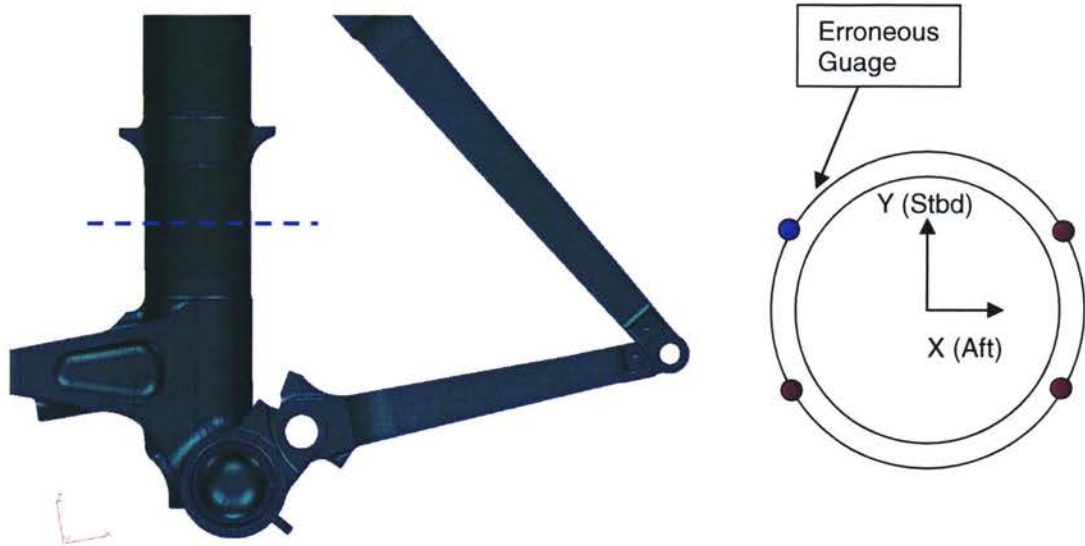


FIGURE 7-36: SAMPLE LOCATIONS FOR PISTON BARREL

For the 30 degree location, the unit stress data and A matrix are as follows:

TABLE 7-8: UNIT STRESS/STRAIN DATA (30 DEG CONFIG)

| Location | Case | Stress (ksi) | | | Strain (μ) | | |
|-----------|------|--------------|------------|-------------|------------------|--------------|---------------|
| | | σ_x | σ_y | τ_{xy} | ϵ_x | ϵ_y | γ_{xy} |
| Aft Inbd | D | -5.181 | 0.177 | 0.643 | -180.6 | 63.3 | 58.6 |
| | S | -3.020 | 0.187 | -0.933 | -106.2 | 39.8 | -84.9 |
| | V | -1.319 | 0.036 | -0.004 | -45.9 | 15.8 | -0.4 |
| | MD | -0.396 | 0.011 | -0.007 | -13.8 | 4.7 | -0.6 |
| | MV | 0.107 | -0.005 | 0.065 | 3.8 | -1.3 | 5.9 |
| Fwd Inbd | D | 5.569 | 0.168 | 0.503 | 190.2 | -55.7 | 45.8 |
| | S | -3.081 | -0.240 | 0.902 | -103.6 | 25.7 | 82.1 |
| | V | 0.123 | 0.038 | 0.001 | 3.8 | 0.0 | 0.1 |
| | MD | -0.444 | -0.036 | -0.010 | -14.9 | 3.6 | -0.9 |
| | MV | 0.110 | 0.003 | -0.066 | 3.8 | -1.1 | -6.0 |
| Fwd Outbd | D | 5.645 | 0.174 | -0.504 | 192.7 | -56.3 | -45.9 |
| | S | 3.222 | 0.245 | 0.904 | 108.4 | -27.1 | 82.3 |
| | V | 0.134 | 0.039 | -0.001 | 4.2 | -0.1 | -0.1 |
| | MD | 0.459 | 0.037 | -0.010 | 15.4 | -3.8 | -0.9 |
| | MV | -0.105 | -0.003 | -0.066 | -3.6 | 1.1 | -6.0 |
| Aft Outbd | D | -5.114 | 0.170 | -0.644 | -178.2 | 62.3 | -58.6 |
| | S | 2.889 | -0.180 | -0.935 | 101.6 | -38.1 | -85.1 |
| | V | -1.312 | 0.036 | 0.004 | -45.6 | 15.7 | 0.4 |
| | MD | 0.382 | -0.010 | -0.007 | 13.3 | -4.6 | -0.6 |
| | MV | -0.111 | 0.005 | 0.065 | -3.9 | 1.4 | 5.9 |
| Torque | D | -0.064 | 0.000 | 0.000 | -6.2 | 2.1 | 0.0 |

| Location | Case | Stress (ksi) | | | Strain (μ) | | |
|----------|------|--------------|------------|-------------|------------------|--------------|---------------|
| | | σ_x | σ_y | τ_{xy} | ϵ_x | ϵ_y | γ_{xy} |
| Link | S | -1.018 | 0.001 | -0.248 | -98.8 | 32.7 | -64.0 |
| | V | -0.009 | 0.000 | 0.000 | -0.8 | 0.3 | 0.0 |
| | MD | -0.015 | 0.000 | -0.006 | -1.5 | 0.5 | -1.5 |
| | MV | -0.796 | 0.002 | -0.164 | -77.3 | 25.7 | -42.2 |

From the data provided in Table 7-8, the system of linear equations is as follows:

$$\begin{pmatrix} -180.6 & -106.2 & -45.9 & -13.8 & 3.8 \\ 190.2 & -103.6 & 3.8 & -14.9 & 3.8 \\ 192.7 & 108.4 & 4.2 & 15.4 & -3.6 \\ -178.2 & 101.6 & -45.6 & 13.3 & -3.9 \\ -6.2 & -98.8 & -0.8 & -1.5 & -77.3 \end{pmatrix} \begin{Bmatrix} D \\ S \\ V \\ MD \\ MV \end{Bmatrix} = \begin{Bmatrix} \epsilon_{OUTBD} \\ \epsilon_{FWD} \\ \epsilon_{AFT} \\ \epsilon_{INBD} \\ \epsilon_{T/L} \end{Bmatrix}$$

Based on the applied loads in section 7.8.1, the predicted strain levels are:

TABLE 7-9: CALCULATED STRAIN LEVELS FOR THE 30 DEG CONFIGURATION

| Time (s) | $\epsilon_x (\mu)$ | | | | |
|----------|--------------------|-------------|-----------|-----------|-----|
| | Aft Inbd | Fwd Inbd | Fwd Outbd | Aft Outbd | T/L |
| 0.094 | -2187 | 1336 | 1360 | -2166 | -59 |

The resulting side load error by varying the strain gauge output is:

TABLE 7-10: SIDE LOAD ERROR FOR THE 30 DEG CONFIGURATION

| Strain Ratio | Fwd-Inbd Reading (μ) | Side Load (kips) |
|--------------|----------------------------|------------------|
| 1.10 | 1469 | 5.958 |
| 1.05 | 1402 | 2.979 |
| 1.00 | 1336 | 0.000 |
| 0.95 | 1269 | -2.979 |
| 0.90 | 1202 | -5.958 |

7.8.1.3 45 Degree Analysis

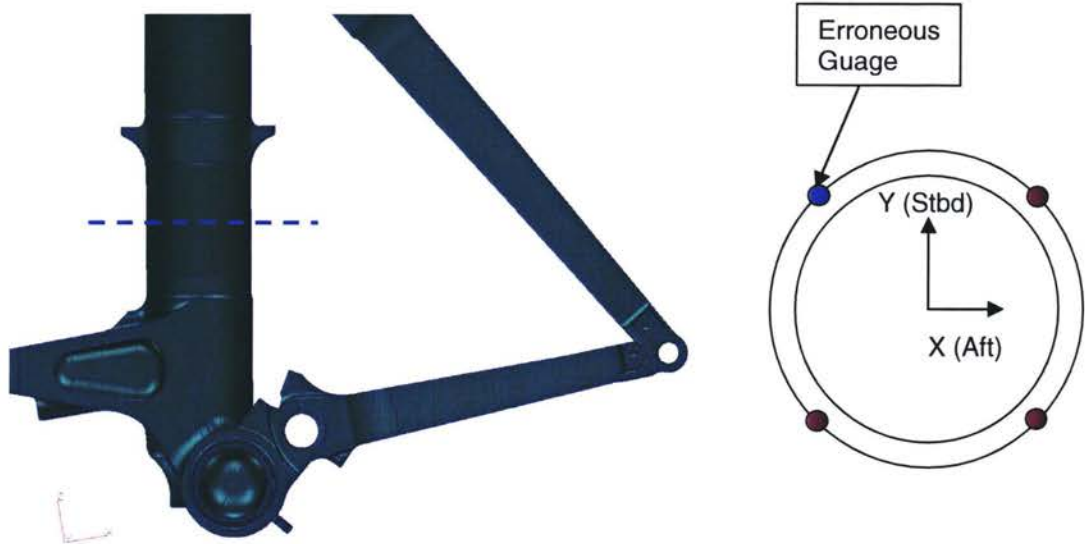


FIGURE 7-37: SAMPLE LOCATIONS FOR PISTON BARREL

For the 45 degree location, the unit stress data and A matrix are as follows:

TABLE 7-11: UNIT STRESS/STRAIN DATA (45 DEG CONFIG)

| Location | Case | Stress (ksi) | | | Strain (μ) | | |
|-----------|------|--------------|------------|-------------|------------------|--------------|---------------|
| | | σ_x | σ_y | τ_{xy} | ϵ_x | ϵ_y | γ_{xy} |
| Aft Inbd | D | -4.168 | 0.169 | 0.913 | -145.6 | 51.8 | 83.1 |
| | S | -4.386 | 0.242 | -0.696 | -153.9 | 56.8 | -63.4 |
| | V | -1.153 | 0.023 | -0.001 | -40.0 | 13.5 | -0.1 |
| | MD | -0.582 | 0.022 | 0.006 | -20.3 | 7.2 | 0.6 |
| | MV | 0.158 | -0.005 | 0.051 | 5.5 | -1.9 | 4.6 |
| Fwd Inbd | D | 4.269 | -0.168 | 0.766 | 149.1 | -52.9 | 69.7 |
| | S | -4.594 | -0.274 | 0.738 | -155.4 | 41.2 | 67.2 |
| | V | -0.032 | -0.013 | 0.001 | -0.9 | -0.1 | 0.1 |
| | MD | -0.657 | -0.038 | -0.004 | -22.2 | 5.9 | -0.4 |
| | MV | 0.162 | 0.003 | -0.053 | 5.6 | -1.7 | -4.9 |
| Fwd Outbd | D | 4.397 | -0.156 | -0.768 | 153.3 | -53.9 | -69.9 |
| | S | 4.709 | 0.270 | 0.740 | 159.4 | -42.7 | 67.4 |
| | V | -0.016 | -0.012 | -0.001 | -0.4 | -0.2 | -0.1 |
| | MD | 0.669 | 0.037 | -0.004 | 22.7 | -6.1 | -0.4 |
| | MV | -0.159 | -0.004 | -0.053 | -5.4 | 1.6 | -4.9 |
| Aft Outbd | D | -4.062 | 0.160 | -0.910 | -141.8 | 50.4 | -82.9 |
| | S | 4.280 | -0.238 | -0.700 | 150.2 | -55.4 | -63.7 |
| | V | -1.141 | 0.022 | 0.002 | -39.6 | 13.4 | 0.1 |
| | MD | 0.571 | -0.021 | 0.006 | 19.9 | -7.0 | 0.5 |
| | MV | -0.161 | 0.005 | 0.051 | -5.6 | 2.0 | 4.6 |
| Torque | D | -0.064 | 0.000 | 0.000 | -6.2 | 2.1 | 0.0 |

| Location | Case | Stress (ksi) | | | Strain (μ) | | |
|----------|------|--------------|------------|-------------|------------------|--------------|---------------|
| | | σ_x | σ_y | τ_{xy} | ϵ_x | ϵ_y | γ_{xy} |
| Link | S | -1.018 | 0.001 | -0.248 | -98.8 | 32.7 | -64.0 |
| | V | -0.009 | 0.000 | 0.000 | -0.8 | 0.3 | 0.0 |
| | MD | -0.015 | 0.000 | -0.006 | -1.5 | 0.5 | -1.5 |
| | MV | -0.796 | 0.002 | -0.164 | -77.3 | 25.7 | -42.2 |

From the data provided in Table 7-11, the system of linear equations is as follows:

$$\begin{pmatrix} -145.6 & -153.9 & -40.0 & -20.3 & 5.5 \\ 149.1 & -155.4 & -0.9 & -22.2 & 5.6 \\ 153.3 & 159.4 & -0.4 & 22.7 & -5.4 \\ -141.8 & 150.2 & -39.6 & 19.9 & -5.6 \\ -6.2 & -98.8 & -0.8 & -1.5 & -77.3 \end{pmatrix} \begin{Bmatrix} D \\ S \\ V \\ MD \\ MV \end{Bmatrix} = \begin{Bmatrix} \epsilon_{OUTBD} \\ \epsilon_{FWD} \\ \epsilon_{AFT} \\ \epsilon_{INBD} \\ \epsilon_{T/L} \end{Bmatrix}$$

Based on the applied loads in section 7.8.1, the predicted strain levels are:

TABLE 7-12: CALCULATED STRAIN LEVELS FOR THE 45 DEG CONFIGURATION

| Time (s) | ϵ_x (μ) | | | | |
|----------|------------------------|------------|-----------|-----------|-----|
| | Aft Inbd | Fwd Inbd | Fwd Outbd | Aft Outbd | T/L |
| 0.094 | -1829 | 961 | 1000 | -1795 | -59 |

The resulting side load error by varying the strain gauge output is:

TABLE 7-13: SIDE LOAD ERROR FOR THE 45 DEG CONFIGURATION

| Strain Ratio | Fwd-Inbd Reading (μ) | Side Load (kips) |
|--------------|----------------------------|------------------|
| 1.10 | 1057 | 3.677 |
| 1.05 | 1009 | 1.839 |
| 1.00 | 961 | 0.000 |
| 0.95 | 913 | -1.839 |
| 0.90 | 865 | -3.677 |

7.8.1.4 60 Degree Analysis

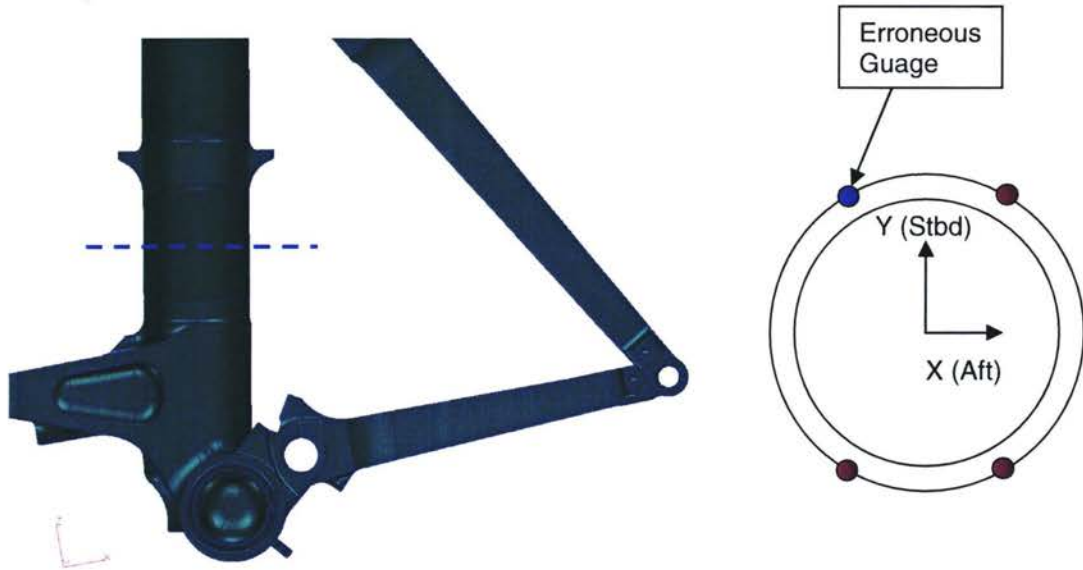


FIGURE 7-38: SAMPLE LOCATIONS FOR PISTON BARREL

For the 60 degree location, the unit stress data and A matrix are as follows:

TABLE 7-14: UNIT STRESS/STRAIN DATA (60 DEG CONFIG)

| Location | Case | Stress (ksi) | | | Strain (μ) | | |
|-----------|------|--------------|------------|-------------|------------------|--------------|---------------|
| | | σ_x | σ_y | τ_{xy} | ϵ_x | ϵ_y | γ_{xy} |
| Aft Inbd | D | -3.319 | 0.091 | 1.036 | -115.5 | 39.8 | 94.3 |
| | S | -5.140 | 0.241 | -0.510 | -179.9 | 65.0 | -46.4 |
| | V | -1.023 | 0.002 | 0.001 | -35.3 | 11.4 | 0.1 |
| | MD | -0.689 | 0.027 | 0.014 | -24.1 | 8.5 | 1.2 |
| | MV | 0.185 | -0.004 | 0.039 | 6.4 | -2.2 | 3.5 |
| Fwd Inbd | D | 2.666 | -0.380 | 0.963 | 96.1 | -42.5 | 87.7 |
| | S | -5.684 | -0.217 | 0.524 | -193.6 | 55.2 | 47.7 |
| | V | -0.228 | -0.056 | 0.000 | -7.2 | 0.6 | 0.0 |
| | MD | -0.805 | -0.024 | 0.003 | -27.5 | 8.0 | 0.3 |
| | MV | 0.201 | 0.003 | -0.037 | 6.9 | -2.1 | -3.3 |
| Fwd Outbd | D | 2.824 | -0.369 | -0.966 | 101.5 | -43.9 | -87.9 |
| | S | 5.762 | 0.205 | 0.523 | 196.4 | -56.5 | 47.6 |
| | V | -0.209 | -0.056 | 0.000 | -6.6 | 0.4 | 0.0 |
| | MD | 0.813 | 0.023 | 0.003 | 27.8 | -8.2 | 0.3 |
| | MV | -0.199 | -0.004 | -0.037 | -6.8 | 2.1 | -3.3 |
| Aft Outbd | D | -3.187 | 0.083 | -1.030 | -110.8 | 38.0 | -93.7 |
| | S | 5.048 | -0.241 | -0.515 | 176.7 | -64.0 | -46.9 |
| | V | -1.007 | 0.001 | 0.000 | -34.8 | 11.2 | 0.0 |
| | MD | 0.679 | -0.027 | 0.013 | 23.7 | -8.4 | 1.2 |
| | MV | -0.187 | 0.004 | 0.039 | -6.5 | 2.2 | 3.5 |
| Torque | D | -0.064 | 0.000 | 0.000 | -6.2 | 2.1 | 0.0 |

| Location | Case | Stress (ksi) | | | Strain (μ) | | |
|----------|------|--------------|------------|-------------|------------------|--------------|---------------|
| | | σ_x | σ_y | τ_{xy} | ϵ_x | ϵ_y | γ_{xy} |
| Link | S | -1.018 | 0.001 | -0.248 | -98.8 | 32.7 | -64.0 |
| | V | -0.009 | 0.000 | 0.000 | -0.8 | 0.3 | 0.0 |
| | MD | -0.015 | 0.000 | -0.006 | -1.5 | 0.5 | -1.5 |
| | MV | -0.796 | 0.002 | -0.164 | -77.3 | 25.7 | -42.2 |

From the data provided in Table 7-14, the system of linear equations is as follows:

$$\begin{pmatrix} -115.5 & -179.9 & -35.3 & -24.1 & 6.4 \\ 96.1 & -193.6 & -7.2 & -27.5 & 6.9 \\ 101.5 & 196.4 & -6.6 & 27.8 & -6.8 \\ -110.8 & 176.7 & -34.8 & 23.7 & -6.5 \\ -6.2 & -98.8 & -0.8 & -1.5 & -77.3 \end{pmatrix} \begin{Bmatrix} D \\ S \\ V \\ MD \\ MV \end{Bmatrix} = \begin{Bmatrix} \epsilon_{OUTBD} \\ \epsilon_{FWD} \\ \epsilon_{AFT} \\ \epsilon_{INBD} \\ \epsilon_{T/L} \end{Bmatrix}$$

Based on the applied loads in section 7.8.1, the predicted strain levels are:

TABLE 7-15: CALCULATED STRAIN LEVELS FOR THE 60 DEG CONFIGURATION

| Time (s) | ϵ_x (μ) | | | | |
|----------|------------------------|----------|-----------|-----------|-----|
| | Aft Inbd | Fwd Inbd | Fwd Outbd | Aft Outbd | T/L |
| 0.094 | -1528 | 476 | 524 | -1486 | -59 |

The resulting side load error by varying the strain gauge output is:

TABLE 7-16: SIDE LOAD ERROR FOR THE 60 DEG CONFIGURATION

| Strain Ratio | Fwd-Inbd Reading (μ) | Side Load (kips) |
|--------------|----------------------------|------------------|
| 1.10 | 523 | 1.996 |
| 1.05 | 499 | 0.998 |
| 1.00 | 476 | 0.000 |
| 0.95 | 452 | -0.998 |
| 0.90 | 428 | -1.996 |

7.8.1.5 Summary of Results – Vertical and Drag Case

Below is a table and graph summarizing the sensitivity results:

TABLE 7-17: SUMMARY OF SIDE LOAD ERROR (VERTICAL + DRAG CASE)

| Strain Ratio | Side Load Error (kips) | | | |
|--------------|------------------------|--------------|--------------|--------------|
| | 0 deg | 30 deg | 45 deg | 60 deg |
| 1.10 | 173.702 | 5.958 | 3.677 | 1.996 |
| 1.05 | 86.851 | 2.979 | 1.839 | 0.998 |
| 1.00 | 0.000 | 0.000 | 0.000 | 0.000 |
| 0.95 | -86.851 | -2.979 | -1.839 | -0.998 |
| 0.90 | -173.702 | -5.958 | -3.677 | -1.996 |

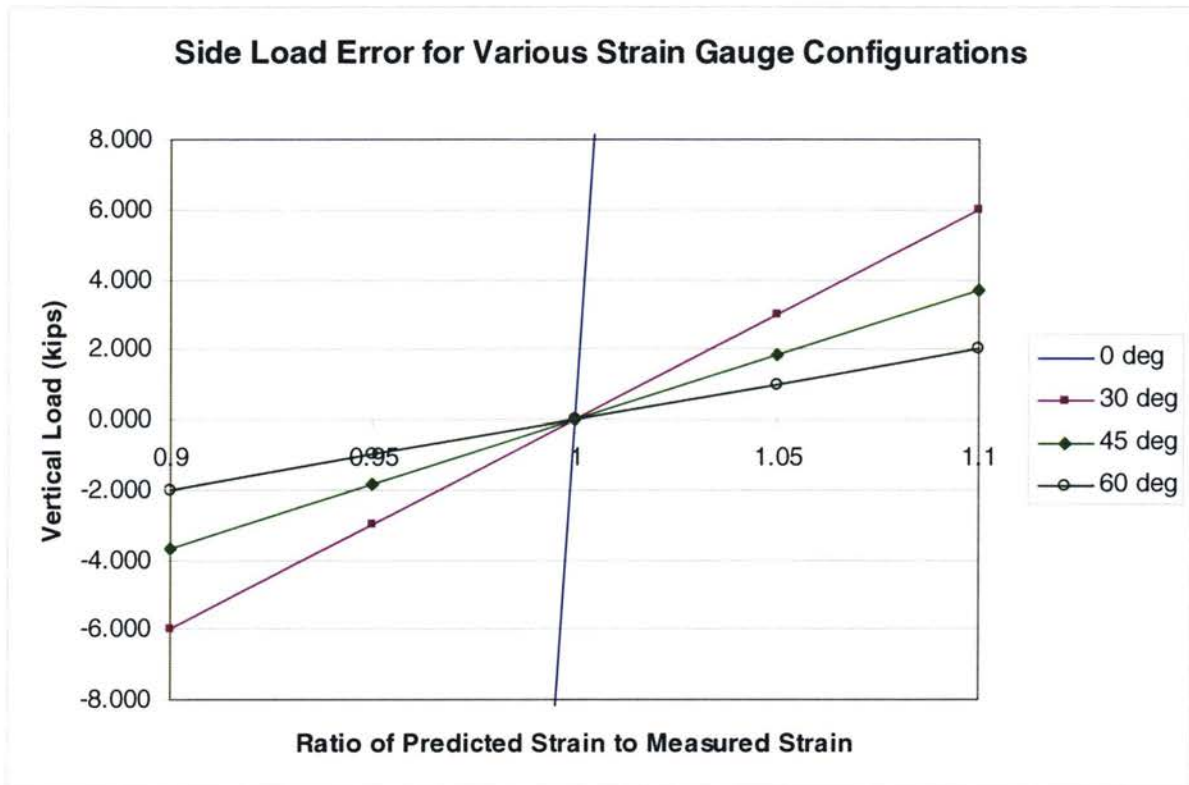


FIGURE 7-39: SUMMARY OF SIDE LOAD ERROR (VERTICAL + DRAG)

From the table and graph above, the 60 degree location is the least sensitive to strain gauge reading inaccuracies due to its shallow slope.

7.8.2 Sensitivity Analysis Results – Vertical and Side

From the previous section, it was concluded that the 60 degree strain gauge configuration is the least sensitive to strain gauge errors. In order to confirm this conclusion, combinations of vertical and side load were analyzed in the same manner as the previous section. The results are summarized in the table and graph below:

| | | | |
|----|--------|--------|-------------------------------------|
| D | 0.000 | kip | } Post Loads used for all scenarios |
| S | 6.583 | kip | |
| V | 21.752 | kip | |
| MD | 0.000 | kip-in | |
| MV | 0.000 | kip-in | |

In this sensitivity study, the aft-inbd location was chosen since this strain gauge will see high strain levels for combinations of vertical and side load.

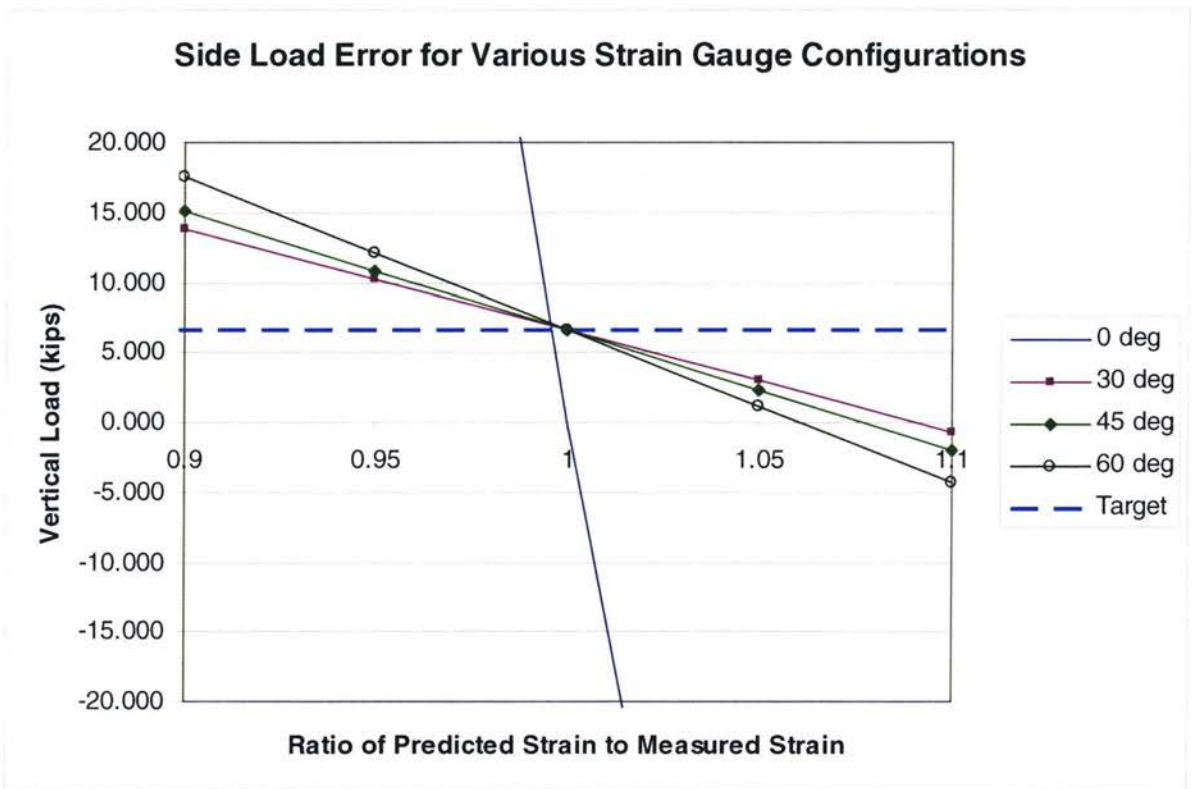


FIGURE 7-40: SUMMARY OF SIDE LOAD ERROR (VERTICAL + SIDE)

From the graph above, the 30 degree location is least sensitive to strain gauge reading errors. Depending on the types of loads the landing gear will undergo while in-service, it may be optimum to place the strain gauges at the 45 degree location in order to minimize the error for side load and drag load cases.

7.9 Data Reduction for Static and Fatigue Analysis

In order to speed up the static and fatigue analysis of the SHM system, the raw strain data will need to be processed and reduced to manageable levels. The data reduction method will attempt to identify two types of data to be eliminated from the analysis:

- data points between peaks and valleys of load eliminated
- small strain-level vibrations eliminated

7.9.1 Intermediate Data Point Elimination

In landing gear structure, applied loads take variable amounts of time to reach their maximum magnitudes. For instance, a ground maneuver may take seconds to generate full load levels whereas a landing case may take milliseconds. As a result, the SHM system must be designed to detect the maximum and minimum ground loads for both types of loading states. This requirement will result in large amounts of strain data that is not useful in the analysis since this data will lie between the maximum and minimum load levels (i.e. peaks and valleys).

An example of intermediate data point elimination is provided below:

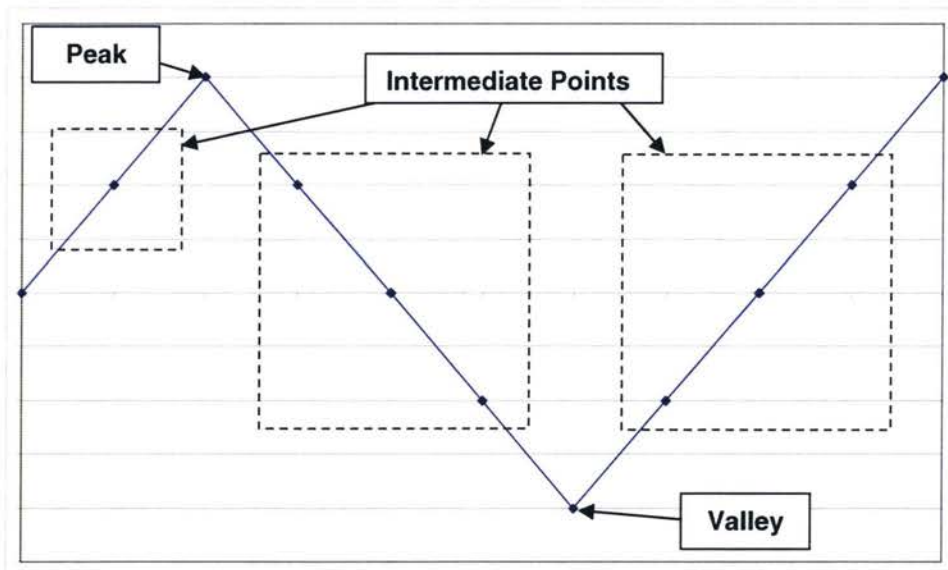


FIGURE 7-41: EXAMPLE OF INTERMEDIATE DATA ELIMINATION

An algorithm will be developed to eliminate these intermediate strain levels. Since the SHM system will require a minimum of 6 strain gauges, the algorithm developed may be quite complex. Initially, the data elimination algorithm will take the absolute strain at each strain gauge and calculate the sum of these strains at each time slice:

$$|\Sigma \varepsilon_T| = \sum_{i=1}^n |\varepsilon_i| \quad (7.9.1)$$

where:

$|\Sigma \varepsilon_T| =$ absolute total strain of all strain gauges for a given time slice

$|\varepsilon_i| =$ absolute strain for a given strain gauge

To prove the fidelity of this algorithm, the landing simulation event provided in section 7.7 is used. The applied ground loads and the resulting strain levels are tabulated below for this simulation:

TABLE 7-18: LANDING SIMULATION GROUND LOADS AND STRAINS

| Time (s) | Stroke (in) | Drag (kips) | Side (kips) | Vertical (kips) | MD (kips-in) | MV (kips-in) | ε_x (μ) | | | | | $ \Sigma \varepsilon_T $ |
|-------------|----------------|----------------|----------------|--------------------|-----------------|-----------------|---------------------------|-------|-------|------|-----|--------------------------|
| | | | | | | | Outbd | Fwd | Aft | Inbd | T/L | |
| 0.000 | 0.00 | 0 | 0 | 0 | 0 | 0 | 0 | 0 | 0 | 0 | 0 | 0 |
| 0.006 | 0.05 | 0.388 | 0 | 2.466 | 0 | 0 | -51 | 103 | -204 | -50 | -4 | 412 |
| 0.013 | 0.34 | 2.015 | 0 | 10.982 | 0 | 0 | -229 | 521 | -966 | -223 | -22 | 1961 |
| 0.019 | 0.68 | 3.577 | 0 | 14.332 | 0 | 0 | -309 | 888 | -1456 | -295 | -34 | 2981 |
| 0.025 | 1.11 | 5.627 | 0 | 18.707 | 0 | 0 | -413 | 1369 | -2097 | -389 | -50 | 4318 |
| 0.031 | 1.58 | 7.233 | 0 | 21.072 | 0 | 0 | -474 | 1739 | -2545 | -441 | -62 | 5262 |
| 0.037 | 2.11 | 7.994 | 0 | 22.804 | 0 | 0 | -515 | 1918 | -2789 | -478 | -69 | 5769 |
| 0.044 | 2.70 | 7.718 | 0 | 23.262 | 0 | 0 | -521 | 1861 | -2755 | -486 | -67 | 5690 |
| 0.050 | 3.36 | 7.941 | 0 | 23.769 | 0 | 0 | -533 | 1913 | -2826 | -497 | -69 | 5838 |
| 0.056 | 3.98 | 9.323 | 0 | 22.828 | 0 | 0 | -529 | 2210 | -3063 | -484 | -77 | 6362 |
| 0.062 | 4.59 | 6.11 | 0 | 21.801 | 0 | 0 | -476 | 1498 | -2352 | -451 | -56 | 4833 |
| 0.069 | 5.24 | -1.099 | 0 | 23.285 | 0 | 0 | -429 | -72 | -946 | -453 | -13 | 1913 |
| 0.075 | 5.73 | -7.744 | 0 | 21.118 | 0 | 0 | -319 | -1545 | 527 | -385 | 30 | 2806 |
| 0.081 | 6.18 | -7.553 | 0 | 21.078 | 0 | 0 | -320 | -1503 | 490 | -385 | 29 | 2727 |
| 0.087 | 6.66 | -0.953 | 0 | 20.676 | 0 | 0 | -381 | -59 | -845 | -402 | -11 | 1698 |
| 0.094 | 7.15 | 6.583 | 0 | 21.752 | 0 | 0 | -480 | 1601 | -2446 | -452 | -59 | 5039 |
| 0.100 | 7.52 | 8.215 | 0 | 21.231 | 0 | 0 | -488 | 1955 | -2755 | -448 | -69 | 5714 |
| 0.106 | 7.86 | 3.096 | 0 | 21.528 | 0 | 0 | -440 | 835 | -1719 | -434 | -37 | 3465 |
| 0.112 | 8.15 | -3.777 | 0 | 22.172 | 0 | 0 | -380 | -667 | -340 | -421 | 5 | 1813 |
| 0.119 | 8.39 | -5.593 | 0 | 23.125 | 0 | 0 | -379 | -1058 | -15 | -432 | 15 | 1901 |
| 0.125 | 8.65 | -1.088 | 0 | 23.511 | 0 | 0 | -434 | -68 | -960 | -457 | -13 | 1931 |
| 0.131 | 8.94 | 4.752 | 0 | 24.199 | 0 | 0 | -508 | 1217 | -2193 | -493 | -50 | 4461 |
| 0.138 | 9.18 | 5.77 | 0 | 23.876 | 0 | 0 | -512 | 1438 | -2386 | -491 | -56 | 4883 |
| 0.144 | 9.41 | 1.441 | 0 | 24.087 | 0 | 0 | -471 | 491 | -1508 | -478 | -29 | 2977 |
| 0.150 | 9.60 | -3.383 | 0 | 23.946 | 0 | 0 | -418 | -568 | -510 | -457 | 1 | 1954 |
| 0.157 | 9.75 | -3.415 | 0 | 23.74 | 0 | 0 | -414 | -576 | -493 | -453 | 1 | 1938 |

| Time (s) | Stroke (in) | Drag (kips) | Side (kips) | Vertical (kips) | MD (kips-in) | MV (kips-in) | $\epsilon_x (\mu)$ | | | | | |
|-------------|----------------|----------------|----------------|--------------------|-----------------|-----------------|--------------------|------|-------|------|-----|----------------------|
| | | | | | | | Outbd | Fwd | Aft | Inbd | T/L | $ \Sigma\epsilon_T $ |
| 0.163 | 9.91 | 0.8 | 0 | 23.499 | 0 | 0 | -453 | 346 | -1347 | -464 | -24 | 2634 |
| 0.169 | 10.06 | 4.085 | 0 | 23.293 | 0 | 0 | -484 | 1065 | -2011 | -473 | -45 | 4076 |
| 0.176 | 10.18 | 2.866 | 0 | 22.736 | 0 | 0 | -460 | 793 | -1732 | -457 | -37 | 3480 |
| 0.182 | 10.27 | -0.871 | 0 | 22.819 | 0 | 0 | -423 | -25 | -969 | -444 | -14 | 1876 |
| 0.188 | 10.29 | -2.654 | 0 | 22.304 | 0 | 0 | -395 | -420 | -577 | -427 | -2 | 1821 |
| 0.195 | 10.29 | -0.588 | 0 | 21.872 | 0 | 0 | -408 | 30 | -980 | -427 | -15 | 1859 |
| 0.201 | 10.32 | 2.336 | 0 | 21.885 | 0 | 0 | -439 | 671 | -1581 | -438 | -33 | 3161 |
| 0.207 | 10.34 | 2.346 | 0 | 20.849 | 0 | 0 | -419 | 666 | -1531 | -418 | -32 | 3065 |

This table can now be summarized in the figure below:

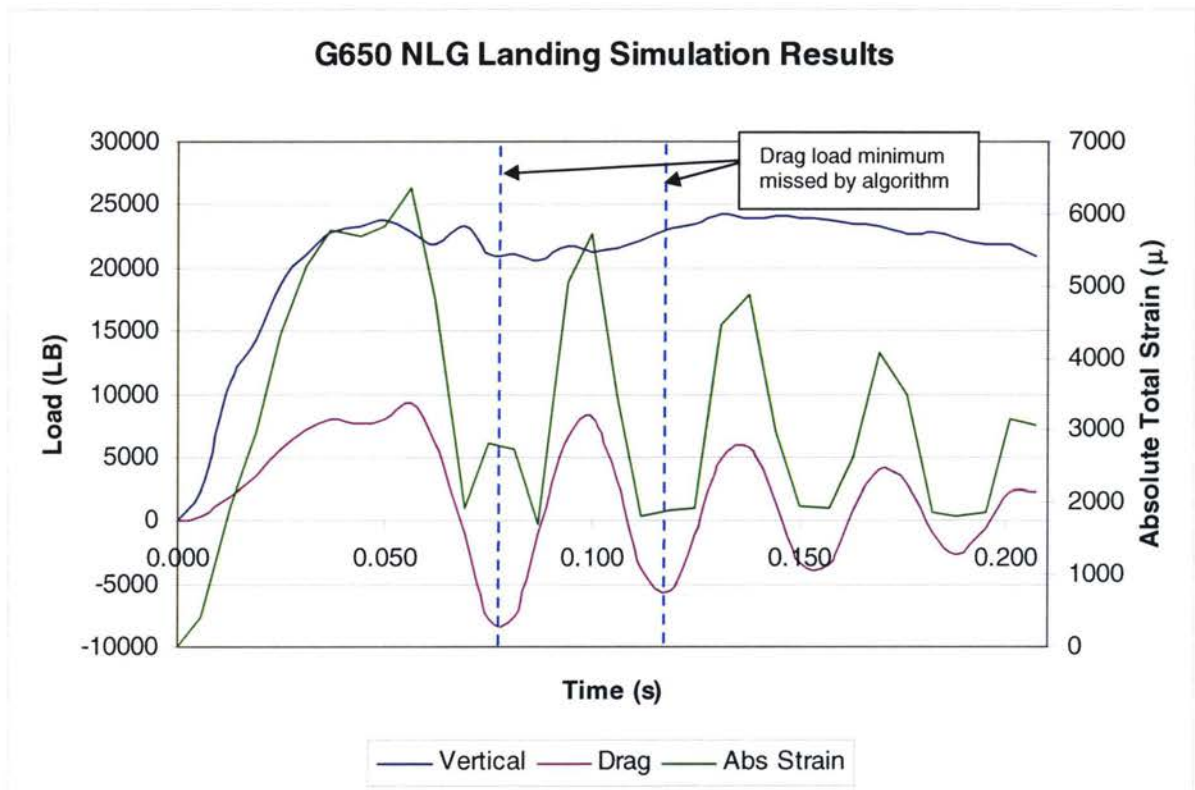


FIGURE 7-42: COMPARISON OF APPLIED LOADS TO ABSOLUTE STRAIN

Generally speaking, the absolute total strain algorithm captures the majority of the peaks and valleys in the landing simulation. Further studies will be necessary to prove the robustness of this technique.

7.9.2 Small-Strain Vibration Elimination

During take-off, landing, and taxiing, landing gear systems undergo large amounts of low-level vibration loading. Typically, these load levels do not affect the structural strength or the fatigue life of landing gear components. As a result, these types of loading events can be removed by the SHM system prior to completing static and fatigue analysis on the landing gear. An example of small vibration strain elimination is provided below:

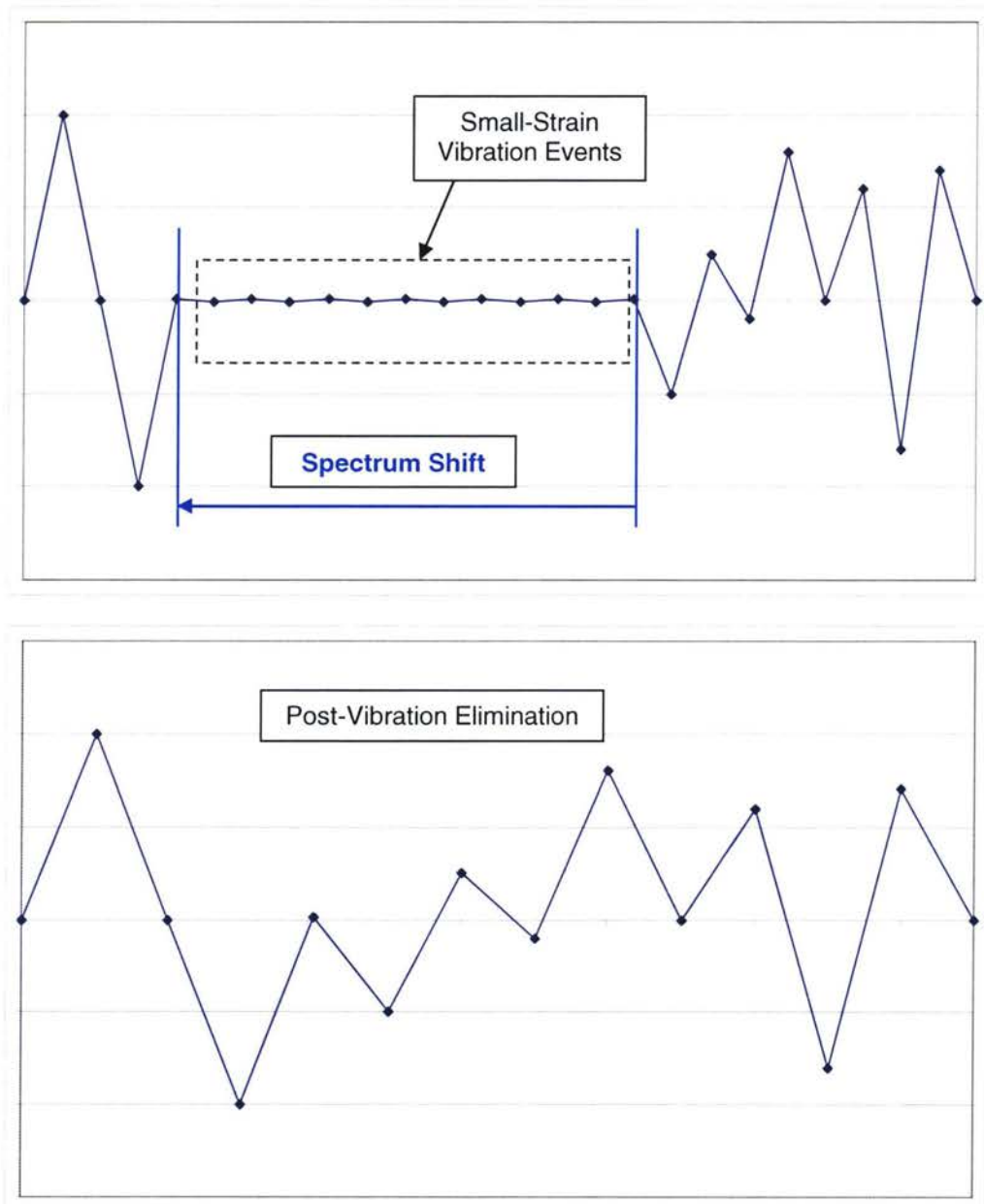


FIGURE 7-43: SMALL-STRAIN VIBRATION EVENTS ELIMINATION

In order to introduce this data reduction procedure, it will be necessary to establish the not to exceed strain level for small-strain vibrations. This value will be landing gear design dependent. However, for example, assume that the not to exceed strain level (NES) has been set to ϵ_{NTS} . The resulting algorithm is as follows:

```

If  $|\Sigma\epsilon_T|_i \leq \epsilon_{NTS}$  then
  Start Loop
  → Read next strain,  $|\Sigma\epsilon_T|_{i+1}$ 
  If  $|\Sigma\epsilon_T|_{i+1} \leq \epsilon_{NTS}$  then
    Remove  $|\Sigma\epsilon_T|_{i+1}$ 
  Loop
Else
  End Loop
End If
End If
  
```

Two examples of this algorithm are provided below:

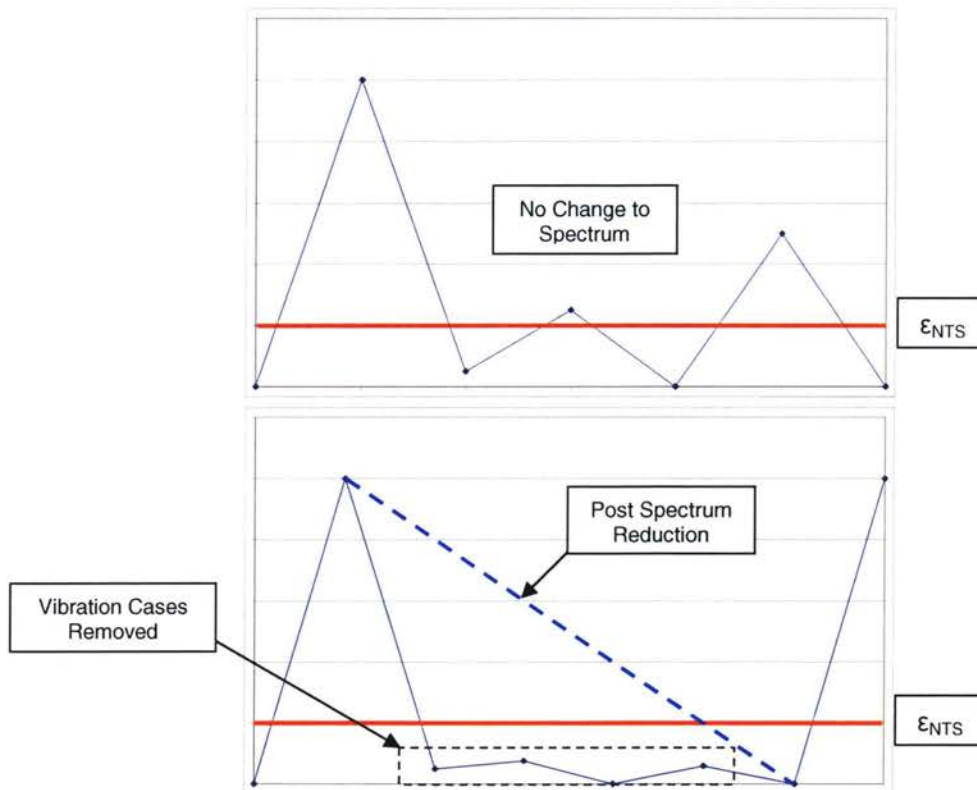


FIGURE 7-44: EXAMPLE OF SMALL-STRAIN VIBRATION EVENT REMOVAL

Chapter 8: Software Development

8.1 Modules

The software created to predict both overload and component fatigue life has been written in Microsoft Visual Basic.Net 2003 computer code. This code was chosen because of its abilities to create interactive, easy to use GUI interfaces. It is divided into individual modules, each of which performs specific calculations. The program architecture is provided below:

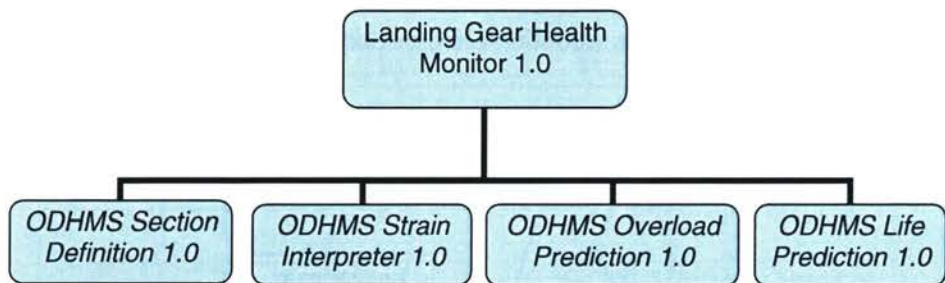


FIGURE 8-1: LANDING GEAR HEALTH MONITORING 1.0

The subsequent pages outline the functions of the individual modules.

Note: I have completed only ODHMS Section Definition 1.0.

8.2 **ODHMS Section Definition 1.0**

This module allows the user to define two different types of component analyses:

- traditional section cut analysis
- FEM nodal stress analysis

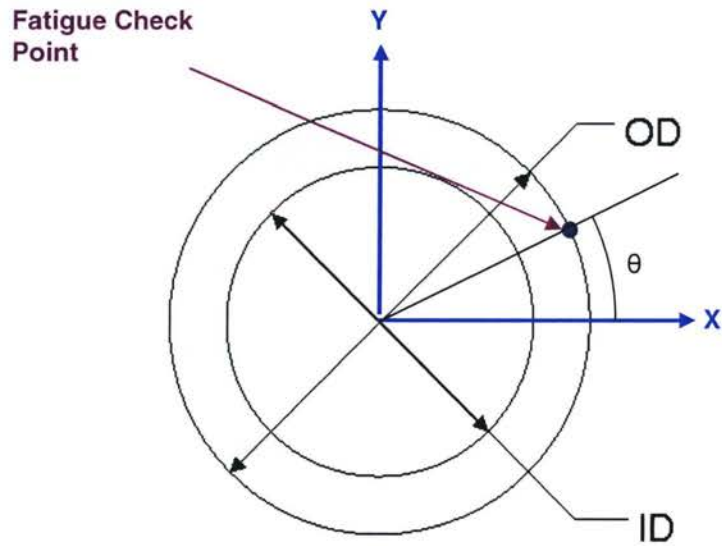
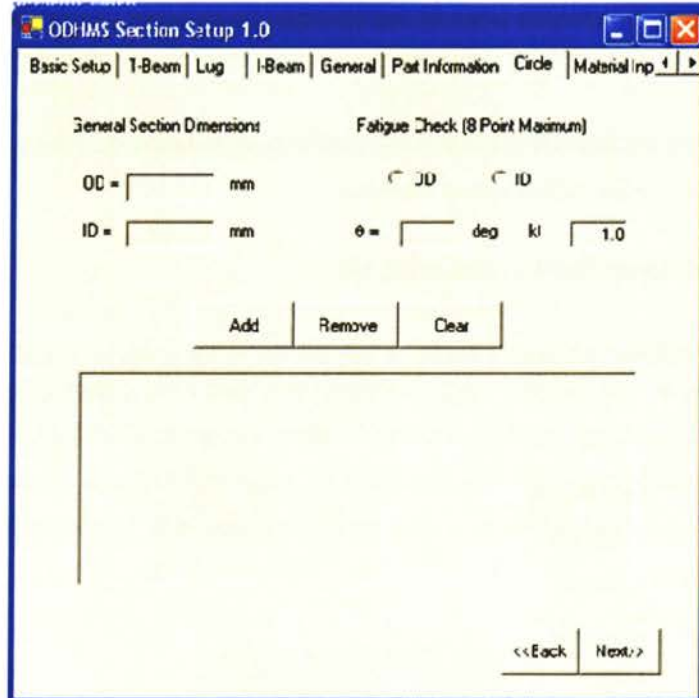
8.2.1 **Traditional Section Cut Analysis**

The following types of sections are available for analysis in the software:

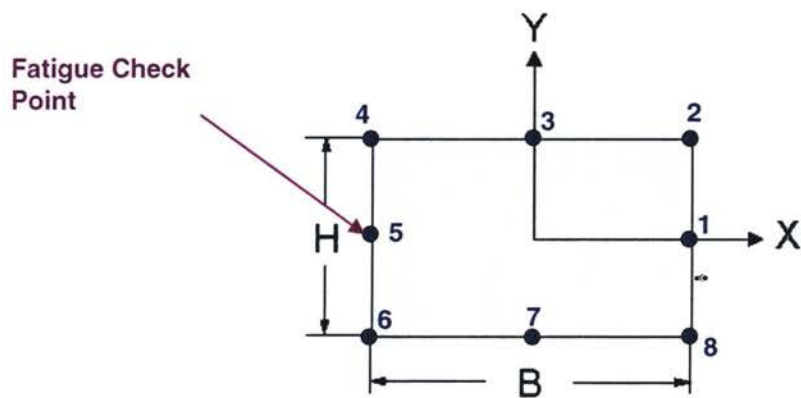
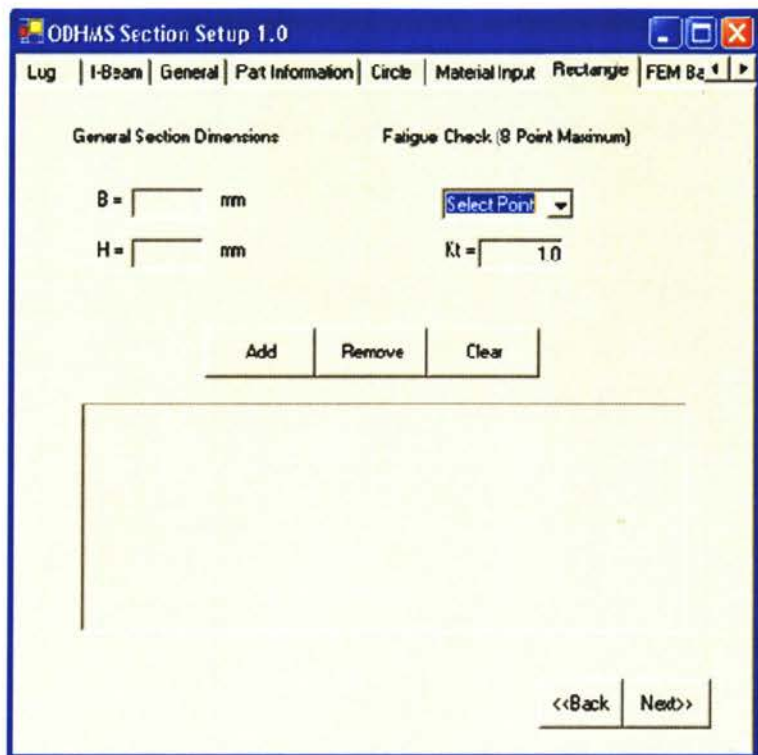
1. Circle
2. Rectangle
3. T-Beam
4. I-Beam
5. General
6. Lug

When calculating the section properties for the types 1-5 above, standard equations for area, moment of inertia, etc. are utilized. The following pages outline each section type and the dimensions required.

Circle



Rectangle



T-Beam

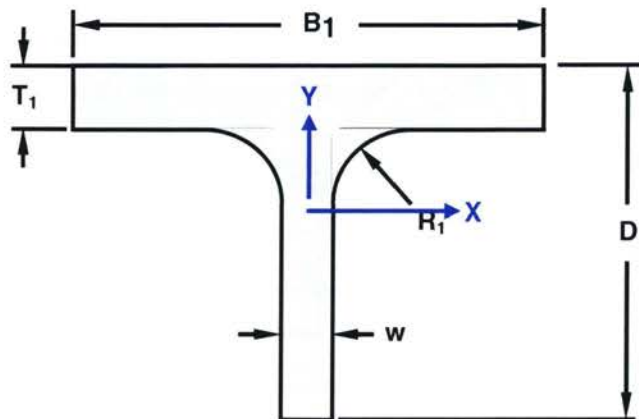
ODHMS Section Setup 1.0

Basic Setup | T-Beam | Lug | I-Beam | General | Part Information | Circle | Material Inp

| General Section Dimensions | Fatigue Check (8 Point Maximum) |
|------------------------------|---------------------------------|
| D = <input type="text"/> mm | x = <input type="text"/> mm |
| B1 = <input type="text"/> mm | y = <input type="text"/> mm |
| T1 = <input type="text"/> mm | kshx = <input type="text"/> |
| R = <input type="text"/> mm | kshy = <input type="text"/> |
| w = <input type="text"/> mm | kt = <input type="text"/> |

Add
 Remove
 Clear

<<Back Next>>



kshx = shear peaking factor in x – direction (i.e. $kshx = \frac{Q_{yy} A}{I_{yy} t_x}$)

kshy = shear peaking factor in y – direction (i.e. $kshy = \frac{Q_{xx} A}{I_{xx} t_y}$)

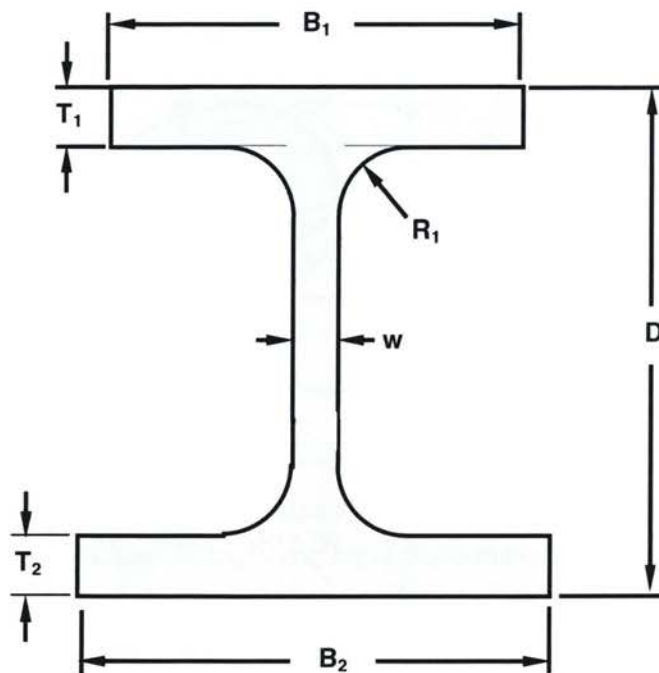
I-Beam

ODHMS Section Setup 1.0

Basic Setup | T-Beam | Lug | I-Beam | General | Part Information | Circle | Material Inp

| General Section Dimensions | Fatigue Check (8 Point Maximum) |
|------------------------------|---|
| D = <input type="text"/> mm | x = <input type="text"/> mm |
| B1 = <input type="text"/> mm | y = <input type="text"/> mm |
| B2 = <input type="text"/> mm | kshx = <input type="text"/> <input type="button" value="Add"/> |
| T1 = <input type="text"/> mm | kshy = <input type="text"/> <input type="button" value="Remove"/> |
| T2 = <input type="text"/> mm | kt = <input type="text"/> <input type="button" value="Clear"/> |
| R = <input type="text"/> mm | |
| w = <input type="text"/> mm | |

<<Back | Next>>



General

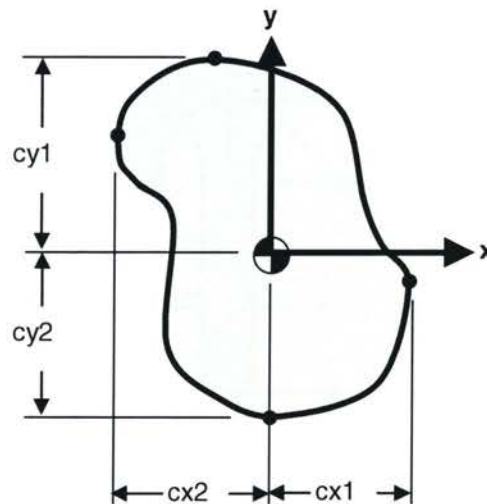
ODHMS Section Setup 1.0

Basic Setup | T-Beam | Lug | I-Beam | General | Part Information | Circle | Material Inp

| General Section Dimensions | Fatigue Check (8 Point Maximum) |
|---|---------------------------------|
| A = <input type="text"/> mm ² | cx = <input type="text"/> mm |
| Qxx = <input type="text"/> mm ³ | cy = <input type="text"/> mm |
| Qyy = <input type="text"/> mm ³ | kshx = <input type="text"/> |
| Ixx = <input type="text"/> mm ⁴ | kshy = <input type="text"/> |
| Iyy = <input type="text"/> mm ⁴ | kt = <input type="text"/> |
| Torz = <input type="text"/> mm ³ | |
| cx1 = <input type="text"/> mm | |
| cx2 = <input type="text"/> mm | |
| cy1 = <input type="text"/> mm | |
| cy2 = <input type="text"/> mm | |
| tx = <input type="text"/> mm | |
| ty = <input type="text"/> mm | |

Add Remove Clear

<<Back Next>>



Torz = torsional modulus (analogous to bending modulus Zxx)

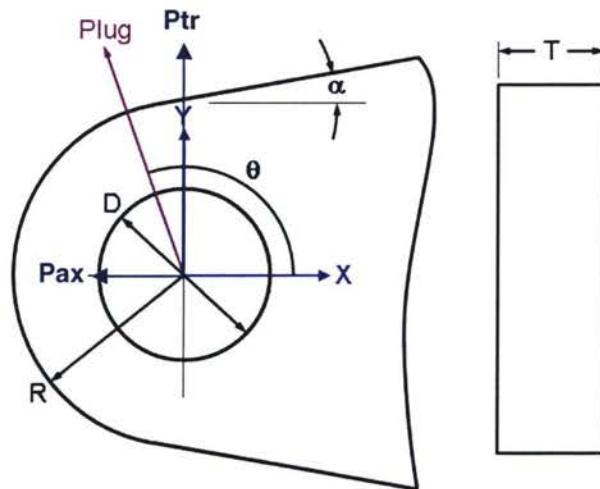
Lug

ODHMS Section Setup 1.0

Basic Setup | T-Beam | Lug | I-Beam | General | Part Information | Circle | Material Inp

| General Section Dimensions | Fatigue Check (8 Point Maximum) |
|-------------------------------------|--|
| R = <input type="text"/> mm | <input type="checkbox"/> Include Angle Range |
| D = <input type="text"/> mm | K1 = <input type="text"/> |
| T = <input type="text"/> mm | K2 = <input type="text"/> |
| α = <input type="text"/> deg | $\theta 1$ = <input type="text"/> deg |
| Pax(all) = <input type="text"/> kN | $\theta 2$ = <input type="text"/> deg |
| Ptr(all) = <input type="text"/> kN | Kt = <input type="text"/> 1.0 |

<<Back | Next>>

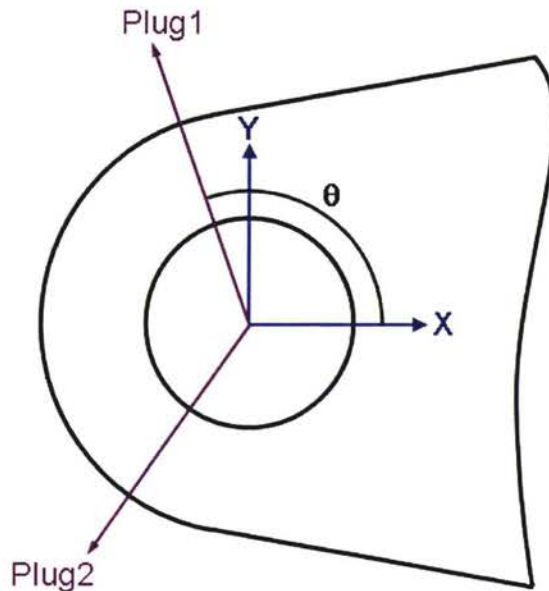


Pax = allowable axial load for lug (using lug analysis method outlined in reference 3)

Ptr = allowable transverse load for lug (using lug analysis method outlined in reference 3)

Lug (cont'd)

For fatigue analysis of lugs, in many cases there are two dominant loading directions acting on the lug (Plug1, Plug2). To account for these two cases, the following algorithm is used for determining the equivalent stress, f_{eq} :



$$\begin{aligned} f_{eq} &= K1 \text{ Plug1} && (\text{for } \theta_1 \leq \theta \leq \theta_2) \\ f_{eq} &= K2 \text{ Plug2} && (\text{for } \theta \leq \theta_1 \text{ and } \theta_2 \leq \theta) \end{aligned}$$

In other instances, the lug load is bidirectional (i.e. Plug1 is positive or negative). For this scenario, the following algorithm is used:

$$\begin{aligned} f_{eq} &= K1 \text{ Plug} && (\text{for } \text{Plug} \geq 0) \\ f_{eq} &= K2 \text{ Plug} && (\text{for } \text{Plug} < 0) \end{aligned}$$

8.2.2 FEM Nodal Stress Analysis

For complex landing gear components, it is sometimes difficult to use traditional section cut analysis to predict the stress levels within the component. As a result, FEA is used extensively for these components as a reliable alternative to section cut analysis. In order to use FEA for predicting stress levels for complex loading scenarios, the principle of superposition is used (see section 4.2). Generally speaking, a series of unit load cases are individually analyzed on a component to determine the unit stress levels within the component. For example:

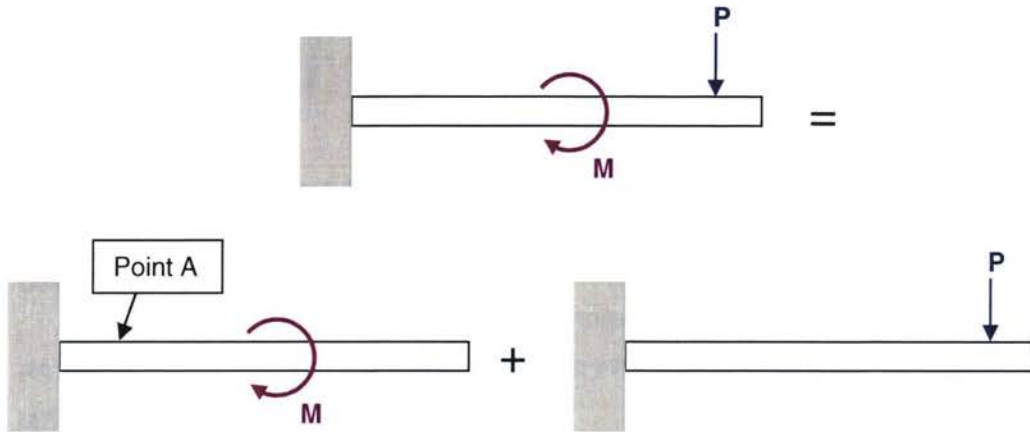


FIGURE 8-2: SAMPLE USE OF FEA RESULTS

Assume that, at point A, the following unit 2D stresses result from the applied shear and moments:

| Load Case | σ_x | σ_y | τ_{xy} |
|-----------|------------|------------|-------------|
| Shear, P | 5.0 | 0.0 | 1.0 |
| Moment, M | 1.0 | 0.0 | 0.0 |

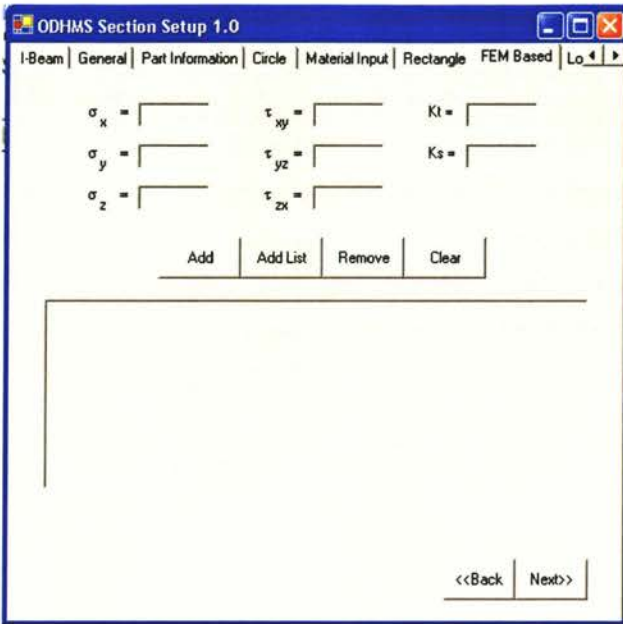
Now, assume that a 10 kip force P and a 100 kip-in moment M are applied to the cantilever beam. The total stress components acting at point are then:

$$\sigma_x = 10 (5.0) + 100(1.0) = 150.0 \text{ ksi}$$

$$\sigma_y = 0.0 \text{ ksi}$$

$$\tau_{xy} = 10 (1.0) + 100(0.0) = 10.0 \text{ ksi}$$

The following page illustrates the input required to utilize unit stress results in both the static and fatigue analyses software presented in sections 8.4 and 8.5.



K_t = additional stress concentration factor to be added to FEM results

K_s = surface finish/coating stress concentration factor

8.2.3 Load Equation Definitions

In order to predict the applied loads throughout the landing gear structure based on either the wheel or post loads (see sections 7.1 and 7.3), load equations must be developed. As an example, assume that the load equations will be developed for the cantilever beam presented in the previous section for section A-A:

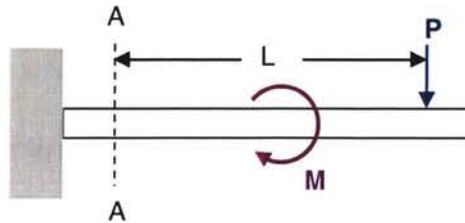


FIGURE 8-3: SAMPLE LOAD EQUATIONS DEVELOPMENT

Load Equations at A-A:

$$PSY = - P$$

$$MBX = PL + M$$

With regards to a landing gear structural beam model (see section 4.1), individual beam elements internal loads would be referenced instead of P and M shown above:

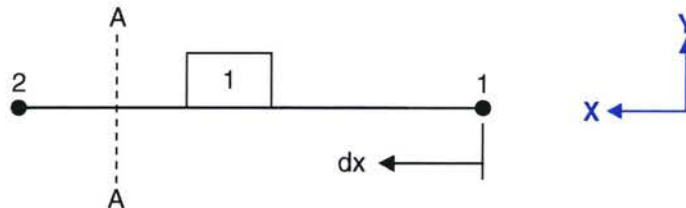


FIGURE 8-4: SAMPLE LOAD EQUATIONS DEVELOPMENT FROM BEAM MODEL

Load Equations at A-A:

$$\text{Axial} = - F_x [M1J1]$$

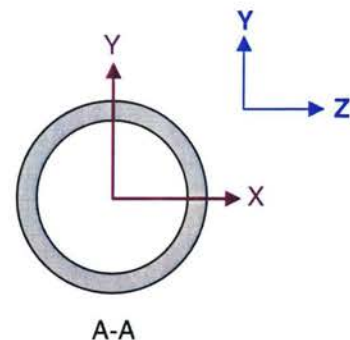
$$PSX = F_z [M1J1]$$

$$PSY = F_y [M1J1]$$

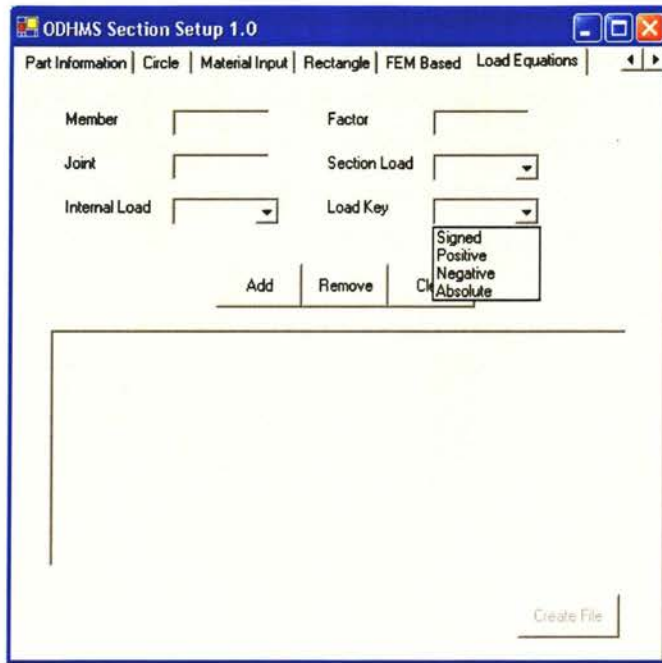
$$MBX = M_z [M1J1] - F_z dx [M1J1]$$

$$MBY = M_y [M1J1] + F_y dx [M1J1]$$

$$\text{Torque} = -M_x [M1J1]$$



The following page illustrates the software load equation inputs.



Load Key:

Signed

Positive

Negative

Absolute

Internal load applied to section when positive or negative

Internal load is only applied to section when positive

Internal load is only applied to section when negative

Internal load is applied as an absolute value

8.3 ODHMS Strain Interpreter 1.0

At the time of publication, the software for ODHMS Strain Interpreter 1.0 is still in development.

This software will read the raw strain data collected by the ODHMS system on the landing gear. The purpose of this software is twofold:

1. Eliminate superfluous strain data from strain history
2. Calculate the wheel or post loads

8.3.1 Elimination of Superfluous Strain Data

Eliminating the superfluous strain data from the strain history file will be the first step in the software program. By eliminating unneeded strain data, the overall speed of the ODHMS software will be greatly improved. Two separate algorithms will be used to eliminate the superfluous data:

1. Intermediate Data Point Elimination (see section 7.9.1)
2. Small-Strain Vibration Elimination (see section 7.9.2)

8.3.2 Calculation of Wheel/Post Loads

Once all of the superfluous strain data has been eliminated from the ODHMS strain history output, the software will determine the wheel or post loads, depending on the ODHMS system specified. If the system chosen measures wheel loads at the axle (see section 7.1), then a combination of Newton's Method of Solving Nonlinear systems of equations and Gaussian elimination will be used (see section 7.2.5). If the system will measure post loads (see section 7.3), then a linear system of equations will be solved using Gaussian elimination (see section 7.4.3).

At the time of publication, the software for ODHMS Overload Prediction 1.0 is still in development.

This software will utilize the section definitions created by ODHMS Section Definition 1.0 (see section 8.2) and the wheel/post loads predicted using ODHMS Strain Interpreter 1.0 (see section 8.3). For these two inputs to be linked properly, a series of unit loads will need to be applied to the landing gear structural beam model (see section 0). As an example, assume that the ODHMS system used predicts post loads. The following unit loads would need to be applied to the beam model for a MLG:

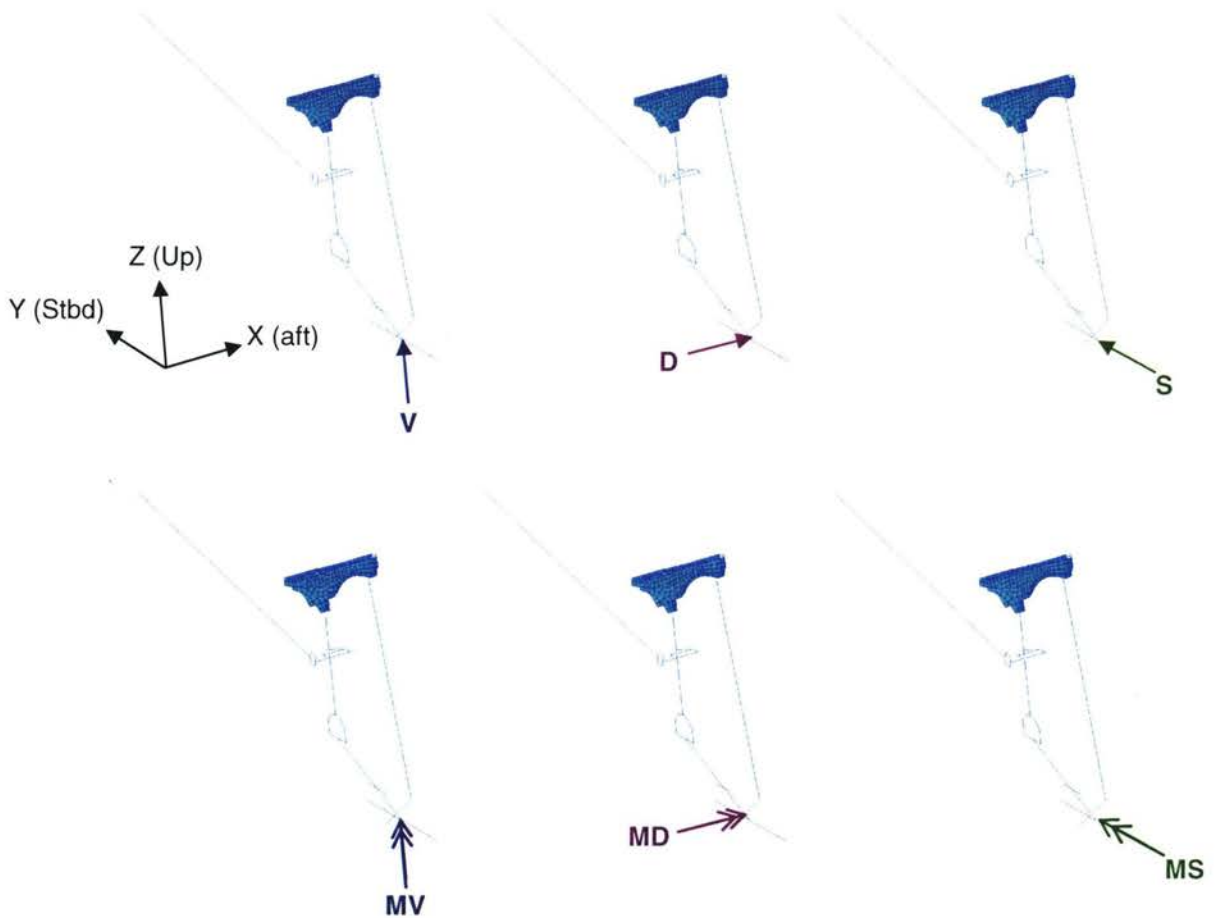


FIGURE 8-5: UNIT POST LOADS APPLIED TO BEAM MODEL

For each unit load case, 6 components of internal loads will result at each beam element. Assuming the principle of superposition (see section 4.2), the unit internal loads results for each post load can be directly combined. As an example, assume that it is required to calculate the axial force acting at member 100, joint 100 for the following post loads:

$$P_{axial} = -F_x [M100J100]$$

$$D = 5 \text{ kips}$$

$$S = 5 \text{ kips}$$

$$V = 30 \text{ kips}$$

$$MD = 100 \text{ kips-in}$$

$$MS = 50 \text{ kips-in}$$

$$MV = 25 \text{ kips}$$

Unit Internal Loads Results for
F_x in Member 100 Joint 100

$$P_{axial} = \{D \quad S \quad V \quad MD \quad MS \quad MV\} \begin{bmatrix} 1.0 \\ 0.2 \\ -0.3 \\ 0.1 \\ 0.05 \\ -0.2 \end{bmatrix} = \{5.0 \quad 5.0 \quad 30.0 \quad 100.0 \quad 50.0 \quad 25.0\} \begin{bmatrix} 1.0 \\ 0.2 \\ -0.3 \\ 0.1 \\ 0.05 \\ -0.2 \end{bmatrix} = 4.5 \text{ kips}$$

Once the unit load results have been combined with the load equations (as shown above), each post load data point will be converted into applied section loads at each section cut analysis location. Based on the cross-section geometry, a yield margin of safety will be calculated and recorded (see section 4.3 for a sample section cut margin calculation). The user will also have the option of calculated the ultimate margin of safety.

ODHMS Life Prediction 1.0

At the time of publication, the software for ODHMS Life Prediction 1.0 is still in development.

Generally speaking, this software utilizes the same techniques to calculate applied loads/stresses as is employed in section 8.4. Instead of calculating margins of safety after stress levels are calculated, the equivalent stress is stored for each load history data point. After stress levels have been calculated for every load history data point, rainflow analysis is completed on the stress history (see section 6.4 for details on rainflow) to determine the stress pairs for fatigue damage assessment. After all of the relevant stress pairs have been identified by the rainflow procedure, strain-life analysis is utilized to predict the accumulated fatigue damage on the sections analyzed. For details on strain-life theory, refer to section 6.2.

Chapter 10: Test Plan

9.1 Cantilever Beam Demonstration Test

As an initial development exercise, a cantilever beam test will be completed. This cantilever beam test will attempt to simulate the applied loads from a wheel to a landing gear axle. In this test, a series of unit load cases will first be applied to calibrate the strain gauges. After calibration is complete, combinations of the unit cases will be applied to confirm the validity of both the calibration and the load equations developed in sections 7.1 and 7.3. A diagram of the test fixture that I have designed is provided below:

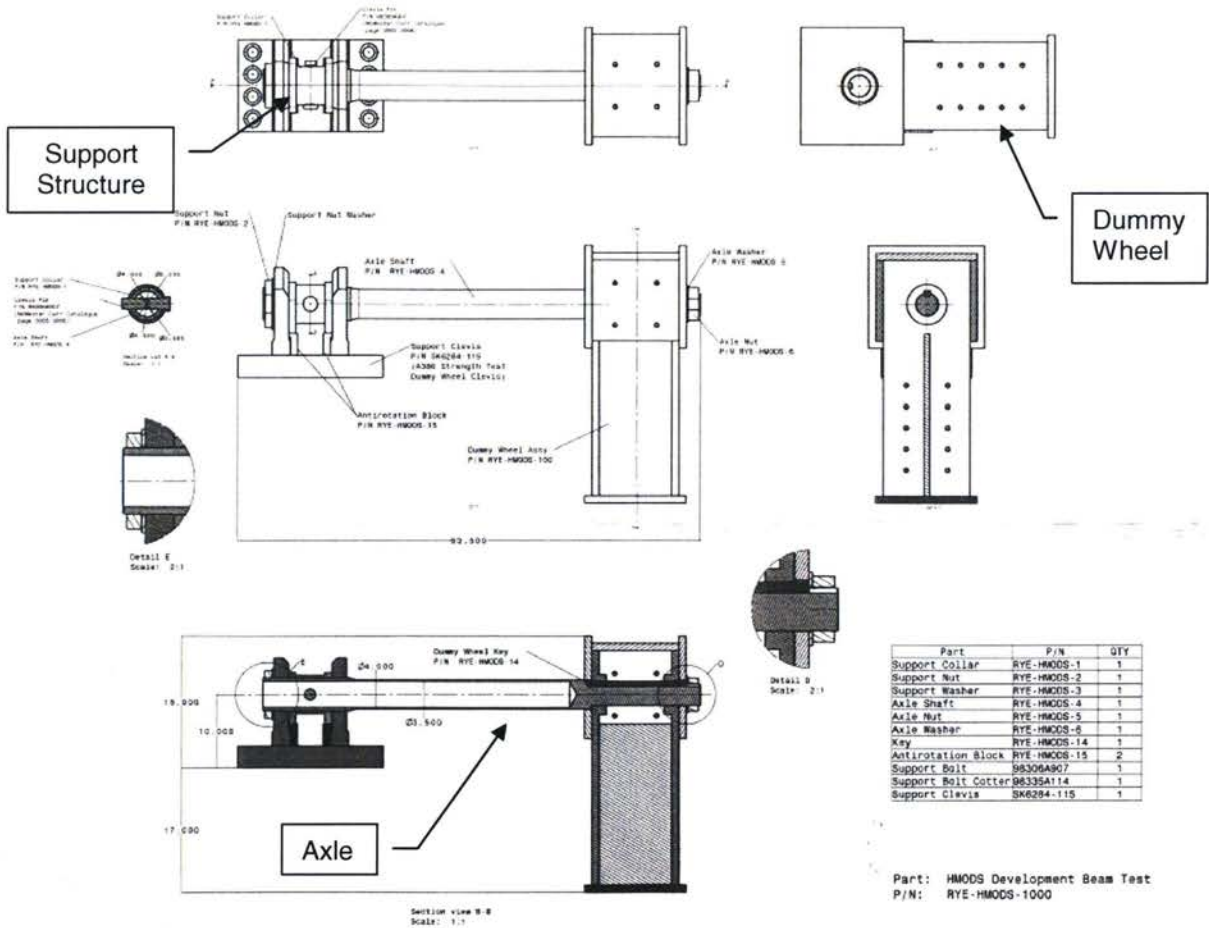


FIGURE 9-1: CANTILEVER BEAM DEMONSTRATION TEST ARTICLE

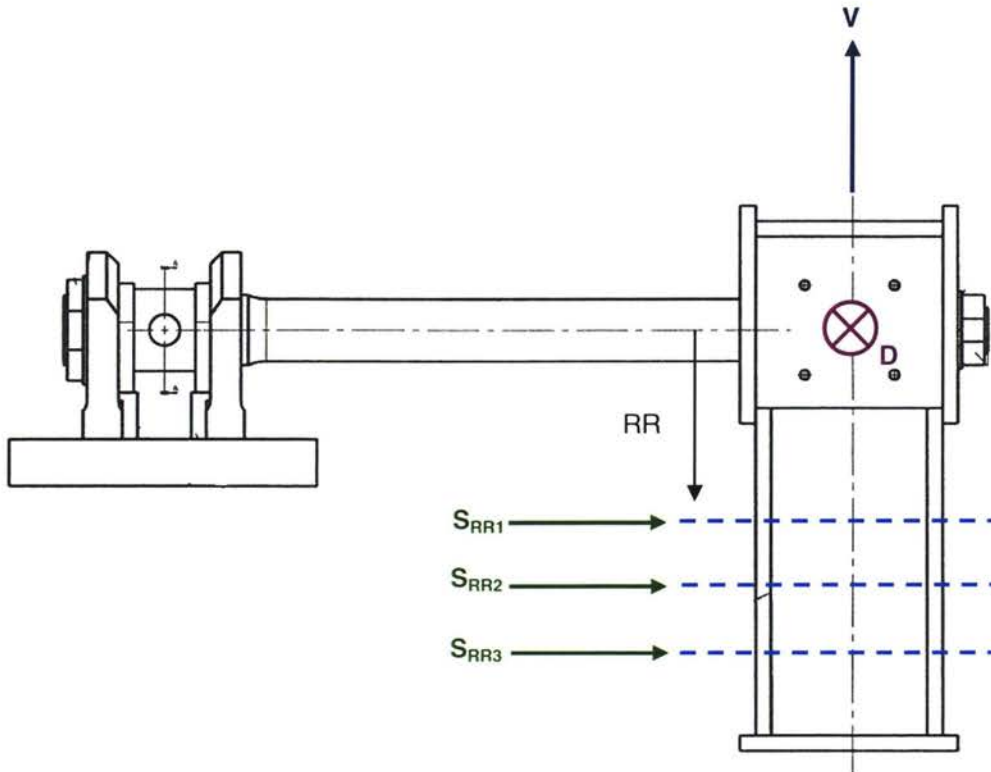


FIGURE 9-2: CALIBRATION LOADS FOR CANTILEVER BEAM TEST

The following calibration loads will be applied to the cantilever beam:

- Vertical
- Drag
- Side at 3 different distances from the beam centreline (RR)

For the side load case, both side load and MD moment will be applied. As a result, it is necessary to apply a constant side load at various distances from the axle centreline in order to separate the effects of side load and MD moment.

9.1.2 Strain Gauge Placement

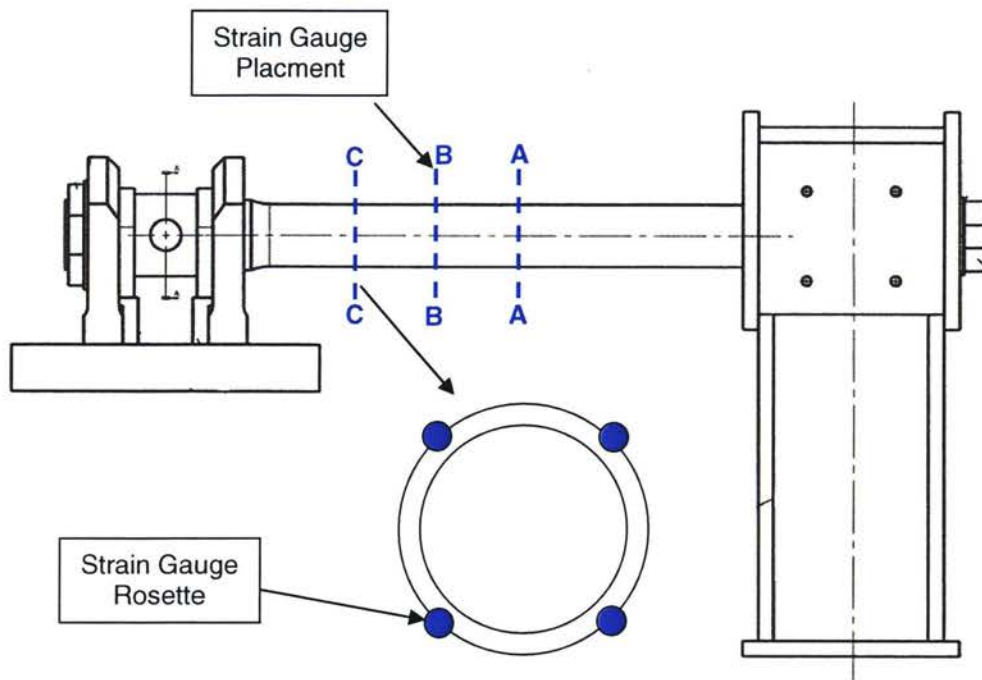


FIGURE 9-3: STRAIN GAUGE PLACEMENT ON CANTILEVER BEAM

For the demonstration test, 3 sets of 4 strain gauge rosettes will be placed on the axle at the locations specified in the figure above. Strain gauge rosettes will be used as a means for confirming the results of the uniaxial strain gauge concept predictions. When rosettes are used, shear, bending, and axial loads can be measured more directly than the uniaxial strain gauge concept proposed for the test.

Three separate locations have been chosen in order to investigate the sensitivity of the strain gauge readings to the magnitude of bending moment.

9.1.3 Finite Element Calibration

Initial calibration of the cantilever beam has been completed via finite element analysis. Refer to the figure below for a picture of the model that I have created:



FIGURE 9-4: CANTILEVER BEAM FINITE ELEMENT MODEL

Two sample Von Mises stress plots are provide below for one force and one moment case.

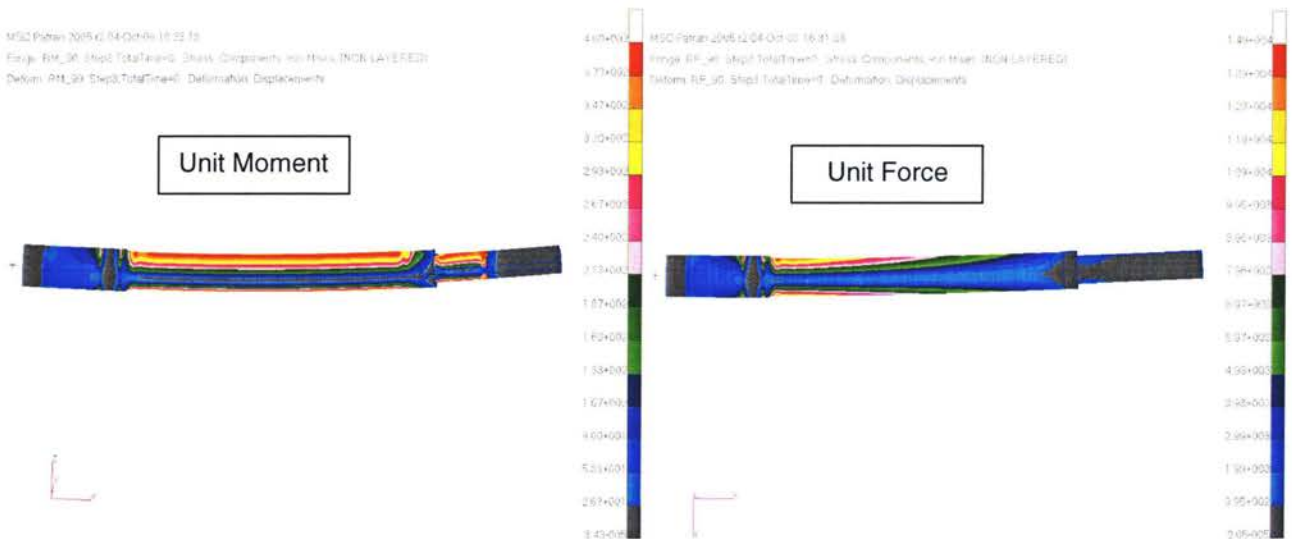


FIGURE 9-5: SAMPLE VON MISES STRESS PLOTS

9.1.4 Load Equation Development

This section shows the derivation of the required coefficients for section C-C as shown in Figure 9-3. The coefficients are based on the following equation derived in section 7.2.4:

$$\varepsilon_x = \varepsilon'_x(RF, \phi_{RF}) + \varepsilon''_x(RM, \phi_{RM}) + \varepsilon'''_x(S)$$

where

$$\varepsilon'_x = RF(A \cos(\theta_{RF} + \phi_{RF}) + B)$$

$$\varepsilon''_x = RM(C \cos(\theta_{RM} + \phi_{RM}) + D)$$

$$\varepsilon'''_x = SE$$

Applied Load Definitions

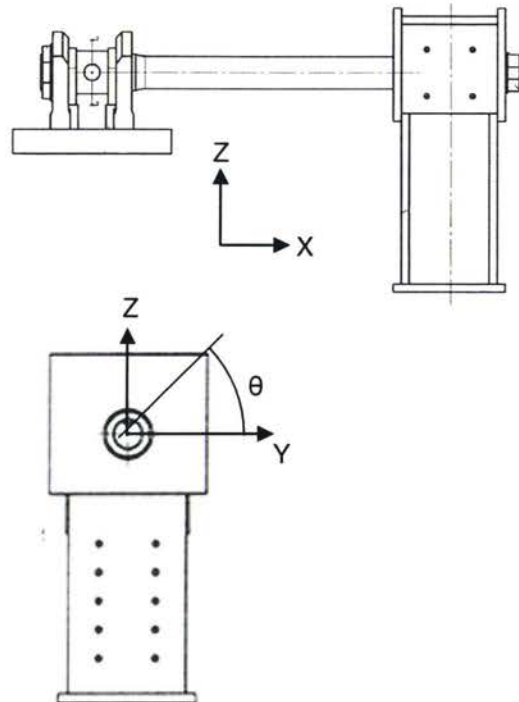
Forces and moments were applied to the finite element model every 45 degrees in order to derive the coefficients in the equations above. The definitions of these load cases are provided below.

| Load Case | Definition |
|-----------|------------|
| 1 | RF_0 |
| 2 | RF_45 |
| 3 | RF_90 |
| 4 | RF_135 |
| 5 | RF_180 |
| 7 | RM_0 |
| 8 | RM_45 |
| 9 | RM_90 |
| 10 | RM_135 |
| 11 | RM_180 |
| 12 | RM_225 |
| 13 | RM_270 |
| 14 | RM_315 |

RF = Resultant Force

RM = Resultant Moment

_xxx = Angle θ



The data provided on the following pages is based on the assumption that a strain gauge could be potentially place at locations every 45 degrees from $\theta = 0$ degrees. The charts refer to shear (RF) and Moment (RM).

Strain Gauge Coefficient Derivations

$\theta = 0$ Degree Location

| Load Case | Definition | Element | Case | θ (deg) | ϵ_x (μ) |
|-----------|------------|---------|------|----------------|------------------------|
| 1 | RF_0 | 93203 | 1 | 0 | -216 |
| 2 | RF_45 | 93203 | 2 | 45 | -157 |
| 3 | RF_90 | 93203 | 3 | 90 | -6 |
| 4 | RF_135 | 93203 | 4 | 135 | 149 |
| 5 | RF_180 | 93203 | 5 | 180 | 216 |
| 6 | Side | 93203 | 6 | - | -12 |
| 7 | RM_0 | 93203 | 7 | 0 | 0 |
| 8 | RM_45 | 93203 | 8 | 45 | -9 |
| 9 | RM_90 | 93203 | 9 | 90 | -13 |
| 10 | RM_135 | 93203 | 10 | 135 | -10 |
| 11 | RM_180 | 93203 | 11 | 180 | 0 |
| 12 | RM_225 | 93203 | 12 | 225 | 9 |
| 13 | RM_270 | 93203 | 13 | 270 | 13 |
| 14 | RM_315 | 93203 | 14 | 315 | 10 |

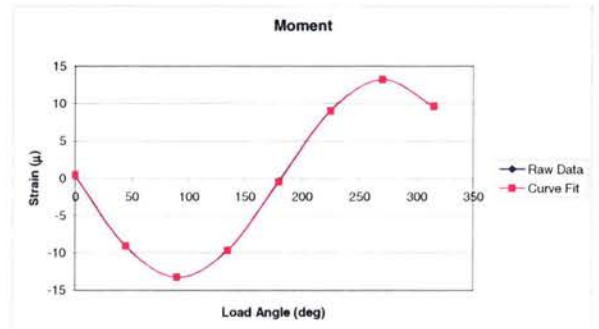
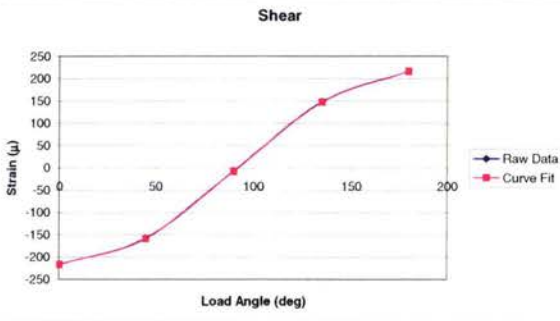
Shear

Max = 216
 Min = -216
 Mean = 0
 Alt = 216
 A = 216
 ϕ_{RF} = 178 deg
 ϕ_{RM} = 3.11 rad
 B = 0

Moment

Max = 13
 Min = -13
 Mean = 0
 Alt = 13
 C = 13
 ϕ_{RM} = 88 deg
 ϕ_{RM} = 1.54 rad
 D = 0

| Load Case | Definition | Element | Case | θ (deg) | ϵ_x (μ) |
|-----------|------------|---------|------|----------------|------------------------|
| 1 | RF_0 | 93203 | 1 | 0 | -216 |
| 2 | RF_45 | 93203 | 2 | 45 | -158 |
| 3 | RF_90 | 93203 | 3 | 90 | -8 |
| 4 | RF_135 | 93203 | 4 | 135 | 147 |
| 5 | RF_180 | 93203 | 5 | 180 | 216 |
| 7 | RM_0 | 93203 | 7 | 0 | 0 |
| 8 | RM_45 | 93203 | 8 | 45 | -9 |
| 9 | RM_90 | 93203 | 9 | 90 | -13 |
| 10 | RM_135 | 93203 | 10 | 135 | -10 |
| 11 | RM_180 | 93203 | 11 | 180 | 0 |
| 12 | RM_225 | 93203 | 12 | 225 | 9 |
| 13 | RM_270 | 93203 | 13 | 270 | 13 |
| 14 | RM_315 | 93203 | 14 | 315 | 10 |



$\theta = 45$ Degree Location

| Load Case | Definition | Element | Case | θ (deg) | ϵ_x (μ) |
|-----------|------------|---------|------|----------------|------------------------|
| 1 | RF_0 | 95163 | 1 | 0 | -151 |
| 2 | RF_45 | 95163 | 2 | 45 | -216 |
| 3 | RF_90 | 95163 | 3 | 90 | -155 |
| 4 | RF_135 | 95163 | 4 | 135 | -3 |
| 5 | RF_180 | 95163 | 5 | 180 | 151 |
| 6 | Side | 95163 | 6 | - | -12 |
| 7 | RM_0 | 95163 | 7 | 0 | 9 |
| 8 | RM_45 | 95163 | 8 | 45 | 0 |
| 9 | RM_90 | 95163 | 9 | 90 | -9 |
| 10 | RM_135 | 95163 | 10 | 135 | -13 |
| 11 | RM_180 | 95163 | 11 | 180 | -9 |
| 12 | RM_225 | 95163 | 12 | 225 | 0 |
| 13 | RM_270 | 95163 | 13 | 270 | 9 |
| 14 | RM_315 | 95163 | 14 | 315 | 13 |

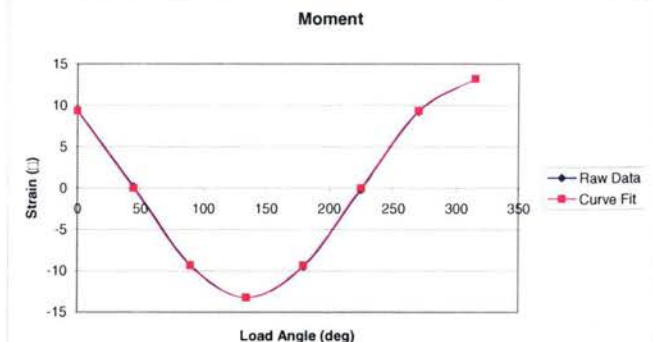
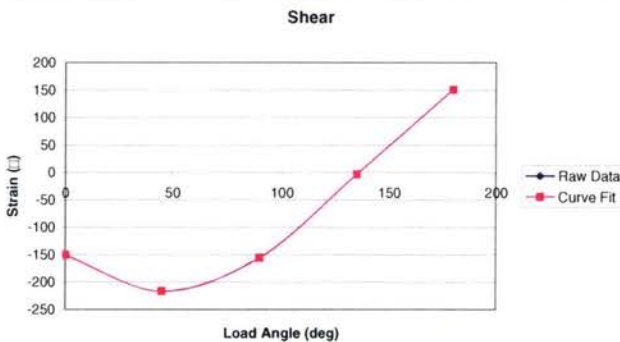
Shear

Max = 151
 Min = -216
 Mean = -33
 Alt = 184
 A = 216
 ϕ_{RF} = 134 deg
 ϕ_{RF} = 2.34 rad
 B = 0

Moment

Max = 13
 Min = -13
 Mean = 0
 Alt = 13
 C = 13
 ϕ_{RM} = 45 deg
 ϕ_{RM} = 0.79 rad
 D = 0

| Load Case | Definition | Element | Case | θ (deg) |
|-----------|------------|---------|------|----------------|
| 1 | RF_0 | 95163 | 1 | 0 |
| 2 | RF_45 | 95163 | 2 | 45 |
| 3 | RF_90 | 95163 | 3 | 90 |
| 4 | RF_135 | 95163 | 4 | 135 |
| 5 | RF_180 | 95163 | 5 | 180 |
| 7 | RM_0 | 95163 | 7 | 0 |
| 8 | RM_45 | 95163 | 8 | 45 |
| 9 | RM_90 | 95163 | 9 | 90 |
| 10 | RM_135 | 95163 | 10 | 135 |
| 11 | RM_180 | 95163 | 11 | 180 |
| 12 | RM_225 | 95163 | 12 | 225 |
| 13 | RM_270 | 95163 | 13 | 270 |
| 14 | RM_315 | 95163 | 14 | 315 |



θ = 90 Degree Location

| Load Case | Definition | Element | Case | θ (deg) | ε _x (μ) |
|-----------|------------|---------|------|---------|--------------------|
| 1 | RF_0 | 97123 | 1 | 0 | 0 |
| 2 | RF_45 | 97123 | 2 | 45 | -153 |
| 3 | RF_90 | 97123 | 3 | 90 | -216 |
| 4 | RF_135 | 97123 | 4 | 135 | -153 |
| 5 | RF_180 | 97123 | 5 | 180 | 0 |
| 6 | Side | 97123 | 6 | - | -12 |
| 7 | RM_0 | 97123 | 7 | 0 | 13 |
| 8 | RM_45 | 97123 | 8 | 45 | 9 |
| 9 | RM_90 | 97123 | 9 | 90 | 0 |
| 10 | RM_135 | 97123 | 10 | 135 | -9 |
| 11 | RM_180 | 97123 | 11 | 180 | -13 |
| 12 | RM_225 | 97123 | 12 | 225 | -9 |
| 13 | RM_270 | 97123 | 13 | 270 | 0 |
| 14 | RM_315 | 97123 | 14 | 315 | 9 |

Shear

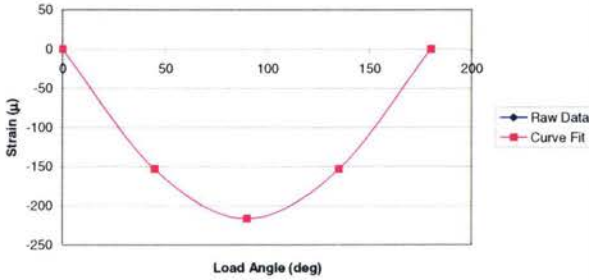
Max = 0
 Min = -216
 Mean = -108
 Alt = 108
 A = 216
 φ_{RF} = 90 deg
 φ_{RM} = 1.57 rad
 B = 0

Moment

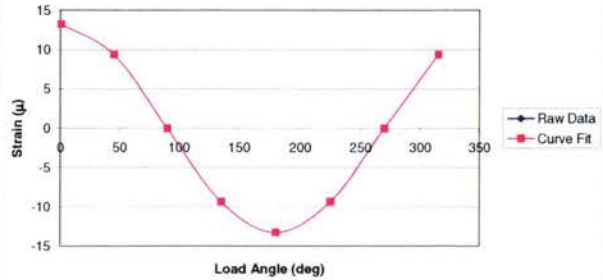
Max = 13
 Min = -13
 Mean = 0
 Alt = 13
 C = 13
 φ_{RM} = 0 deg
 φ_{RM} = 0.00 rad
 D = 0

| Load Case | Definition | Element | Case | θ (deg) | ε _x (μ) |
|-----------|------------|---------|------|---------|--------------------|
| 1 | RF_0 | 97123 | 1 | 0 | 0 |
| 2 | RF_45 | 97123 | 2 | 45 | -153 |
| 3 | RF_90 | 97123 | 3 | 90 | -216 |
| 4 | RF_135 | 97123 | 4 | 135 | -153 |
| 5 | RF_180 | 97123 | 5 | 180 | 0 |
| 7 | RM_0 | 97123 | 7 | 0 | 13 |
| 8 | RM_45 | 97123 | 8 | 45 | 9 |
| 9 | RM_90 | 97123 | 9 | 90 | 0 |
| 10 | RM_135 | 97123 | 10 | 135 | -9 |
| 11 | RM_180 | 97123 | 11 | 180 | -13 |
| 12 | RM_225 | 97123 | 12 | 225 | -9 |
| 13 | RM_270 | 97123 | 13 | 270 | 0 |
| 14 | RM_315 | 97123 | 14 | 315 | 9 |

Shear



Moment



θ = 135 Degree Location

| Load Case | Definition | Element | Case | θ (deg) | ε _x (μ) |
|-----------|------------|---------|------|---------|--------------------|
| 1 | RF_0 | 99083 | 1 | 0 | 151 |
| 2 | RF_45 | 99083 | 2 | 45 | -3 |
| 3 | RF_90 | 99083 | 3 | 90 | -155 |
| 4 | RF_135 | 99083 | 4 | 135 | -216 |
| 5 | RF_180 | 99083 | 5 | 180 | -151 |
| 6 | Side | 99083 | 6 | - | -12 |
| 7 | RM_0 | 99083 | 7 | 0 | 9 |
| 8 | RM_45 | 99083 | 8 | 45 | 13 |
| 9 | RM_90 | 99083 | 9 | 90 | 9 |
| 10 | RM_135 | 99083 | 10 | 135 | 0 |
| 11 | RM_180 | 99083 | 11 | 180 | -9 |
| 12 | RM_225 | 99083 | 12 | 225 | -13 |
| 13 | RM_270 | 99083 | 13 | 270 | -9 |
| 14 | RM_315 | 99083 | 14 | 315 | 0 |

Shear

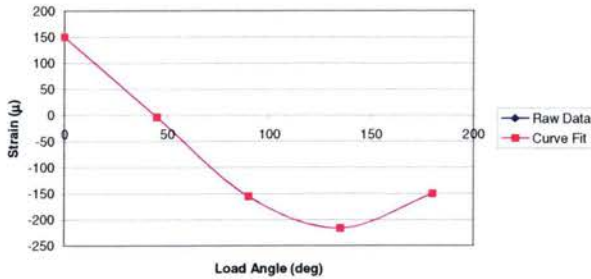
Max = 151
 Min = -216
 Mean = -33
 Alt = 184
 A = 216
 φ_{RF} = 46 deg
 φ_{RM} = 0.80 rad
 B = 0

Moment

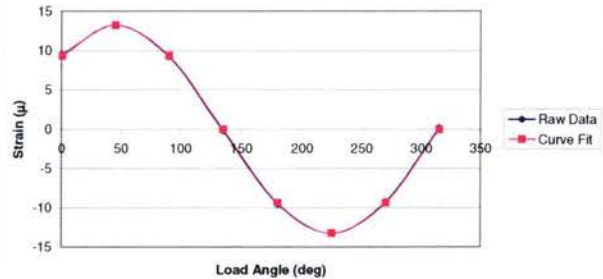
Max = 13
 Min = -13
 Mean = 0
 Alt = 13
 C = 13
 φ_{RM} = -45 deg
 φ_{RM} = -0.79 rad
 D = 0

| Load Case | Definition | Element | Case | θ (deg) | ε _x (μ) |
|-----------|------------|---------|------|---------|--------------------|
| 1 | RF_0 | 99083 | 1 | 0 | 150 |
| 2 | RF_45 | 99083 | 2 | 45 | -4 |
| 3 | RF_90 | 99083 | 3 | 90 | -156 |
| 4 | RF_135 | 99083 | 4 | 135 | -216 |
| 5 | RF_180 | 99083 | 5 | 180 | -150 |
| 7 | RM_0 | 99083 | 7 | 0 | 9 |
| 8 | RM_45 | 99083 | 8 | 45 | 13 |
| 9 | RM_90 | 99083 | 9 | 90 | 9 |
| 10 | RM_135 | 99083 | 10 | 135 | 0 |
| 11 | RM_180 | 99083 | 11 | 180 | -9 |
| 12 | RM_225 | 99083 | 12 | 225 | -13 |
| 13 | RM_270 | 99083 | 13 | 270 | -9 |
| 14 | RM_315 | 99083 | 14 | 315 | 0 |

Shear



Moment



θ= 180 Degree Location

| Load Case | Definition | Element | Case | θ (deg) | ε _x (μ) |
|-----------|------------|---------|------|---------|--------------------|
| 1 | RF_0 | 101043 | 1 | 0 | 216 |
| 2 | RF_45 | 101043 | 2 | 45 | 149 |
| 3 | RF_90 | 101043 | 3 | 90 | -6 |
| 4 | RF_135 | 101043 | 4 | 135 | -157 |
| 5 | RF_180 | 101043 | 5 | 180 | -216 |
| 6 | Side | 101043 | 6 | - | -12 |
| 7 | RM_0 | 101043 | 7 | 0 | 0 |
| 8 | RM_45 | 101043 | 8 | 45 | 10 |
| 9 | RM_90 | 101043 | 9 | 90 | 13 |
| 10 | RM_135 | 101043 | 10 | 135 | 9 |
| 11 | RM_180 | 101043 | 11 | 180 | 0 |
| 12 | RM_225 | 101043 | 12 | 225 | -10 |
| 13 | RM_270 | 101043 | 13 | 270 | -13 |
| 14 | RM_315 | 101043 | 14 | 315 | -9 |

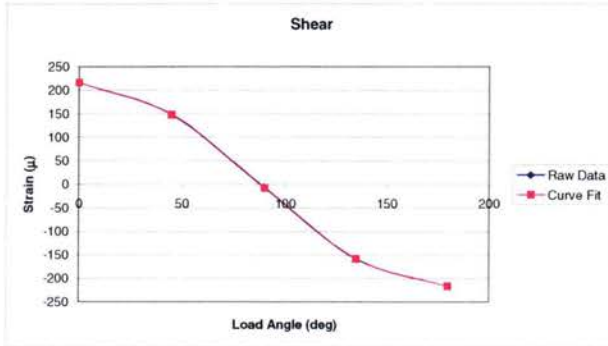
Shear

Max = 216
 Min = -216
 Mean = 0
 Alt = 216
 A = 216
 φ_{RF} = 2 deg
 φ_{RM} = 0.03 rad
 B = 0

Moment

Max = 13
 Min = -13
 Mean = 0
 Alt = 13
 C = 13
 φ_{RM} = -90 deg
 φ_{RM} = -1.57 rad
 D = 0

| Load Case | Definition | Element | Case | θ (deg) | ε _x (μ) |
|-----------|------------|---------|------|---------|--------------------|
| 1 | RF_0 | 101043 | 1 | 0 | 216 |
| 2 | RF_45 | 101043 | 2 | 45 | 148 |
| 3 | RF_90 | 101043 | 3 | 90 | -8 |
| 4 | RF_135 | 101043 | 4 | 135 | -158 |
| 5 | RF_180 | 101043 | 5 | 180 | -216 |
| 7 | RM_0 | 101043 | 7 | 0 | 0 |
| 8 | RM_45 | 101043 | 8 | 45 | 9 |
| 9 | RM_90 | 101043 | 9 | 90 | 13 |
| 10 | RM_135 | 101043 | 10 | 135 | 9 |
| 11 | RM_180 | 101043 | 11 | 180 | 0 |
| 12 | RM_225 | 101043 | 12 | 225 | -9 |
| 13 | RM_270 | 101043 | 13 | 270 | -13 |
| 14 | RM_315 | 101043 | 14 | 315 | -9 |



θ= 225 Degree Location

| Load Case | Definition | Element | Case | θ (deg) | ε _x (μ) |
|-----------|------------|---------|------|---------|--------------------|
| 1 | RF_0 | 103003 | 1 | 0 | 151 |
| 2 | RF_45 | 103003 | 2 | 45 | 216 |
| 3 | RF_90 | 103003 | 3 | 90 | 155 |
| 4 | RF_135 | 103003 | 4 | 135 | 3 |
| 5 | RF_180 | 103003 | 5 | 180 | -151 |
| 6 | Side | 103003 | 6 | - | -12 |
| 7 | RM_0 | 103003 | 7 | 0 | -9 |
| 8 | RM_45 | 103003 | 8 | 45 | 0 |
| 9 | RM_90 | 103003 | 9 | 90 | 9 |
| 10 | RM_135 | 103003 | 10 | 135 | 13 |
| 11 | RM_180 | 103003 | 11 | 180 | 9 |
| 12 | RM_225 | 103003 | 12 | 225 | 0 |
| 13 | RM_270 | 103003 | 13 | 270 | -9 |
| 14 | RM_315 | 103003 | 14 | 315 | -13 |

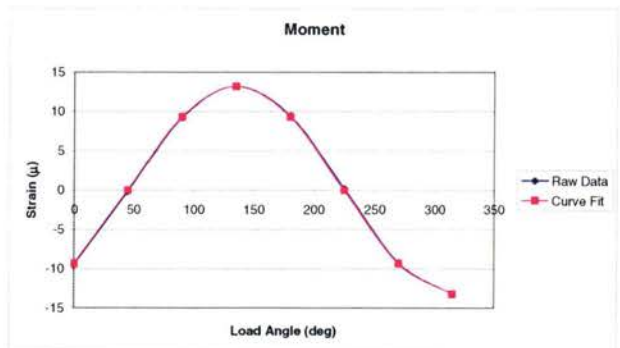
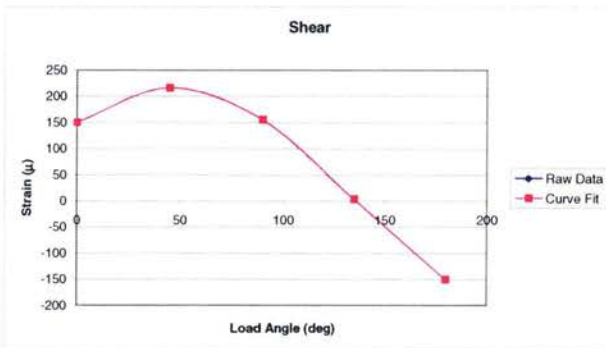
Shear

Max = 216
 Min = -151
 Mean = 33
 Alt = 183
 A = 216
 φ_{RF} = -46 deg
 φ_{RM} = -0.80 rad
 B = 0

Moment

Max = 13
 Min = -13
 Mean = 0
 Alt = 13
 C = 13
 φ_{RM} = -135 deg
 φ_{RM} = -2.36 rad
 D = 0

| Load Case | Definition | Element | Case | θ (deg) | ε _x (μ) |
|-----------|------------|---------|------|---------|--------------------|
| 1 | RF_0 | 103003 | 1 | 0 | 150 |
| 2 | RF_45 | 103003 | 2 | 45 | 216 |
| 3 | RF_90 | 103003 | 3 | 90 | 156 |
| 4 | RF_135 | 103003 | 4 | 135 | 4 |
| 5 | RF_180 | 103003 | 5 | 180 | -150 |
| 7 | RM_0 | 103003 | 7 | 0 | -9 |
| 8 | RM_45 | 103003 | 8 | 45 | 0 |
| 9 | RM_90 | 103003 | 9 | 90 | 9 |
| 10 | RM_135 | 103003 | 10 | 135 | 13 |
| 11 | RM_180 | 103003 | 11 | 180 | 9 |
| 12 | RM_225 | 103003 | 12 | 225 | 0 |
| 13 | RM_270 | 103003 | 13 | 270 | -9 |
| 14 | RM_315 | 103003 | 14 | 315 | -13 |



θ= 270 Degree Location

| Load Case | Definition | Element | Case | θ (deg) | ε _x (μ) |
|-----------|------------|---------|------|---------|--------------------|
| 1 | RF_0 | 89283 | 1 | 0 | -12 |
| 2 | RF_45 | 89283 | 2 | 45 | 144 |
| 3 | RF_90 | 89283 | 3 | 90 | 216 |
| 4 | RF_135 | 89283 | 4 | 135 | 161 |
| 5 | RF_180 | 89283 | 5 | 180 | 12 |
| 6 | Side | 89283 | 6 | - | -12 |
| 7 | RM_0 | 89283 | 7 | 0 | -13 |
| 8 | RM_45 | 89283 | 8 | 45 | -10 |
| 9 | RM_90 | 89283 | 9 | 90 | -1 |
| 10 | RM_135 | 89283 | 10 | 135 | 9 |
| 11 | RM_180 | 89283 | 11 | 180 | 13 |
| 12 | RM_225 | 89283 | 12 | 225 | 10 |
| 13 | RM_270 | 89283 | 13 | 270 | 1 |
| 14 | RM_315 | 89283 | 14 | 315 | -9 |

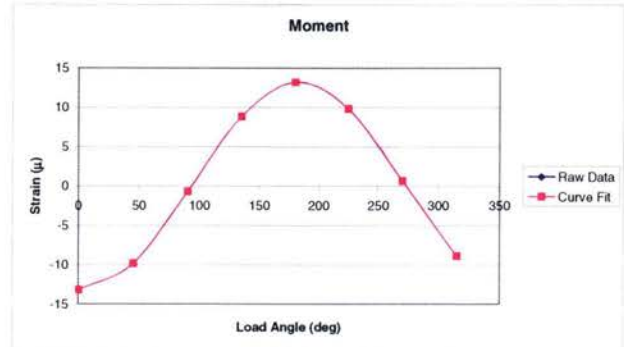
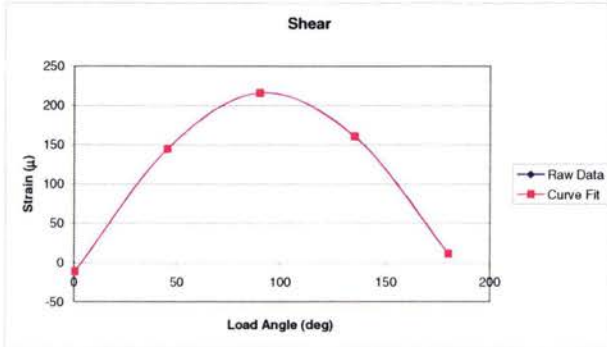
Shear

Max = 216
 Min = -12
 Mean = 102
 Alt = 114
 A = 216
 $\phi_{RF} = -93 \text{ deg}$
 $\phi_{RM} = -1.62 \text{ rad}$
 B = 0

Moment

Max = 13
 Min = -13
 Mean = 0
 Alt = 13
 C = 13
 $\phi_{RM} = -183 \text{ deg}$
 $\phi_{RM} = -3.19 \text{ rad}$
 D = 0

| Load Case | Definition | Element | Case | θ (deg) | ε _x (μ) |
|-----------|------------|---------|------|---------|--------------------|
| 1 | RF_0 | 89283 | 1 | 0 | -11 |
| 2 | RF_45 | 89283 | 2 | 45 | 145 |
| 3 | RF_90 | 89283 | 3 | 90 | 216 |
| 4 | RF_135 | 89283 | 4 | 135 | 161 |
| 5 | RF_180 | 89283 | 5 | 180 | 11 |
| 7 | RM_0 | 89283 | 7 | 0 | -13 |
| 8 | RM_45 | 89283 | 8 | 45 | -10 |
| 9 | RM_90 | 89283 | 9 | 90 | -1 |
| 10 | RM_135 | 89283 | 10 | 135 | 9 |
| 11 | RM_180 | 89283 | 11 | 180 | 13 |
| 12 | RM_225 | 89283 | 12 | 225 | 10 |
| 13 | RM_270 | 89283 | 13 | 270 | 1 |
| 14 | RM_315 | 89283 | 14 | 315 | -9 |



θ= 315 Degree Location

| Load Case | Definition | Element | Case | θ (deg) | ε _x (μ) |
|-----------|------------|---------|------|---------|--------------------|
| 1 | RF_0 | 90963 | 1 | 0 | -151 |
| 2 | RF_45 | 90963 | 2 | 45 | 3 |
| 3 | RF_90 | 90963 | 3 | 90 | 155 |
| 4 | RF_135 | 90963 | 4 | 135 | 216 |
| 5 | RF_180 | 90963 | 5 | 180 | 151 |
| 6 | Side | 90963 | 6 | - | -12 |
| 7 | RM_0 | 90963 | 7 | 0 | -9 |
| 8 | RM_45 | 90963 | 8 | 45 | -13 |
| 9 | RM_90 | 90963 | 9 | 90 | -9 |
| 10 | RM_135 | 90963 | 10 | 135 | 0 |
| 11 | RM_180 | 90963 | 11 | 180 | 9 |
| 12 | RM_225 | 90963 | 12 | 225 | 13 |
| 13 | RM_270 | 90963 | 13 | 270 | 9 |
| 14 | RM_315 | 90963 | 14 | 315 | 0 |

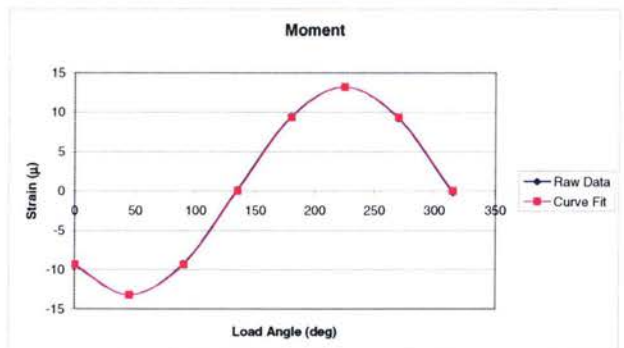
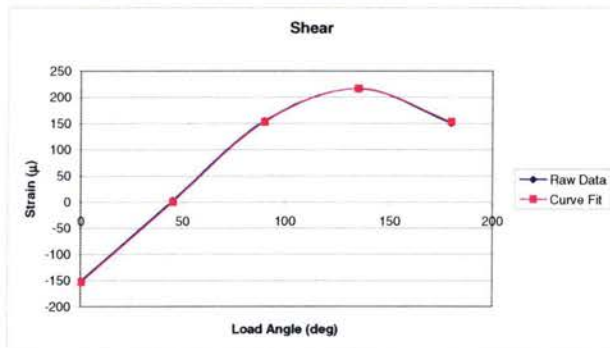
Shear

Max = 216
 Min = -151
 Mean = 33
 Alt = 183
 A = 216
 $\phi_{RF} = -135 \text{ deg}$
 $\phi_{RF} = -2.36 \text{ rad}$
 B = 0

Moment

Max = 13
 Min = -13
 Mean = 0
 Alt = 13
 C = 13
 $\phi_{RM} = -225 \text{ deg}$
 $\phi_{RM} = -3.93 \text{ rad}$
 D = 0

| Load Case | Definition | Element | Case | θ (deg) | ε _x (μ) |
|-----------|------------|---------|------|---------|--------------------|
| 1 | RF_0 | 90963 | 1 | 0 | -153 |
| 2 | RF_45 | 90963 | 2 | 45 | 0 |
| 3 | RF_90 | 90963 | 3 | 90 | 153 |
| 4 | RF_135 | 90963 | 4 | 135 | 216 |
| 5 | RF_180 | 90963 | 5 | 180 | 153 |
| 7 | RM_0 | 90963 | 7 | 0 | -9 |
| 8 | RM_45 | 90963 | 8 | 45 | -13 |
| 9 | RM_90 | 90963 | 9 | 90 | -9 |
| 10 | RM_135 | 90963 | 10 | 135 | 0 |
| 11 | RM_180 | 90963 | 11 | 180 | 9 |
| 12 | RM_225 | 90963 | 12 | 225 | 13 |
| 13 | RM_270 | 90963 | 13 | 270 | 9 |
| 14 | RM_315 | 90963 | 14 | 315 | 0 |



Strain Gauge Coefficient Summary

Based on the data presented in the previous pages, the following table provides the predicted coefficients at all three strain gauge locations shown in Figure 9-3 (i.e. A-A, B-B, C-C).

TABLE 9-1: SUMMARY OF PREDICTED COEFFICIENTS FOR CANTILEVER BEAM

| Section | Location (deg) | Element | A | ϕ_{RF} (rad) | B | C | ϕ_{RM} (rad) | D | E |
|------------|----------------|---------|-------|-------------------|-----|------|-------------------|-----|-------|
| A-A | 0 | 93347 | 406.3 | 3.142 | 0.0 | 13.2 | 1.571 | 0.0 | -11.7 |
| | 45 | 95307 | 406.3 | 2.356 | 0.0 | 13.2 | 0.785 | 0.0 | -11.7 |
| | 90 | 97267 | 406.3 | 1.571 | 0.0 | 13.2 | 0.000 | 0.0 | -11.7 |
| | 135 | 99227 | 406.3 | 0.785 | 0.0 | 13.2 | -0.785 | 0.0 | -11.7 |
| | 180 | 101187 | 406.3 | 0.000 | 0.0 | 13.2 | -1.571 | 0.0 | -11.7 |
| | 225 | 103147 | 406.3 | -0.785 | 0.0 | 13.2 | -2.356 | 0.0 | -11.7 |
| | 270 | 89427 | 406.3 | -1.623 | 0.0 | 13.2 | -3.194 | 0.0 | -11.7 |
| | 315 | 91107 | 406.3 | -2.356 | 0.0 | 13.2 | -3.927 | 0.0 | -11.7 |
| | 360 | 93347 | 406.3 | 3.142 | 0.0 | 13.2 | 1.571 | 0.0 | -11.7 |
| B-B | 0 | 93275 | 311.3 | 3.107 | 0.0 | 13.2 | 1.536 | 0.0 | -11.7 |
| | 45 | 95235 | 311.3 | 2.339 | 0.0 | 13.2 | 0.785 | 0.0 | -11.7 |
| | 90 | 97195 | 311.3 | 1.571 | 0.0 | 13.2 | 0.000 | 0.0 | -11.7 |
| | 135 | 99155 | 311.3 | 0.785 | 0.0 | 13.2 | -0.785 | 0.0 | -11.7 |
| | 180 | 101115 | 311.3 | 0.000 | 0.0 | 13.2 | -1.571 | 0.0 | -11.7 |
| | 225 | 103075 | 311.3 | -0.785 | 0.0 | 13.2 | -2.356 | 0.0 | -11.7 |
| | 270 | 89355 | 311.3 | -1.623 | 0.0 | 13.2 | -3.194 | 0.0 | -11.7 |
| | 315 | 91035 | 311.3 | -2.356 | 0.0 | 13.2 | -3.927 | 0.0 | -11.7 |
| | 360 | 93275 | 311.3 | 3.107 | 0.0 | 13.2 | 1.536 | 0.0 | -11.7 |
| C-C | 0 | 93203 | 216.3 | 3.107 | 0.0 | 13.2 | 1.536 | 0.0 | -11.7 |
| | 45 | 95163 | 216.3 | 2.339 | 0.0 | 13.2 | 0.785 | 0.0 | -11.7 |
| | 90 | 97123 | 216.3 | 1.571 | 0.0 | 13.2 | 0.000 | 0.0 | -11.7 |
| | 135 | 99083 | 216.3 | 0.803 | 0.0 | 13.2 | -0.785 | 0.0 | -11.7 |
| | 180 | 101043 | 216.3 | 0.035 | 0.0 | 13.2 | -1.571 | 0.0 | -11.7 |
| | 225 | 103003 | 216.3 | -0.803 | 0.0 | 13.2 | -2.356 | 0.0 | -11.7 |
| | 270 | 89283 | 216.3 | -1.623 | 0.0 | 13.2 | -3.194 | 0.0 | -11.7 |
| | 315 | 90963 | 216.3 | -2.356 | 0.0 | 13.2 | -3.927 | 0.0 | -11.7 |
| | 360 | 93203 | 216.3 | 3.107 | 0.0 | 13.2 | 1.536 | 0.0 | -11.7 |

After the initial calibration load cases, the coefficients provided in the table above will be adjusted based on the actual strain gauge readings from the tests. Any corrections needed between the FEA predicted strain levels and the actual strain gauge data will be investigated.

9.1.5 Test Cases

In order to test the fidelity of the load equations developed for the cantilever beam test, a series of typical in-service landing gear loads were used. A Microsoft Excel spreadsheet in combination with a VBA macro was utilized to test the load equations. The steps to confirm the fidelity of the load equations are as follows:

1. Based on the applied loads to the cantilever beam, calculate the strain levels based on the strain equations and appropriate coefficients derived in the previous section
2. Input the strain levels calculated from step 1 for a given load case
3. Use Newton's method to solve for the appropriate ground loads to match the inputted strain levels
4. Compare the known applied loads to the predicted strain levels using Newtons Method

Sample Case

Input

Strain Gauge Coefficients

| Section | Location (deg) | Element | A | ϕ_{RF} (rad) | B | C | ϕ_{RM} (rad) | D | E |
|---------|----------------|---------|-------|-------------------|-----|------|-------------------|-----|-------|
| B-B | 0 | 93275 | 311.3 | 3.107 | 0.0 | 13.2 | 1.536 | 0.0 | -11.7 |
| | 45 | 95235 | 311.3 | 2.339 | 0.0 | 13.2 | 0.785 | 0.0 | -11.7 |
| | 90 | 97195 | 311.3 | 1.571 | 0.0 | 13.2 | 0.000 | 0.0 | -11.7 |
| | 135 | 99155 | 311.3 | 0.785 | 0.0 | 13.2 | -0.785 | 0.0 | -11.7 |
| | 180 | 101115 | 311.3 | 0.000 | 0.0 | 13.2 | -1.571 | 0.0 | -11.7 |
| | 225 | 103075 | 311.3 | -0.785 | 0.0 | 13.2 | -2.356 | 0.0 | -11.7 |
| | 270 | 89355 | 311.3 | -1.623 | 0.0 | 13.2 | -3.194 | 0.0 | -11.7 |
| | 315 | 91035 | 311.3 | -2.356 | 0.0 | 13.2 | -3.927 | 0.0 | -11.7 |
| | 360 | 93275 | 311.3 | 3.107 | 0.0 | 13.2 | 1.536 | 0.0 | -11.7 |

L = 30.6 in

Applied Loads

Case = 24
Ref Row = 31

| | |
|------|----------------|
| V = | 1.574 kip |
| D = | -0.016 kip |
| S = | -1.036 kip |
| RR = | 19.675 in |
| MD = | -20.375 kip-in |
| MV = | -0.017 kip-in |

In-service slow turn maneuver example

RF = 1.575 kip
RM = 20.375 kip-in
 θ_{RF} = 1.581 rad
 θ_{RM} = 3.142 rad

90.6 deg
180.0 deg

Strain Calculations

| Location (deg) | ϵ' (μ) | ϵ'' (μ) | ϵ''' (μ) | ϵ (μ) |
|----------------|-----------------------|------------------------|-------------------------|----------------------|
| 0 | -12 | -9 | 12 | -9 |
| 45 | -349 | -190 | 12 | -527 |
| 90 | -490 | -270 | 12 | -748 |
| 135 | -350 | -191 | 12 | -529 |
| 180 | -5 | 0 | 12 | 7 |
| 225 | 343 | 190 | 12 | 545 |
| 270 | 490 | 269 | 12 | 771 |
| 315 | 350 | 190 | 12 | 553 |
| 360 | -12 | -9 | 12 | -9 |

Calculated Strain Levels at Different Locations at Section B-B

Output

Strain Readings

| Section | Location (deg) | ϵ (μ) |
|---------|----------------|----------------------|
| B-B | 0 | -9 |
| | 90 | -748 |
| | 180 | 7 |
| | 270 | 771 |
| | 315 | 553 |

Input based on Data on Previous Page

Calculations

Applied Loads

RF = 1.575 kip
 RM = 20.375 kip
 θ_{RF} = 265.475 rad 15210.6 deg
 θ_{RM} = -3.141 rad -180.0 deg
 S = -1.036 kip

Strain Readings

| Location (deg) | ϵ' (μ) | ϵ'' (μ) | ϵ''' (μ) | ϵ (μ) | f | f^2 |
|----------------|-----------------------|------------------------|-------------------------|----------------------|---|-------|
| 0 | -12 | -9 | 12 | -9 | 0 | 0 |
| 90 | -490 | -270 | 12 | -748 | 0 | 0 |
| 180 | -5 | 0 | 12 | 7 | 0 | 0 |
| 270 | 490 | 269 | 12 | 771 | 0 | 0 |
| 315 | 350 | 190 | 12 | 553 | 0 | 0 |

J-Matrix

| RF | RM | θ_{RF} | θ_{RM} | S |
|--------|---------|---------------|---------------|-------|
| -7.8 | -0.450 | 489.978 | 269.321 | -11.7 |
| -311.3 | -13.234 | 4.892 | 0.227 | -11.7 |
| -3.1 | -0.011 | -490.106 | -269.514 | -11.7 |
| 311.0 | 13.191 | 20.764 | 13.859 | -11.7 |
| 222.3 | 9.348 | 343.098 | 190.156 | -11.7 |

Inverse J-Matrix

| RF | RM | θ_{RF} | θ_{RM} | S |
|--------|---------|---------------|---------------|--------|
| -1.816 | 1.718 | -1.613 | 1.538 | 0.172 |
| 42.354 | -40.467 | 38.119 | -36.754 | -3.232 |
| -1.206 | 0.060 | 0.420 | -1.700 | 2.426 |
| 2.213 | -0.127 | -0.748 | 3.076 | -4.415 |
| -0.047 | 0.001 | -0.042 | -0.005 | 0.007 |

$J^{-1} \cdot F$

0.00
 0.00
 0.00
 0.00
 0.00

Latest Guess

RF = 2 kip Iteration = 18
 RM = 20 kip
 θ_{RF} = 265 rad
 θ_{RM} = -3 rad
 S = -1.036 kip

Analysis Check

Input

V = 1.574 kip
 D = -0.016 kip
 S = -1.036 kip
 RR = 19.675 in
 MD = -20.375 kip-in
 MV = -0.017 kip-in

Output

V = 1.574 kip
 D = -0.016 kip
 S = -1.036 kip
 RR = 19.675 in
 MD = -20.375 kip-in
 MV = -0.017 kip-in

Input and Output Match

In total, over 200 typical in-service loading conditions were checked to determine if Newton's Method would consistently converge and accurately predict the ground loads applied. For all cases, Newton's Method converged. The embedded spreadsheet below contains both the calculations and results for all of these cases.



CantileverBeam_Equ
ation_Solver.xls

9.2 G650 NLG Drop Test

For each new landing gear design, a series of drop tests are required to certify the performance of the landing gear shock strut. These tests require that the landing gear be dropped at specific sink and tire rotation speeds. Drop tests are the best means of testing dynamic loading scenarios prior to flight test.

As a technology demonstration test, the post-style strain gauge configuration proposed in this thesis (see section 7.3) will be placed on the G650 NLG drop test unit. This test will investigate the strain gauge configuration's ability to measure strain levels during highly dynamic loading events. Based on the strain levels measured, the resulting ground loads will be calculated and compared to the dynamic simulation results.

9.3 G650 NLG Static Test

Many loading events experienced by landing gear are quasi-static in nature. These loading events include turning, braking, taxiing, etc. As a result, it will be necessary to demonstrate that the proposed load monitoring system is able to predict these types of loading events.

As a part of the technology demonstration, the strain gauge configuration proposed in section 7.3 will be placed on the G650 NLG static test unit. This test will demonstrate the proposed strain gauge configuration's ability to predict the applied loads for quasi-static load events.

9.4 G650 NLG Fatigue Test

In conjunction with the static and drop test technology demonstrations, the proposed strain gauge configuration will also be placed on the G650 NLG fatigue test unit. The purpose of this demonstration is twofold:

1. fidelity of post load predictions under cyclic loading (most representative of in-service loading)
2. ability of system to maintain ability to accurately measure strains over long periods of time under cyclic loading

9.5

G650 Flight Test

As a final step in the technology demonstration of the ODHMS system, the proposed strain gauge configuration will be placed on the G650 flight test aircraft (shown below).

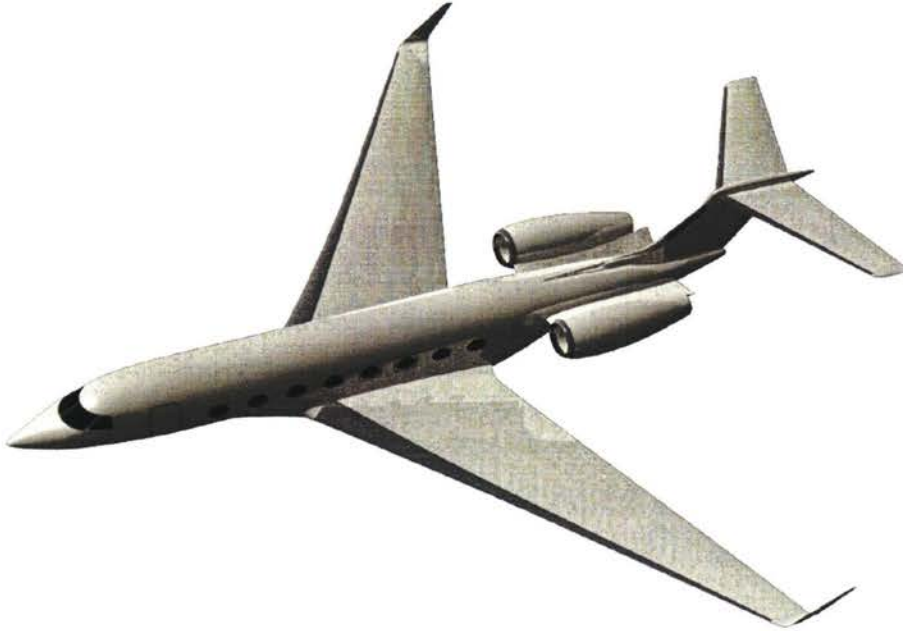


TABLE 9-2: GULFSTREAM G650 BUSINESS JET

Assuming that the drop, static, and fatigue demonstration tests are successful, the proposed system will be placed on the G650 flight test aircraft to demonstrate the system's ability for actual in-service measurements.

Chapter 10: Discussion

In future aircraft platforms, there is an opportunity to provide both airframe manufacturers and airline customers a sensing system for landing gear overload detection and long-term health monitoring. I have named this system as 'Overload Detection and Health Monitoring System' (ODHMS). At present, there are many innovative sensing system options that could be used in an ODHMS system. This system would utilize either direct or indirect measurement of strain at key locations on the landing gear structure. A few of these sensing options include fibre optic strain gauges and silicon MEMS strain gauges developed by Goodrich Corporation.

The keys to developing an ODHMS system that both airline customers and airframe manufacturers will allow to be placed on the landing gear are:

- Minimize the number of sensors required to predict overload and fatigue life
- Minimize the need for replacement and/or maintenance of sensing system
- Minimize the weight and power consumption of the system
- Minimize complexity of system which reduces the probability of system failure

For an ODHMS system to be viable, there are two options:

1. Place sensors on key structural components of landing gear
2. Place sensors at a few key locations to predict ground loads

Option 1 would involve a high number of sensors. As an example, if resistance strain gauges were chosen as the sensor, a minimum of 100 channels would be required to accurately predict the loads acting on all key structural components on the landing gear. Placing this many sensors on the landing gear system pose many issues:

- Many cables required to connect all strain gauges to data acquisition system (DAC). This many cables may not be physically possible since the landing gear will need to retract and extend (i.e. cables may not bend or could interfere with retraction sequence)
- Weight of all of the cables and the increased power requirements for system could be prohibitive

- Introduction of high sensor count increases risk of maintenance/replacement as well as system failure

Option 2 is a much more viable option and is the focus of my thesis. By placing a minimum amount of sensors close to the ground loads application points (i.e. wheels), the input forces and moments acting on the landing gear can be measured. With the use of standard landing gear structural beam models, the internal loads throughout the structure can be predicted analytically instead of by direct measurement. These structural beam models are validated during prototype landing gear testing therefore the accuracy of the internal load predictions will be acceptable. In my proposal, I investigate two different sensor configurations:

1. Wheel Load Sensing
2. Post Load Sensing

Wheel load sensing (see section 7.1) is the most accurate way of determining the applied ground loads to the landing gear since the sensors will be measuring directly adjacent to the wheel. By measuring at the wheel, the distribution of forces and moments at each wheel can be accurately determined. However, there are some difficulties of implementing this type of sensing system:

1. Sensors will need to be placed on the inner diameter (ID) of the axle. For smaller landing gears (i.e. less than 150 passengers), the ID's are relatively small and installing the sensors here would require special tooling.
2. Since the brakes typically rest on the axle, the sensors would be exposed to high temperatures (in the range of 250 °C maximum). If standard bonding techniques are utilized to attach the sensors to the axle, these bonds may not withstand the temperature. Special bonding agents may need to be utilized to withstand the high temperature exposure.
3. The moment due to braking would not be measured at the wheel. Instead, it would be the brake supplier's responsibility to provide brake torque data to the ODHMS system.

Post load sensing (see section 7.3) requires that sensors be placed on the outer diameter of the piston and on the lower (or upper) torque link. This system is capable of measuring the total forces and moments acting on the landing gear but cannot accurately predict the loads acting at each individual wheel. Therefore, for any wheel and axle analyses, assumptions about the distribution the total load at each wheel will need to be made (aviation authorities typically require that a minimum of 60% distribution at each will be assumed). This system requires only five (for NLG) and six (for MLG) sensors to predict the post loads acting on the landing gear.

Comparing the two systems, the post load measurement technique is best for smaller landing gears that have one or two wheels. The assumptions made in terms of wheel load distributions are minimized since there are a maximum of two wheels to consider. For larger aircraft with landing gears that have 4 or more wheels, the wheel load monitoring system is ideal since the need to make assumptions about wheel load distributions is eliminated.

The two sensing system configurations that I have proposed require that the sensors output strain levels. The sensors chosen must be capable of accurately sensing strain (direct or indirect) for dynamic, quasi-static, and static loading events. The sensing system must be capable of accurately reading strain levels in dynamic loading events at ranges of 256 – 1000 Hz. Technologies today can provide this type of accuracy for dynamic loading events. During flight test programs for prototype aircraft, the airframe manufacturer typically requires that the landing gear manufacturer calibrate their landing gear designs with resistance strain gauges. The strain data collected by these strain gauges includes all regimes of flight (dynamic, quasi-static, and static). The strain data accumulated during flight test is then used to validate both aircraft dynamic and structural models used to predict ground loads.

Chapter 11: Conclusion

In future aircraft landing gear development programs, an opportunity exists for landing gear suppliers such as GLG to provide customers with both an overload detection and health monitoring system. If companies such as GLG can provide a low cost, low-maintenance system to detect the health of their landing gear products, both airframe manufacturers and airline customers will be willing to absorb additional up-front costs to purchase the system. In the long-term, the airline customers will save costs since inspections for both overload and fatigue may be reduced and/or eliminated.

This thesis has proposed a system strain gauge configuration that could accurately measure the ground loads experienced by a landing gear over its life. This configuration is independent of the choice of strain measurement type so that, over time, improved measurement techniques may be implemented with little to no impact to the algorithms presented in this report.

The proposed strain gauge configuration will be demonstrated in a series of tests of escalating complexity which are listed below:

1. Cantilever Beam Test
2. G650 NLG Static Test
3. G650 NLG Drop Test
4. G650 NLG Fatigue Test
5. G650 NLG Flight Test

If these technology demonstration tests are successful, both in-service and future aircraft platforms will be able to place a system similar to ODHMS on their landing gear systems. This system will be able to predict overload, service-life, and aircraft weights and balance.

REFERENCES

Textbooks

1. Bannantine, Julie, Comer, Jess, and James Handrock. *Fundamentals of Metal Fatigue Analysis*. Englewood Cliffs, NJ: Prentice-Hall, Inc., 1990.
2. Beer, Ferdinand, and E. Russell Johnston. *Mechanics of Materials*. 2nd Edition. Toronto, ON: McGraw-Hill, 1992.
3. Bruhn, E.F. *Analysis and Design of Flight Vehicle Structures*. 2nd Edition. USA. Tri-State Offset Company, 1973.
4. Burden, Richard L. and J. Douglas Faires. *Numerical Analysis*. 6th Edition. Toronto, Brooks/Cole Publishing Company, 1997.
5. Dieter, George E. *Mechanical Metallurgy*. 3rd Edition. Toronto, ON: McGraw-Hill, 1986.
6. Roark, Warren C. *Roark's Formulas for Stress and Strain*. 6th Edition. Toronto, McGraw-Hill, Inc., 1989.
7. MMPDS-03. *Metallic Materials Properties Development and Standardization*. Federal Aviation Administration, 2006.

Papers

8. Giurgiutiu, Victor (2000) "Active Sensors for Health Monitoring of Aging Aerospace Structures" *SPIE's 7th International Symposium on Smart Structures and Materials*, Newport Beach, CA, March 5-9, 2000.
9. *Best Practices Guide: Inspection Process following High Load Events*. Publication 05-01. Aerospace Industries Association (AIA), April 8, 2005.
10. *Airplane Hard Landing Indication System*. US Patent 6,676,075, August 30, 2001.

Goodrich Documents

11. EM-005. *Engineering Structural Manual*. Goodrich Landing Gear. Oakville, Ontario, 2008. Goodrich Proprietary.
12. S471. *GVI Nose Landing Gear Internal Loads Report*. Revision B. Goodrich Landing Gear. Oakville, Ontario, 2007. Goodrich Proprietary.
13. ECM B-BFG-AUK-1018, "Update to Hard Landing Inspection procedures – includes rationale for the inspection locations", Issue A, 2006. Goodrich Proprietary.